

**INVESTIGATION OF AIR BUBBLE MOTION
IN COUNTER-CURRENT WATER FLOW CONDITIONS**

Uğur BEZDEGÜMELİ

SEPTEMBER 2003

**INVESTIGATION OF AIR BUBBLE MOTION
IN COUNTER-CURRENT WATER FLOW CONDITIONS**

**A THESIS SUBMITTED TO
THE GRADUATE SCHOOL OF NATURAL AND APPLIED SCIENCES
OF
THE MIDDLE EAST TECHNICAL UNIVERSITY**

BY

UĞUR BEZDEĞÜMELİ

**IN PARTIAL FULFILLMENT OF THE REQUIREMENTS FOR THE DEGREE OF
DOCTOR OF PHILOSOPHY
IN
THE DEPARTMENT OF MECHANICAL ENGINEERING**

SEPTEMBER 2003

Approval of the Graduate School of Natural and Applied Sciences

Prof.Dr. Canan ÖZGEN
Director

I certify that this thesis satisfies all the requirements as a thesis for the degree of Doctor of Philosophy.

Prof.Dr. Kemal İDER
Head of Department

This is to certify that we have read this thesis and that in our opinion it is fully adequate, in scope and quality, as a thesis for the degree of Doctor of Philosophy.

Prof. Dr. A. Orhan YEŞİN
Supervisor

Examining Committee Members

Prof. Dr. Cahit ÇIRAY

Prof. Dr. A. Orhan YEŞİN

Prof. Dr. Hasbi YAVUZ

Prof. Dr. Zafer DURSUNKAYA

Asst.Prof. Dr. Derek BAKER

ABSTRACT

INVESTIGATION OF AIR BUBBLE MOTION IN COUNTER-CURRENT WATER FLOW CONDITIONS

Bezdegümelı, Uğur

Ph.D., Department of Mechanical Engineering

Supervisor: Prof. Dr. A. Orhan YEŞİN

September 2003, 103 pages

In this thesis study, air bubble motion in counter-current water flow conditions in a vertical pipe is investigated experimentally. For this purpose, a test set-up was designed and constructed. Images of motions of single bubbles, having different diameters in the range of 3.0-4.8 mm, generated by specially designed bubble injectors were recorded by using a monochrome camera, an image capture card and a PC. Recorded video images were processed to obtain the necessary data for the purpose of the study.

The purpose of the study is to determine

- bubble axial velocity and
- bubble drag coefficient

variation as a function of the equivalent bubble diameter, water flow velocity and related dimensionless numbers; Reynolds, Re ; Eötvös, Eo ; and Weber, We , and is to investigate the bubble shapes and bubble travel paths.

Bubble behaviour was investigated at six different counter-current water flow velocities (6.5 cm/s, 7.9 cm/s, 10.5 cm/s, 12.9 cm/s, 15.4 cm/s, and 18.2 cm/s) in addition to stagnant water condition which is taken as the reference case. The

direction of the bubble motion is upwards and the direction of the water flow is downwards (i.e. counter-current). Distilled water was used in the experiments.

The results of this thesis study for the stagnant water condition have shown good consistency with the previous theoretical and experimental studies found in the literature. For the studied range of bubble diameters, it is observed that the bubble average relative velocity for a certain bubble diameter is less under counter-current water flow conditions than that under stagnant water condition and the drag coefficient values for a certain bubble diameter is higher under counter-current water flow conditions than those under stagnant water condition.

Keywords: Air bubble
Bubble motion
Bubble velocity
Bubble drag coefficient
Counter-current flow condition

ÖZ

TERS YÖNLÜ SU AKIŞ KOŞULLARINDA HAVA KABARCIĞI HAREKETİNİN İNCELENMESİ

Bezdegümelı, Uğur

Doktora, Makına Mühendisliđi Bölümü

Tez Yöneticisi: Prof. Dr. A. Orhan YEŞİN

Eylül 2003, 103 sayfa

Bu çalışmada, düşey yöndeki bir boru içerisinde ve ters yönlü su akış koşullarında hava kabarcıklarının hareketleri deneysel olarak incelenmiştir. Bu amaçla bir test düzeneđi tasarlanmıř ve kurulmuřtur. Özel olarak tasarlanmıř ve imal edilmiř şırıngalarla oluşturulan ve çapları 3.0-4.8 mm aralıđında deđişen hava kabarcıklarının hareket görüntüleri bir siyah-beyaz kamera, bir görüntü yakalama kartı ve bilgisayar kullanılarak kaydedilmiştir.

Kaydolan video görüntüleri, çalışmanın amaçları çerçevesinde ihtiyaç duyulan verileri elde etmek amacıyla işlenmiştir.

Çalışmanın amacı

- kabarcık aksenal hızı ve
- kabarcık direnç katsayısı

deđişiminin kabarcık eşdeđer çapı, su akış hızı ve ilgili boyutsuz sayıların (Reynolds, Re ; Eötvös, Eo ; ve Weber, We) fonksiyonu olarak belirlenmesi ve kabarcık şekilleri ile kabarcıkların izlediđi yolların incelenmesidir.

Kabarcık hareketi, referans olarak alınan “durgun su koşulu”na ilaveten altı farklı ters yönlü su akış koşulunda (6,5 cm/sn, 7,9 cm/sn, 10,5 cm/sn, 12,9 cm/sn, 15,4

cm/sn, ve 18,2 cm/sn) incelenmiştir. Kabarcık hareketi yönü yukarı, su akış yönü aşağıya doğrudur (ters yönlü akış). Deneyleerde damıtık su kullanılmıştır.

Bu tez çalışmasının durgun su koşulları için olan bölümü literatürde bulunan önceki teorik ve deneysel çalışmalarla iyi bir uyum göstermektedir. Çalışılmış kabarcık çapı aralığında; belirli bir kabarcık çapı için kabarcık ortalama göreceli hızının ters yönlü su akış koşullarında durgun su koşuluna nazaran daha düşük olduğu görülmüş ve belirli bir kabarcık çapı için direnç katsayısı değerleri durgun su koşuluna nazaran daha yüksek bulunmuştur.

Anahtar Kelimeler : Hava kabarcığı
Kabarcık hareketi
Kabarcık hızı
Kabarcık direnç katsayısı
Ters yönlü akış koşulu

To my family

ACKNOWLEDGMENTS

I express my sincere appreciation to Prof. Dr. Orhan Yeşin for his guidance, encouragement and insight throughout the research.

I would like to thank to Prof. Dr. Cahit Çıray and Prof. Dr. Zafer Dursunkaya, members of my Ph.D. Progress Committee, for their valuable suggestions and comments.

I would also like to thank to Prof. Dr. Hasbi Yavuz who provided some important reports used in this work and encouraged me with his valuable suggestions.

I would like to express my gratitude to Technician Mr. İbrahim Özdemir and to my friend Mr. Sancak Özdemir for their considerable assistance provided during the construction of the test section and conduction of the experiments.

I would like to extend my thanks to Dr. Fahri Ağlar and Ayhan Yılmaz for their assistance provided during the preparation of this dissertation and for their comments.

Last but not least, I wish to express my special thanks to my wife and to my son for their patience, understanding and morale support.

TABLE OF CONTENTS

ABSTRACT	iii
ÖZ	v
ACKNOWLEDGMENTS	viii
TABLE OF CONTENTS	ix
LIST OF TABLES	xi
LIST OF FIGURES	xii
NOMENCLATURE	xv
CHAPTER	
1. INTRODUCTION AND THE IMPORTANCE OF THE THESIS	
SUBJECT	1
2. LITERATURE SURVEY	3
2.1 Bubble Shape	3
2.1.1 Shape Regimes for Bubbles	9
2.2 Bubble Motion	10
2.2.1 Summary of Previous Theoretical Studies on Bubble	
Motion	11
2.2.2 Wakes of Deformed Bubble	16
2.2.3 Secondary Motion	17
2.2.4 Effect of Surface-Active Contaminants and Internal	
Circulation	18
2.2.5 Experimental Studies for Air Bubbles in Water	19
2.2.6 Simple Analysis of the Motion of an Air Bubble Rising	
Through Liquid	30
3. TEST SET-UP AND EXPERIMENT PROCEDURE	32
3.1 Test Set-up	32
3.2 Minimization of the Optical Deformations	35
3.3 Experiment Procedure	36

3.4 The Error Arising from Flow-meter Calibration and the Tank Water Temperature Change	38
4. ACQUISITION AND PROCESS OF THE EXPERIMENTAL DATA	44
4.1 Measurement of the Bubble Diameter	46
5. DISCUSSION OF EXPERIMENTAL RESULTS	57
5.1 Bubble Path, Bubble Shape Behavior, Bubble Axial Relative Velocity Change and Effect of the Water Velocity	57
5.2 Bubble Average Relative Velocity and Effect of the Water Velocity	63
5.2.1 Stagnant Water Condition	63
5.2.2 Counter-Current Water Flow Conditions	65
5.3 Drag Coefficient	68
5.4 Conclusion and Recommendations for Future Studies	69
REFERENCES	88
APPENDICES	
A. UNCERTAINTIES REFERENCES	92
B. FORCES AFFECTING SHAPE OF AN AIR BUBBLE RISING IN WATER REFERENCES	94
C. EXPERIMENTAL RESULTS REFERENCES	97
VITA	103

LIST OF TABLES

TABLE

2.1 Shape of air bubbles rising in stagnant water [3]	6
B.1 Forces affecting on bubble shape (mili Newton)	96
C.1 Data for $V_w = 0.0$ cm/s	97
C.2 Data for $V_w = 6.5$ cm/s	98
C.3 Data for $V_w = 7.9$ cm/s	98
C.4 Data for $V_w = 10.5$ cm/s	99
C.5 Data for $V_w = 12.9$ cm/s	99
C.6 Data for $V_w = 15.4$ cm/s	100
C.7 Data for $V_w = 18.2$ cm/s	100
C.8 Data for $V_w = 0.0$ cm/s	101
C.9 Data for $V_w = 6.5$ cm/s	101
C.10 Data for $V_w = 7.9$ cm/s	101
C.11 Data for $V_w = 10.5$ cm/s	101
C.12 Data for $V_w = 12.9$ cm/s	102
C.13 Data for $V_w = 15.4$ cm/s	102
C.14 Data for $V_w = 18.2$ cm/s	102

LIST OF FIGURES

FIGURES

2.1 Shape regimes for bubbles and drops in unhindered gravitational motion through liquids. [2]	7
2.2 Dimensions of ellipsoids	8
2.3 Deformation of drops and bubbles in pure water. [2]	8
2.4 Drag coefficients for bubbles in pure mediums: predictions of numerical, Galerkin, and BL theories compared with selected experimental data. [2]	15
2.5 The rise velocity of air bubbles in the stagnant water at 20 ⁰ C. [2]	20
2.6 Drag coefficient as function of Re for air bubbles in stagnant water (in comparison with the standard drag curve for a sphere). [2]	21
2.7.a Mean air bubble rise speed in stagnant water. [13]	23
2.7.b Bubble drag coefficient. [13]	24
2.8.a Variation of C_D with Reynolds number. [3]	24
2.8.b Variation of the bubble maximum and average velocities. [3]	25
2.9 Velocities for free-rise conditions in quiescent water. [16]	26
2.10.a Variation of bubble relative velocity with equivalent radius. [14]	26
2.10.b Variation of bubble relative velocity with equivalent radius. [14]	27
2.11.a Variation of the average rise velocity with equivalent bubble diameters: for bubbles in co- current water flow. [15]	27
2.11.b Variation of $C_{D,z}$ with Reynolds number: for bubbles in co-current water flow. [15]	28
2.11.c Variation of C_D with Reynolds number. [15]	29
3.1.a Test Set-up	40
3.1.b Test Section	41
3.1.c Air line	42
3.2 Buffer tank	42
3.3 The bubble injection section	43

3.4 Design of the brass bubble injectors	43
4.1 Process of the images by using Paint Shop Pro computer program ..	47
4.2 Motion of a bubble having 4.60 mm diameter ($V_w = 0.0\text{cm/s}$)	48
4.3 Motion of a bubble having 4.30 mm diameter ($V_w = 6.5\text{ cm/s}$)	49
4.4 Motion of a bubble having 4.53 mm diameter ($V_w = 12.9\text{ cm/s}$)	51
4.5 Motion of a bubble having 3.28 mm diameter ($V_w = 18.2\text{ cm/s}$)	53
5.1.a The bubble average relative velocity change as a function of the equivalent bubble diameter and water velocity	71
5.1.b The bubble average relative velocity change as a function of d_e (comparison with the results of Ref.3 and Ref.15)	72
5.2 The bubble relative velocity change with the vertical distance ($d_e= 3.23\text{ mm}$)	73
5.3 The bubble relative velocity change with the vertical distance ($d_e= 4.06\text{ mm}$)	74
5.4 The bubble relative velocity change with the vertical distance ($d_e= 4.63\text{ mm}$)	75
5.5 Change of the bubble relative velocity with the vertical distance ($d_e=4.0\text{ mm}$, $V_w=0\text{ cm/s}$)	76
5.6 Change of the bubble relative velocity with the vertical distance ($d_e=4.0\text{ mm}$, $V_w=10.5\text{ cm/s}$)	76
5.7 Change of the bubble relative velocity with the vertical distance ($d_e=4.14\text{ mm}$, $V_w=0\text{ cm/s}$)	77
5.8.a The bubble relative vertical velocity change with the vertical distance ($d_e=2.8\text{ mm}$) [3]	78
5.8.b The bubble relative vertical velocity change with the vertical distance ($d_e=2.8\text{ mm}$) [3]	78
5.9.a The bubble relative vertical velocity change with the vertical distance ($d_e=3.57\text{ mm}$) [3]	79
5.9.b The bubble relative vertical velocity change with the vertical distance ($d_e=3.57\text{ mm}$) [3]	79
5.10.a The bubble relative vertical velocity change with the vertical distance ($d_e=4.18\text{ mm}$) [3]	80
5.10.b The bubble relative vertical velocity change with the vertical distance ($d_e=4.18\text{ mm}$) [3]	80
5.11 Drag coefficient change as a function of Eötvös number	81

5.12 Drag coefficient change as a function of Weber number	81
5.13.a Drag coefficient change as a function of the equivalent bubble diameter and the water velocity	82
5.13.b Drag coefficient change as a function of d_e (comparison with the results of Ref.3 and Ref.15)	83
5.14 Change of Weber number as a function of the bubble diameter	84
5.15 Change of Eötvös number as a function of the bubble diameter	84
5.16.a Drag coefficient change as a function of the bubble Reynolds number and water velocity	85
5.16.b Drag coefficient change as a function of the bubble Reynolds number and water velocity	85
5.16.c Drag coefficient change as a function of Re_b and water velocity (comparison with the results of Ref.3 and Ref.15)	86
5.16.d Drag coefficient change as a function of Re_b and water velocity (comparison with the results of Ref.3 and Ref.15)	87
B.1 Magnitudes of some important forces affecting the bubble shape	96

NOMENCLATURE

A	projected area, m^2
C_D	drag coefficient
$C_{D,av}$	drag coefficient based on $V_{av,r}$
$C_{D,St}$	Stokes' drag coefficient
d_b	bubble diameter, m
d_e	equivalent bubble diameter, m
D_h	hydraulic diameter, m
e	plexiglas pipe wall thickness, m
E	aspect ratio
E_o	Eötvös number
F_b, F_{buo}	buoyancy force, N
F_D	drag force, N
F_{st}	surface tension force, N
F_{vis}	viscous force, N
g	gravitational acceleration, m/s^2
L	required length for fully developed flow, m
M	Morton number
m	mass, kg
n_1	refraction index of the water
n_2	refraction index of the plexiglas pipe
R	radius of sphere, m
Re, Re_b	Reynolds number based on the relative velocity of the bubble and the bubble diameter
Re_w	Reynolds number corresponding to water flow velocity in the plexiglas pipe section
U	relative velocity of the bubble, m/s
U_o	free stream velocity of the liquid, m/s

U_T	terminal velocity, m/s
$U_{T,ob}$	bubble observed terminal velocity, m/s
$U_{T,r}$	bubble relative terminal velocity, m/s
$V_{av,r}$	bubble average relative velocities between the distance 5-10 cm, m/s
V_b	bubble volume, m ³
V_w	water flow velocity in the plexiglas pipe section, m/s
v	bubble velocity, m/s
v_l	surrounding liquid velocity, m/s
v_{ob}	observed bubble velocity, m/s
v_r	bubble relative velocity, m/s
We	Weber number

Greek Symbols:

$\Delta\rho$	density difference, $(\rho_l - \rho_b)$, kg/m ³
δ	linear deviation of the incoming light beam
θ	angle between the incoming light beam and normal to the plexiglas pipe surface, rad
κ	dynamic viscosity ratio (μ_b / μ_l)
μ_b	dynamic (absolute) viscosity of the bubble, kg/m.s
μ_l	dynamic (absolute) viscosity of the surrounding liquid, kg/m.s
ν	water kinematic viscosity, m ² /s
ρ_l	liquid density, kg/m ³
ρ_b	bubble density, kg/m ³
σ	surface tension, N/m

CHAPTER I

INTRODUCTION AND THE IMPORTANCE OF THE THESIS SUBJECT

Bubbly two-phase flows appear in many industrial facilities such as nuclear power plants and chemical reactors. In order to reach the desired level of safety and to obtain high operating efficiency at those facilities, the statistical and time averaged characteristics of bubbly flow, such as phase distribution and bubble size, have been extensively investigated. In general, bubbly flows are very complex and detailed knowledge about all phenomena involved should be obtained to predict the motion of bubbles. Recently, investigations have focused on the basic flow mechanisms in order to make clear the phenomenon of bubbly flow. Therefore, the behaviour of a single bubble is regarded as one of the basic elements characterizing the bubbly flow.

It is very complicated to perform fully satisfactory theoretical analyses of the subject due to the following reasons:

- internal circulation in the bubble,
- shape deformation and oscillations causing bubble geometry change,
- secondary motion resulting in non-linear bubble path,
- irregular rotation causing irregular bubble orientations and hence projected area change, and
- effect of the external water flow if the surrounding liquid is not stagnant.

There is no fully satisfactory theoretical model for the bubble motion at moderate Reynolds numbers. Therefore, it is necessary to conduct experimental studies to fully understand the issue and to obtain the necessary data. Although we may get some useful quantitative and qualitative information from the theoretical models, it

is usually not sufficient for many cases, especially for deformed bubbles moving in a liquid medium, hence we should rely on the experimental studies.

An extensive literature survey has shown that there are adequate numbers of experimental studies investigating the air bubble motion in stagnant water condition and only a few experimental studies for co-current water flow conditions in which the direction of the moving bubble and the water flow are upwards. Experimental studies for co-current water flow conditions have indicated that external water flow has an effect on the bubble motion and results are different from those for stagnant water condition. Nevertheless, according to the author's knowledge till the completion of this study, there was not any experimental study conducted for counter-current water flow conditions in which the direction of the moving bubble is upward and the direction of the water flow is downward.

The cases where generated steam or air bubbles move opposite to the water flow occur in the once-through steam generators of power systems during some transient or accident conditions, in U-tube steam generators of nuclear reactors especially during insufficient secondary side cooling, and in the feeders of CANDU nuclear reactors in which the flow reversal occurs during natural circulation cooling mode. Because of its effect on heat transfer rates, an understanding of the subject is important for the design and safety evaluation of those systems. Since the analysis of the issue is so complicated, understanding of bubble behaviour is essential. Therefore, to develop theoretical models which enable to simulate the motion of bubbles, at first, it is necessary to fully understand the behaviour of an individual bubble and then to obtain reliable and sufficient drag coefficient data for the range of bubble sizes under consideration.

Considering the importance of the subject and that there is not any previous experimental study conducted for counter-current water flow conditions, a contribution has been made for the air bubbles having diameters 3.0-4.8 mm (deformed bubble range) moving under counter-current water flow conditions.

It is hoped that the results of this study would provide a valuable base and data for future theoretical or experimental studies.

CHAPTER II

LITERATURE SURVEY

2.1 Bubble Shape

The shape and size of a bubble significantly affects its motion as well as the associated heat and mass transfer processes. The drag force depends on the bubble shape and it is one of the factors that determine the magnitude of the bubble velocity.

If there is a relative motion of a gas bubble that exists in the surrounding liquid, the shape is naturally influenced by the forces in this surrounding liquid. Bubble has a shape so that the normal and shear forces are balanced at the interface between the bubble and surrounding liquid.

The surface tension force, when it has a constant value over the surface, acts to minimize the surface energy. Since the surface to volume ratio is the smallest for the sphere in comparison with the other shape geometries, surface tension force tends to keep a pure fluid particle in a perfect spherical shape. The cohesive forces between liquid molecules are responsible for the surface tension. The molecules at the surface do not have other like molecules on all sides of them and consequently they cohere more strongly to those directly associated with them on the surface.

A bubble will deform only when it is subject to non-uniform or non-symmetric forces such as those due to motion, pressure, or temperature variations that may overcome the stabilizing influence of surface tension. In the presence of surface-active contaminants (surfactants), the surface distribution of the surface-active agent will influence the shape [1,2]. Also, the dynamic forces resulting from the internal circulation may contribute to the deformation.

When the shape of the bubble is deformed significantly, theoretical approaches have limited success to predict the exact bubble shape. The predictions become less

realistic with increasing bubble size and deformation because of increasing error in the assumed or calculated bubble surface dynamic pressure distribution. The shape and trajectory of a bubble moving in a liquid are the consequences of the forces acting on. Some of those forces also depend on the shape and trajectory of the bubble. A bubble shape can't be exactly determined theoretically unless magnitudes and distributions of those forces through out the bubble surface are accurately calculated. Although there are some attempts for slightly deformed bubbles that are successful with some degree of accuracy, it is unavoidable to rely on experimental data for the determination of the exact deformed bubble shape. Therefore, analyses mostly rely on the relevant dimensionless numbers that are Reynolds number, Re , Weber number, We , and Eötvös number, Eo . Recent theoretical studies on the bubble shape and motion are extensively benefiting and are using the experimental data that give the bubble shape as a function of these dimensionless numbers.

Reynolds number is a measure of the relative importance of the inertia force compared to the viscous force and it is defined as

$$Re = \rho_l U d_b / \mu_l \quad (2.1)$$

where U is the relative velocity of the bubble, d_b is the bubble diameter, ρ_l is the bubble density and μ_l is the dynamic (absolute) viscosity of the surrounding fluid.

The Weber number is a measure of the relative importance of the dynamic pressure force compared to the surface tension force. It is given as

$$We = U^2 d_b \Delta\rho / \sigma \quad (2.2)$$

where σ is surface tension and $\Delta\rho$ is the density difference, $(\rho_l - \rho_b)$, of surrounding liquid (ρ_l) and bubble gas (ρ_b). When dynamic pressure forces are dominant, the appropriate parameter to be considered in a study of bubble deformation is the Weber number.

The Eötvös number is a measure of the importance of the buoyancy force compared to the surface tension force. It is defined as

$$Eo = \Delta\rho g d_b^2 / \sigma \quad (2.3)$$

where g is the gravitational acceleration. When buoyancy force is dominant, the appropriate parameter to be considered in a study of bubble deformation is the Eötvös number.

In summary, at a given Reynolds number, the two dimensionless numbers of interest for determining the gas bubble shape deformation are the Weber number and the Eötvös number.

Another parameter that is commonly used and which exclusively characterizes the physical properties of the bubble-liquid system is the Morton number. It is defined as

$$M = g \mu_i^4 \Delta \rho / (\rho_l^2 \sigma^3). \quad (2.4)$$

The Morton number value for air bubbles in water is approximately 10^{-11} .

Determination of bubble shapes as a function of the related dimensionless numbers has been studied experimentally for sixty years. However, all of the current available data are based on studies conducted for bubbles rising in stagnant water. Also, most of the data come from the experimental systems using non-purified water that contains surface-active contaminants (surfactants). On the other hand, it is known that the contamination in the liquid is an effective factor on the bubble shape. The other factor that may affect the bubble shape is the wall effect for the narrowly contained experimental systems. The wall tends to elongate the bubble in the opposite direction of the bubble motion.

One of the important studies performed on the determination of shape of the bubble in motion is the study of Grace and co-workers [2]. They have discussed the various shape regimes and parameters for fluid particles (gas bubbles or liquid drops) rising or falling freely in infinite media. It is possible to prepare a generalized graphical correlation in terms of the Eötvös number, Morton number, and Reynolds number. The resulting plot is shown in Figure 2.1. Since Reynolds number is the only one of the three groups to contain the bubble terminal velocity, Figure 2.1 may be used to estimate terminal velocities as well as the shape regime. It is notable that the dynamic viscosity of the bubble, μ_b , is assumed not to play an important role in determining terminal velocities and shape regimes since it does

not appear in any of the three dimensionless groups used to construct Figure 2.1. However, the role of μ_b may be significant for very pure (surfactant-free) liquid mediums due effect of the internal circulation.

Figure 2.1 shows boundaries between the three principal shape regimes described below, as given by Grace [2]. While the boundaries between the principal shape regimes are somewhat arbitrary, it is clear that bubbles and drops are ellipsoidal at relatively high Re and intermediate Eo while the spherical or ellipsoidal-cap regime requires that both Eo and Re be large. Various sub regimes may also be mapped, and some of these are included in Figure 2.1. Again the boundaries are somewhat arbitrary. Nevertheless, Figure 2.1 is a useful tool for demonstrating the wide range of bubble and drop behavior.

The term ellipsoidal covers a variety of shapes, many of which are far from true ellipsoids. Many bubbles and drops in this regime undergo marked shape oscillations. Also, drops and bubbles in highly purified mediums are significantly more deformed than those in contaminated mediums. Increased flattening of fluid particles in pure mediums results from increased dynamic pressure forces related to the increased terminal velocities. Table 2.1 shows the results of the study of Tapucu [3,4,5] for bubble motion in stagnant tap water.

Table 2.1 Shape of air bubbles rising in stagnant water [3]

Equivalent diameter (mm)	Weber number	Aspect ratio (E)	Shape of the bubble
0-0.83	0-0.62	1	Spherical
0.83-2.00	0.62-3.7	1-0.5	Ellipsoidal
2.00-4.20	3.7-5.5	0.5-0.25	Ellipsoidal with surface oscillation
>4.20	>5.5	-	Distorted bubble with a spherical cap

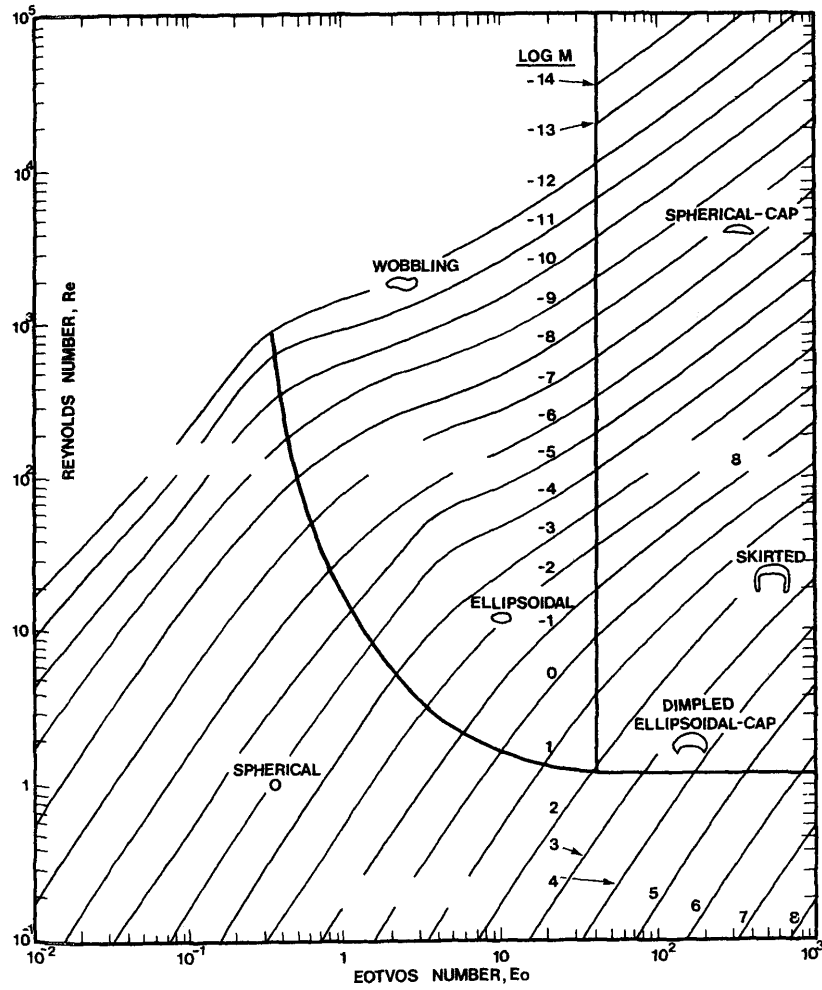


Figure 2.1 Shape regimes for bubbles and drops in un hindered gravitational motion through liquids. [2]

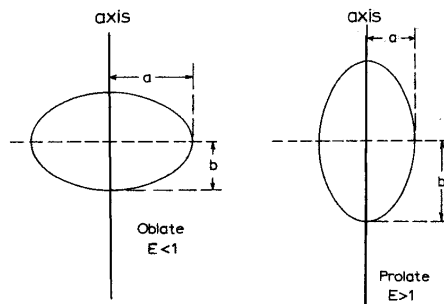


Figure 2.2 Dimensions of ellipsoids

The aspect ratio, b/a , of the bubble is denoted by E . It is an important parameter especially for the definition of the shape and the type of ellipsoidal bubbles. Figure 2.2 shows the notation used here: the axial dimension of the particle is $2b$ while the maximum dimension normal to the axis of symmetry is $2a$.

Some experimental results for liquid drops and gas bubbles in water (low M systems) are also shown in Figure 2.3 [2]. Small bubbles and drops are spherical ($E=1$) and larger ones approach $E=0.24$ no matter how pure the medium is. In addition, medium purity has the greatest effect at low κ . $\kappa = \mu_b / \mu_l$ is the dynamic viscosity ratio ($\kappa = 1.84 \times 10^{-5} \text{ kg/ms} / 8.9 \times 10^{-4} \text{ kg/ms} \approx 0.02$ for air bubbles in water).

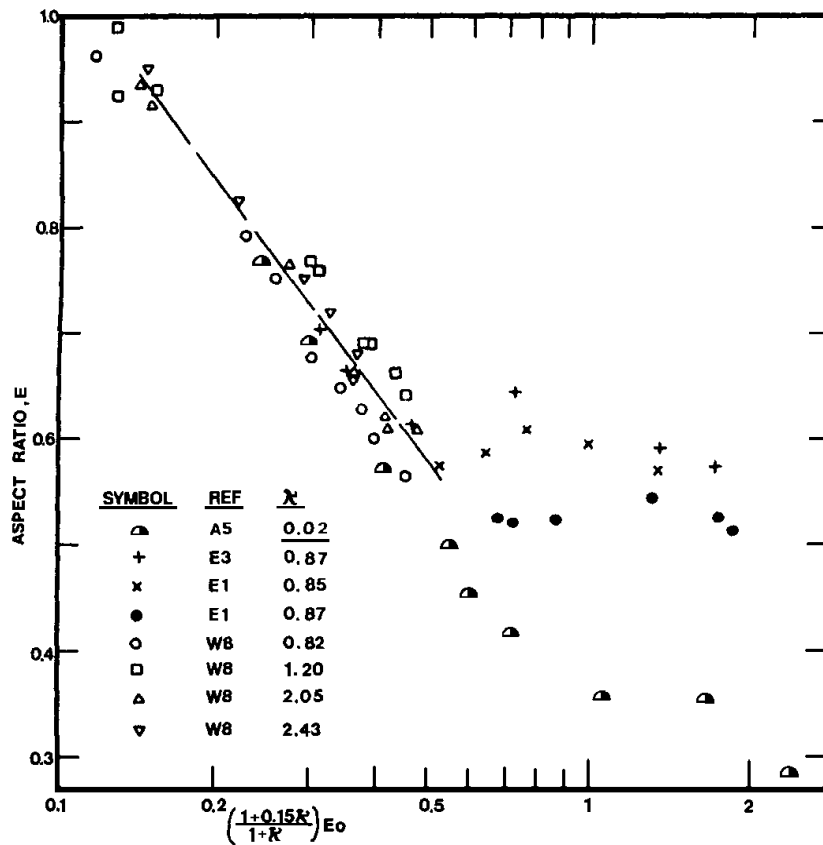


Figure 2.3 Deformation of drops and bubbles in pure water. [2]

2.1.1 Shape Regimes for Bubbles

When compared with the infinite number of shapes possible for solid particles, bubbles at steady state are severely limited in the number of possibilities since such features as sharp corners or protuberances are precluded by the interfacial force balance.

Bubbles in free rise in an infinite medium under the influence of buoyancy are generally grouped under the following three categories:

(a) “Spherical”: Generally speaking, bubbles are closely approximated by spheres if interfacial (surface) tension and/or viscous forces are much more important than dynamic pressure forces. Bubbles are usually termed "spherical" if the minor to major axis ratio lies within 10% of unity.

For $Re < 1$, the fluid particle will remain essentially spherical independent of the magnitude of Re , level of contamination, and value of the surface tension. With regard to the effect of the physical properties of the system, at $Re \leq 1$, unless $M \geq 1$, the particle remains nearly spherical. In usual applications, a fluid particle at $Re \leq 1$ may be assumed to be spherical independent of the Weber and Eötvös numbers. Bubbles remain nearly spherical at moderate Reynolds numbers (e.g., at $Re = 400$) if surface tension forces are sufficiently strong [2].

(b) “Ellipsoidal”: The term "ellipsoidal" is generally used to refer to bubbles which are oblate with a concave interface (viewed from inside) around the entire surface. It must be noted that actual shapes may differ considerably from true ellipsoids and that fore-and-aft symmetry must not be assumed. Moreover, ellipsoidal bubbles commonly undergo periodic dilations or random wobbling motions that make characterization of the shape particularly difficult.

For bubbles rising in liquid mediums, significant deformations from the spherical occur for all $Re > 600$ [2]. At higher values of Reynolds and Eötvös numbers (larger-sized bubble), the bubble becomes an oblate spheroid of revolution (ellipsoidal regime) and eventually becomes a part of the spherical-cap regime. The boundary between the spherical and ellipsoidal regimes is less definite and its

location may be dependent on the amount of surfactant present in the medium. With low M systems, an ellipsoidal fluids undergoes random wobbling motions.

(c) "Spherical-cap" or "ellipsoidal-cap": Large bubbles tend to adopt flat or indented bases and to lack any semblance of fore-and-aft symmetry. Such bubbles may look very similar to segments cut from spheres or from oblate spheroids of low eccentricity; in these cases the terms "spherical-cap" and "ellipsoidal-cap" are used. The leading edge of the cap is spherical and the trailing edge is flat. If the bubble has an indentation at the rear, it is often called "dimpled." Large spherical- or ellipsoidal-caps may also trail thin envelopes of dispersed fluid referred to as "skirts."

2.2 Bubble Motion

The fundamental physical laws governing motion of and heat transfer to bubbles moving in fluids are Newton's second law of motion, the principle of conservation of mass, and the first law of thermodynamics. Application of those laws to an infinitesimal element of material or to an infinitesimal control volume leads to the well-known Navier-Stokes, continuity, and energy equations. For a system with two phases (e.g. air bubble and water), these equations need to be solved for both phases. Interfacial relationships are then required to close the problem. In a moving gas bubble there exists an internal velocity field, or internal circulation, and the internal circulation velocity at different locations on the bubble can be different. Additional boundary conditions are required to completely close the Navier-Stokes and continuity equations.

Exact analytical solutions to the continuity, momentum, and energy equations have been derived only under restricted conditions. More usually, it is necessary to solve the equations numerically or to resort to approximate techniques where certain terms are omitted or modified in favour of those which are known to be more important. Boundary conditions must also be specified carefully to solve the equations. In many cases, especially for deformed bubbles moving in a liquid medium, we should rely on the experimental data.

In the following subsections, previous theoretical and experimental studies reported in the available literature, which are pertaining to the analysis of bubble motion in liquids, are discussed in some details.

2.2.1 Summary of Previous Theoretical Studies on Bubble Motion

As the most simple case, Stokes obtained the solution of drag for a rigid sphere immersed in a fluid flow. His solution is the well-known equation,

$$F_D = 6 \pi \mu_l R U_o \quad (2.5)$$

in which R is the radius of the sphere, U_o is the free stream velocity of the fluid and μ_l is fluid dynamic viscosity. This relationship holds true for $Re < 0.1$ but may be used with negligible error up to $Re = 0.2$. In this range, often referred to as *Stokes flow*, the drag coefficient may be calculated by equating the general drag equation to the Stokes solution,

$$\frac{1}{2} C_D \rho U_o^2 A = 6 \pi \mu_l R U_o$$

where $A = \pi R^2$

so that

$$C_D = 12 \mu_l / \rho U_o R = 24 \mu_l / \rho U_o d, \quad (2.6)$$

where $d = 2R$ is the diameter of the sphere. $Re = \rho U_o d / \mu_l$, based on the sphere diameter, and, therefore, Equation (2.6) yields

$$C_{D,St} = 24 / Re \quad \text{for } Re < 0.2 \quad (2.7)$$

Two thirds of the drag given by the Equation (2.7) arises from skin friction and one third from pressure (form) drag. The corresponding terminal velocity is

$$U_T = 2 g R^2 \Delta\rho / 9 \mu_l = g d^2 \Delta\rho / 18 \mu_l \quad (2.8)$$

Oseen suggested that the Navier-Stokes equation should be linearized by simplifying the non-linear convective acceleration term rather than neglecting this term [2]. Therefore, the drag coefficient formula obtained from his solution has given greater values than the Stokes law values ($C_{D,St}$).

$$C_D = \frac{24}{\text{Re}} \left[1 + \frac{3}{16} \text{Re} \right] \quad (2.9)$$

One of the most important analytic solutions in the study of bubbles was derived independently by Hadamard and Rybczynski [2-7]. A fluid sphere is considered, with its interface assumed to be completely free from surface-active contaminants, so that the interfacial (surface) tension is constant. Their solution gives the following result

$$C_D = \frac{8}{\text{Re}} \left(\frac{2 + 3\kappa}{1 + \kappa} \right) \quad (2.10)$$

where κ is the dynamic viscosity ratio of the bubble and the surrounding fluid (μ_b/μ_l). The terminal velocity of a fluid particle is obtained by equating the total drag to the net buoyancy force, $4\pi R^3 \Delta\rho g / 3$, giving

$$U_T = \frac{2}{3} \frac{g R^2 \Delta\rho}{\mu_l} \left(\frac{1 + \kappa}{2 + 3\kappa} \right) \quad (2.11)$$

For an air bubble ($\kappa \approx 0$), the overall drag coefficient is

$$C_D = \frac{16}{\text{Re}} \quad (2.12)$$

The Hadamard-Rybczynski theory [2] predicts that the terminal velocity of a fluid (gas bubble or liquid drop) sphere should be up to 50% higher than that of a rigid sphere of the same size and density. However, it is commonly observed that small bubbles and drops tend to obey Stokes' law, Equation 2-8, rather than the corresponding Hadamard-Rybczynski result, Equation 2-11. With increasing diameter, there is a sharp increase in bubble velocity towards the Hadamard-Rybczynski value.

Boussinesq obtained an exact solution to the flow equations, analogous to the Hadamard-Rybczynski result but with surface viscosity included [2-4,6,7]. The resulting terminal velocity is

$$U_T = \frac{2}{3} \frac{g R^2 \Delta\rho}{\mu_l} \left[\frac{1 + \kappa + C / \mu_l}{2 + 3\kappa + 3C / \mu_l} \right] \quad (2.13)$$

where C is equal to the surface dilational viscosity divided by 1.5 times the radius. Although Equation (2.13) reduces to Equations (2.11) and (2-8) for $C=0$ and $C= \infty$, respectively, the transition between these results with decreasing radius is in practice much sharper than predicted. A further difficulty with surface viscosity is that it is very difficult to obtain reliable measurements.

Analytic solutions for flow around and transfer from rigid and fluid spheres are effectively limited to $Re < 1$. In the absence of analytic results, sources of information include experimental observations, numerical solutions, and boundary-layer approximations. At intermediate Reynolds numbers when flow is steady and axisymmetric, numerical solutions give more reliable information. Once flow becomes unsteady, complete calculation of the flow field is no longer feasible. Description is then based primarily on experimental results, with additional information from the boundary layer theory. When a fluid sphere exhibits little internal circulation, either because of high κ or because of surface-active contaminants, the external flow is indistinguishable from that around a solid sphere at the same Re .

As for rigid spheres, numerical solutions of the complete Navier-Stokes and transfer equations provide useful quantitative and qualitative information at intermediate Reynolds numbers (typically $Re < 300$) for fluid spheres. More limited success has been achieved with approximate techniques based on Galerkin's method [2]. Boundary layer solutions have also been devised for $Re > 50$. Numerical solutions give the most complete and probably the most reliable results, but Galerkin's method has the advantage of giving analytic expressions. The boundary layer theories also lead to analytic forms for the drag coefficient.

An equation which gives a good fit to numerical predictions of drag on spherical bubbles is:

$$C_D = 14.9 Re^{-0.78} \quad (\kappa \rightarrow 0, Re > 2) \quad (2.14)$$

Moore solved the boundary layer equations analytically, and improved drag estimate as [2,3,4,6,7]

$$C_D = \frac{48}{\text{Re}} \left[1 - \frac{2.21}{\text{Re}^{1/2}} + O(\text{Re}^{-5/6}) \right]. \quad (2.15)$$

The first term reflects the Stokes' solution where the non-linear terms of the Navier-Stokes equation are not considered (which is justifiable for very low Re) and the second term take the non-linear convective terms of the same Navier-Stokes equation. Thus the application for higher Reynolds numbers is possible.

Equations (2.14) and (2.15) are compared with the results of some numerical and experimental studies in Figure 2.4 [2].

All theoretical studies discussed so far has been subjected to the assumptions that the fluid particles (gas bubbles or liquid drops) remain perfectly spherical and that surface-active contaminants play a negligible role. Deformation from a spherical shape tends to increase the drag on a bubble. Likewise, any retardation at the interface leads to an increase in drag. Hence the theories presented above provide lower limits for the drag and upper limits for the internal circulation of fluid particles at intermediate and high Re, just as the Hadamard-Rybczynski solution does at low Re.

In practice, few systems approach the drag coefficient values predicted by the theoretical treatments. Since the theories provide lower limits on drag, it is reasonable to compare their predictions with the lowest available experimental values. From the restrictions noted, these will be systems of (i) low Morton number ($M < 10^{-8}$) and (ii) low surface pressure (i.e., free of surfactants). Figure 2.4 compares selected C_D data on bubbles in very pure mediums with theoretical predictions. The different theoretical approaches are in good agreement with each other and drag is predicted to be less than for rigid spheres. There is reasonable agreement with the experimental results.

Unfortunately there is little quantitative data, e.g., concerning internal and external velocity profiles, with which to test other aspects of the theories. However, the theories are supported by the agreement between the numerical and boundary layer

approaches in their common ranges and by such qualitative features as secondary internal vortices, forward displacement of the internal stagnation ring, delayed boundary layer separation with increasing medium purity, and increasing dimensionless internal fluid velocities with increasing Re .

The difference between the drag coefficients for rigid and fluid spheres becomes considerably wider as Re increases (see Fig. 2.4). Hence the influence of surface-active contaminants can be even more marked at high Re than at low Re .

Unfortunately, accurate experimental data with known surface-active contaminant concentrations do not appear to be available. Thus theories can not be tested except by fitting the surface-active contaminant concentration to match the data [2].

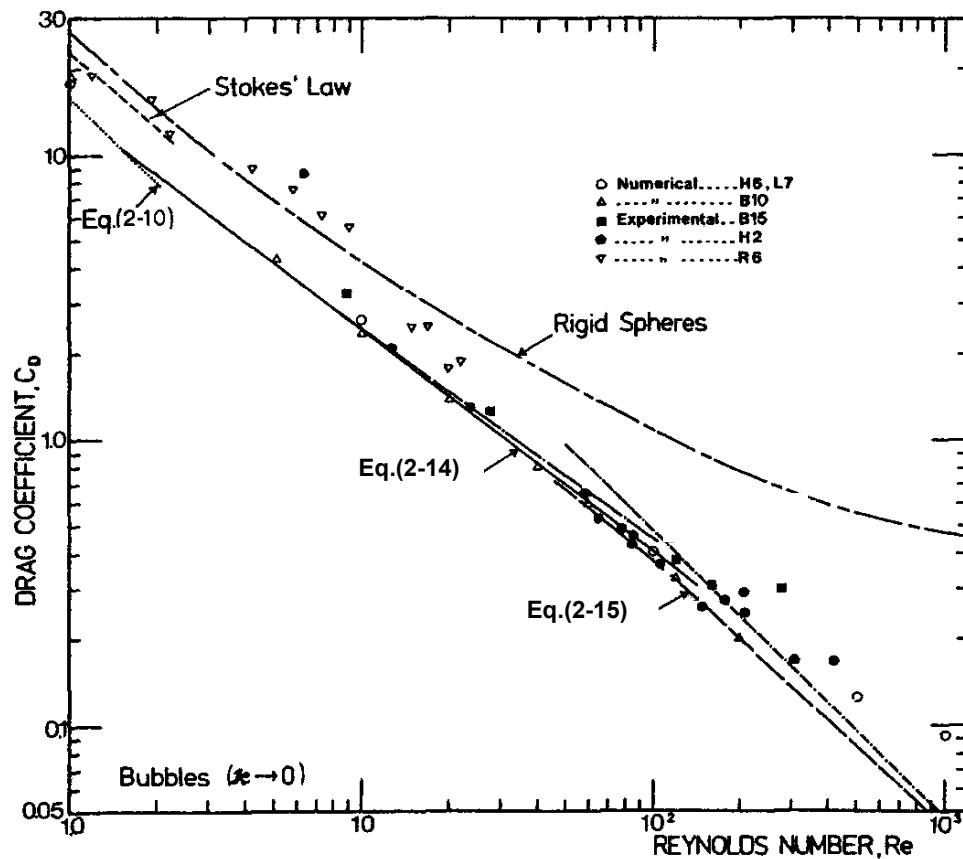


Figure 2.4 Drag coefficients for bubbles in pure mediums: predictions of numerical, Galerkin, and BL theories compared with selected experimental data. [2]

Attempts to obtain theoretical solutions for deformed gas bubbles are very limited in the literature. A simplifying assumption that the bubble is perfectly ellipsoidal was mostly adopted in these solutions. Saffman [2,9] considered flow at the front of a ellipsoidal bubble in spiral or zigzag motion. Results are in fair agreement with experiments. Moore [2-4,10] applied a boundary layer approach to a ellipsoidal bubble. The interface is again assumed to be completely free of contaminants. The drag is given by [2,10]

$$C_D = \frac{48}{\text{Re}} f_1(E) \left[1 + \frac{f_2(E)}{\text{Re}^{1/2}} \right] \quad (2.16)$$

which is similar in character to Equation (2.15).

Harper [2,11] tabulated values of $f_1(E)$ and $f_2(E)$ and plotted drag curves for four values of M . E is the aspect ratio as defined in section 2.1. The curves show minima and are in qualitative agreement with observed $C_D(\text{Re})$ curves for bubbles [12].

2.2.2 Wakes of Deformed Bubble

The formation of an attached wake and the subsequent onset of wake shedding tend to be promoted by increasing oblateness and by the tendency of surface-active contaminants to damp out internal circulation. Experiments have been conducted with dyes added to enable attached wakes and shedding phenomena to be visualized and wake volumes to be measured for bubbles [2]. Since dyes tend to be surface active, the results of these experiments are probably relevant to grossly contaminated mediums. Other tracers have also been used in wake visualization studies. The appearance of an attached wake for impure mediums and the onset of wake shedding occur at Re values of about 20 and 200, respectively, as for rigid spheres, or somewhat lower values (e.g., 5 and 100) if significant deformation has already taken place before these values of Re are achieved.

For carefully purified mediums, interfacial mobility can significantly delay both the formation of an attached eddy and wake shedding, especially for low κ . For example, wake shedding which began at $\text{Re}=200$ for a contaminated medium was

delayed to $Re=800$ for a carefully purified medium of virtually identical properties. Moreover, at a given Re , the wake volume is smaller for pure mediums. Few observations have been reported on wakes of ellipsoidal bubbles at $Re>1000$. Yeheskel and Kehat characterized shedding in this case as random [2]. However, Lindt studied air bubbles in water and distinguished a regular periodic component of drag associated with an open helical vortex wake structure [2].

2.2.3 Secondary Motion

Bubbles and drops of intermediate size show two types of secondary motion:

- i. "Rigid body" type, e.g., rocking from side to side, or following a zigzag or spiral trajectory.
- ii. Shape dilations, usually referred to as "oscillations."

These two types of motion are often superimposed, so that the motion of intermediate size fluid particles can be particularly complex.

While other explanations have been proposed, secondary motions are most plausibly related to wake shedding [2,8]. The onset of oscillations coincides with the onset of wake shedding. For high κ or contaminated drops and bubbles, the onset of oscillations therefore occurs at a Reynolds number of about 200, while for pure mediums at relatively low κ , the onset of oscillations is delayed, but seldom beyond $Re=1000$. In viscous liquids where Re never reaches 200 over the range of practical interest (see Fig. 2.1), no oscillations occur. While a critical Weber number has often been suggested for the onset of oscillations in pure, low κ systems, no agreement has been reached on what the critical value should be, and the value of Re and purity of the medium appear to be better indicators of the likelihood of secondary motion [8].

While wake shedding appears to provide the excitation for shape oscillations, the frequency of the two phenomena may differ. In general, these shape oscillations may be oblate-prolate, oblate-spherical, or oblate-less oblate. Correlations of the amplitude of fluctuation have been given, but these are at best approximate since the amplitude varies erratically as noted above. For low Morton systems, secondary

motion may become marked, leading to what has been described as "random wobbling".

Oscillating bubbles may travel along zigzag or spiral (helical) paths. Some authors have observed only one of these modes while others have observed both. There is some evidence that the type of secondary motion is affected by the mode of release [8]. Saffman [9] performed a careful series of experiments on air bubbles in water. Rectilinear motion was found to become unstable, and gave rise to zigzag motion which in turn gave way to spiral motion for larger bubbles.

The paths followed by gas bubbles under-going secondary motion are no doubt associated with the type of wake [2,8]. Secondary motion plays an important role in increasing drag.

2.2.4 Effect of Surface-Active Contaminants and Internal Circulation

Surface-active contaminants (surfactants) tend to accumulate at the interface between the gas bubble and liquid, thereby reducing the surface tension. When a bubble moves through a liquid medium, adsorbed surfactants are swept to the rear, leaving the frontal region relatively uncontaminated. The concentration gradient results in a tangential gradient of surface tension which in turn causes a tangential stress tending to retard surface motion.

Surfactants play an important role in damping out internal circulation in deformed bubbles, as in spherical fluid particles. The influence of surfactants is most significant for low values of κ , since at large κ the viscous resistance of the internal fluid limits internal motion even for pure mediums. Surface-active contaminants play a particularly important role in high σ systems (e.g., air/water) since surface tension reductions are largest for these systems.

Surface-active contaminants have the greatest influence on terminal velocity near the point of transition from rectilinear to oscillating motion. This is presumably because internal circulation can drastically alter the wake structure of a fluid particle leading to delayed boundary layer separation, smaller wakes, and delayed wake shedding.

No systematic visualization of internal motion in ellipsoidal bubbles has been reported. However, there are indications that deformations tend to decrease internal circulation velocities significantly. No secondary vortex of opposite sense to the prime internal vortex has been observed, even when the external boundary layer was found to separate.

Internal circulation can drastically alter the wake structure of a fluid particle leading to delayed boundary layer separation, smaller wakes, and delayed wake shedding.

Also, the dynamic forces resulting from the internal circulation contribute considerably to deformation.

2.2.5 Experimental Studies for Air Bubbles in Water

An extensive literature survey has shown that there are adequate numbers of experimental studies investigating the air bubble motion in stagnant water conditions. Experimental studies conducted for stagnant water conditions are mostly related to the investigation of bubble velocities, bubble travel paths and wall effect on the bubble velocities.

One of the most important reference documents on this subject is a book prepared by the Cliff, Grace and Weber [2]. This book give a comprehensive critical review of the literature dealing with the dynamics, heat transfer, and mass transfer of single bubbles, drops and solid particles. The information presented in this reference book for gas bubbles is limited to the stagnant water conditions.

Figure 2.5, which was taken from this reference book, shows the experimental data of terminal velocities for air bubbles rising in the stagnant water. It is a compilation of the experimental data for the ellipsoidal regime and adjacent parts of the spherical and spherical-cap regimes. Some of the spread in the experimental data results from surface contamination. For air bubbles in water, κ is so small that there is little viscous resistance to internal circulation, and hence the drag and terminal velocity are sensitive to the presence of surface-active contaminants.

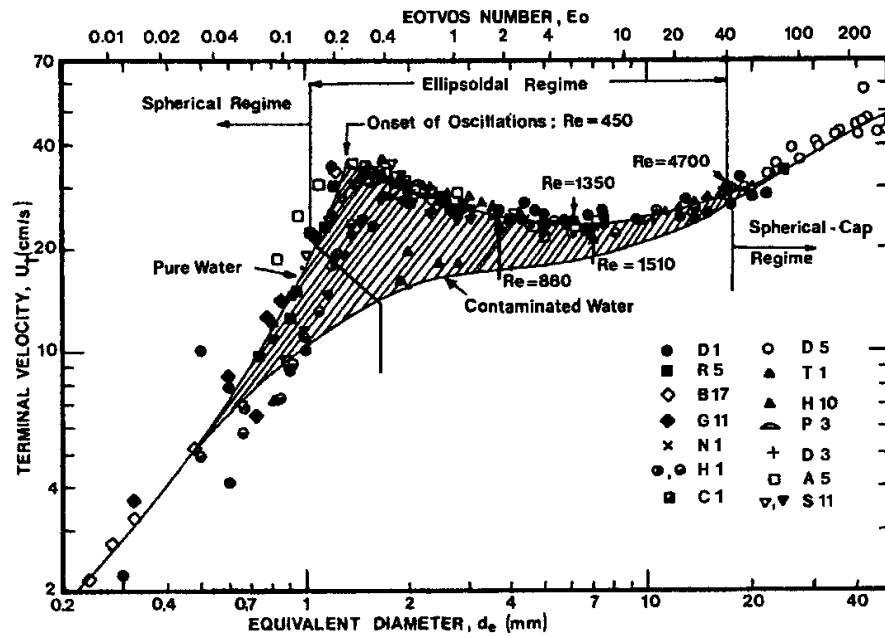


Figure 2.5 The rise velocity of air bubbles in the stagnant water at 20 °C. [2]

The two curves in Figure 2.6 [2] are based on those given by Gaudin for distilled water and for water with surface-active contaminant added. The curves converge for small (spherical) bubbles, since even distilled water tends to contain sufficient surface-active contaminants to prevent circulation in this range, and for large (spherical-cap) bubbles, where surface tension forces cease to be important. Surface-active contaminants affect the rise velocity most strongly in the ellipsoidal range. Drag coefficients corresponding to these two curves appear in Figure 2.6, and show that C_D for bubbles lies below the rigid sphere curve when internal circulation is present, but above if there is no internal circulation and the drag is dominated by deformation.

Specific experimental results, which were used for the comparison of the results of this thesis study for air bubbles rising in stagnant water, are shown in Figures 2.7.a, 2.7.b, 2.8.a, 2.8.b, and 2.9.

Figures 2.7.a and 2.7.b show the results of the studies of Zun and Groselj [13]. They investigated the air bubble rise velocity, the bubble mean lateral

displacement and the mean frequency as functions of bubble diameter in the range of 0.4-6.5 mm for pure and contaminated water, in free rise and agitated-rise conditions. They performed their tests with a 16x16x145 cm glass column filled with water. The bubbles were illuminated from 85 to 115 cm from the bubble generator nozzle to photograph their discrete locations. The bubble equivalent diameter was determined either by measuring the distance that the liquid piston travelled through the horizontal capillary from the pressure chamber or with an MKS flow meter. The other experimental data were obtained from the recorded photographs.

Figures 2.8.a and 2.8.b show the results of Tapucu's study [3]. He conducted an experimental study on bubbles having diameters in the range of 0.83 to 7.11 mm for the stagnant water conditions in tap water. He determined the air bubble rise velocity and drag coefficient, bubble path and shape change as a function of the investigated bubble diameter range. He also investigated the wall effect phenomenon and the effect of the water temperature on the bubble rise velocity.

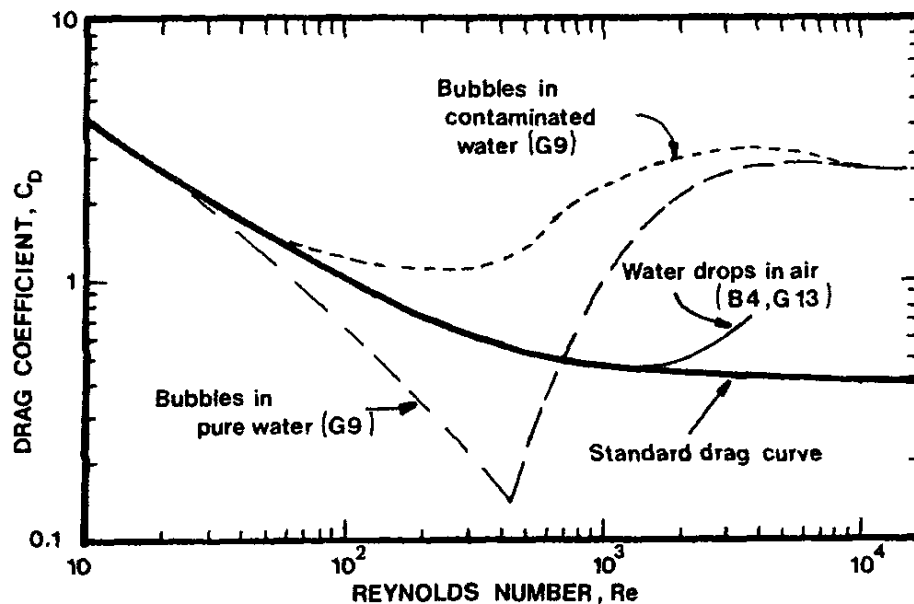


Figure 2.6 Drag coefficient as function of Re for air bubbles in stagnant water (in comparison with the standard drag curve for a sphere). [2]

He performed his tests with a square crystal glass wall tank with dimensions of 17x17x100 cm. He used a new technique that consists of photo tubes, light beams, and an electronic circuit to measure the bubble velocities at different locations of the test-section. The size and the deformation of the bubble were determined by a photographic technique.

However, literature survey has shown that there are only a few experimental studies investigating the air bubble motion for co-current water flow conditions that the direction of the moving bubble and the water flow are upwards.

The first experimental study on the air bubble motion for co-current water flow conditions was performed by Baker and Chao [14]. They investigated the motion of individual air bubbles having diameters in the range of 0.38 to 7.0 mm in tap water flowing turbulently in a 10x10x120 cm conduit by a photographic technique. The turbulent water Reynolds numbers were in a range of 48,600 to 386,000. They determined the bubble velocity and drag coefficient as function of the investigated range of the bubble diameter. Figures 2.10.a and 2.10.b show the results of his study.

The other important experimental study for co-current water flow conditions was conducted by Yavuz [15]. He investigated the effect of co-current water flow on the bubble velocities, drag coefficients and paths for individual bubbles having diameters in the range of 0.97 to 2.72 mm in distilled water. He also investigated the effect of the water temperature on the bubble velocities. The investigated water Reynolds numbers are 15,415 and 21,430. He performed his tests with a 65 cm long cylindrical plexiglas tube having inner radius of 4.75 cm. A square aquarium was fixed on to the test section and filled with water in order to minimize the optical deformation to a negligible level. He used a technique which is similar to the one used by Tapucu [3] to measure bubble velocities. Also, a photographic technique was used to determine the bubble's diameter and path. Figures 2.11.a, 2.11.b, and 2.11.c show the results of his study.

Both experimental studies [14 and 15] have indicated that the bubble average velocity for a certain bubble diameter is higher under co-current flow conditions than that under stagnant water condition and drag coefficient value for a certain

bubble diameter is lower under co-current flow conditions than that under stagnant water condition. The difference from the values of stagnant water condition increases with the increasing flow water. Both studies indicate that the external flow field has an effect on the bubble motion, which is not seen for bubbles moving in the stagnant water.

According to the author's knowledge there is not any experimental study conducted for counter-current water flow conditions that the direction of the moving bubble is upward and the direction of the water flow is downward. In the light of these experimental studies that reported in References 14 and 15, it is necessary to conduct experimental studies also for counter-current water flow conditions.

Other documents and papers [23-52], which were reviewed and benefited, but not directly referred in this dissertation are also given in "References" section.

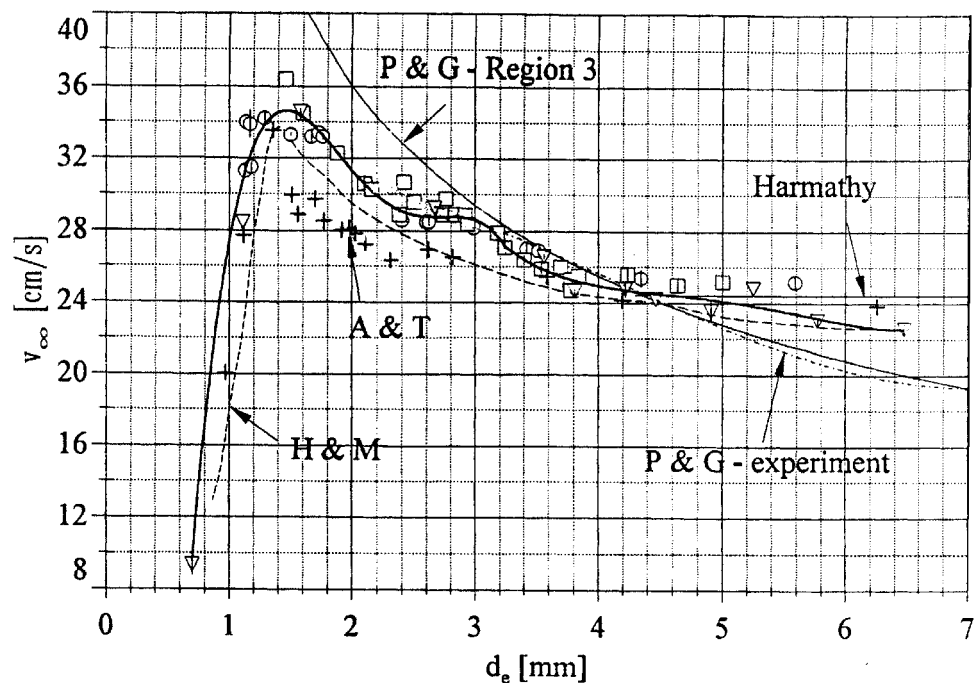


Figure 2.7.a Mean air bubble rise speed in stagnant water. [13]

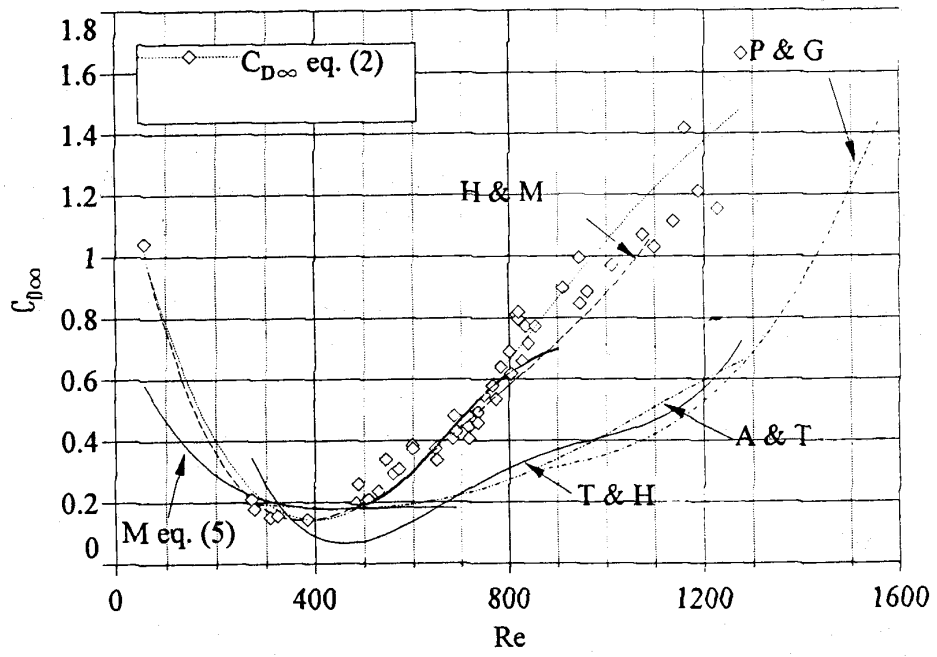


Figure 2.7.b Bubble drag coefficient. [13]

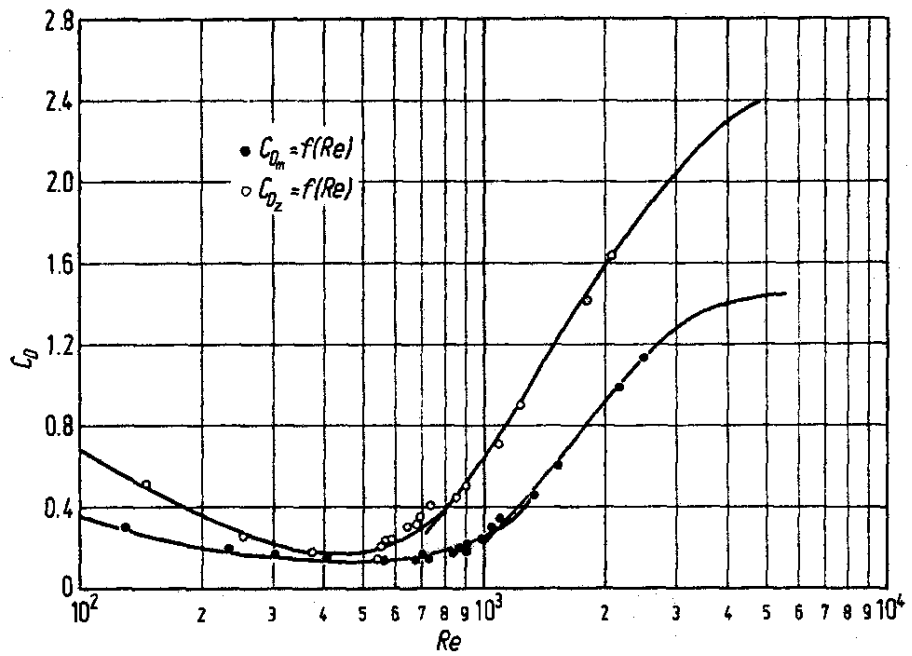


Figure 2.8.a Variation of C_D with Reynolds number. [3]

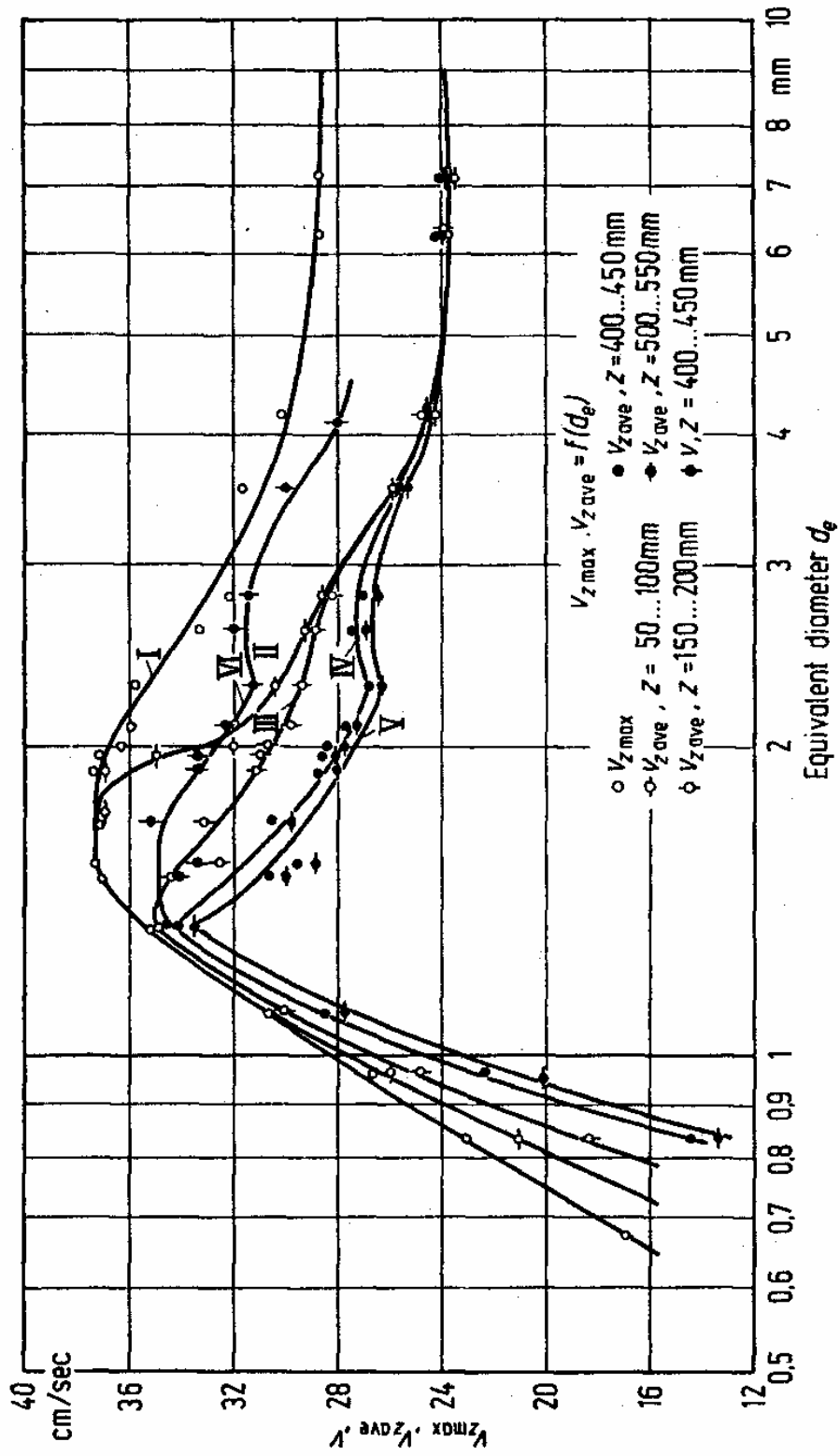


Figure 2.8.b Variation of the bubble maximum and average velocities. [3]

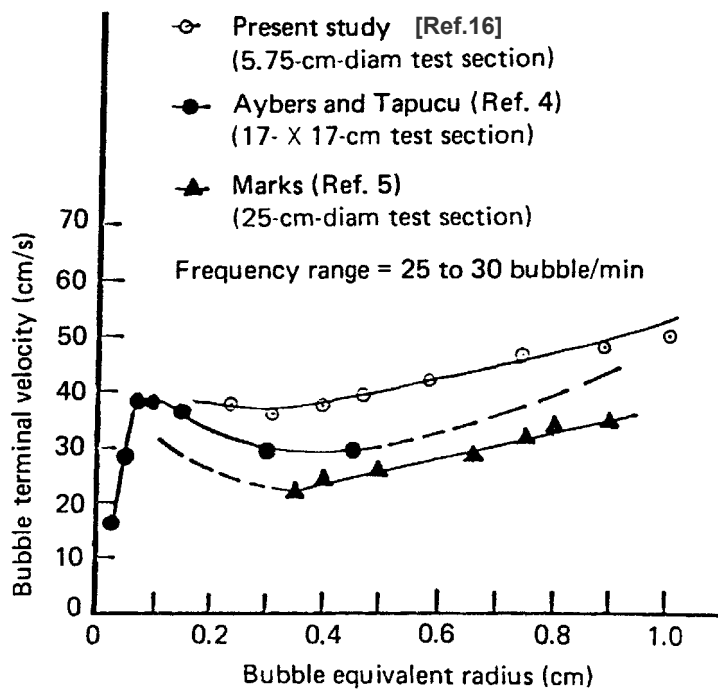


Figure 2.9 Velocities for free-rise conditions in quiescent water. [16]

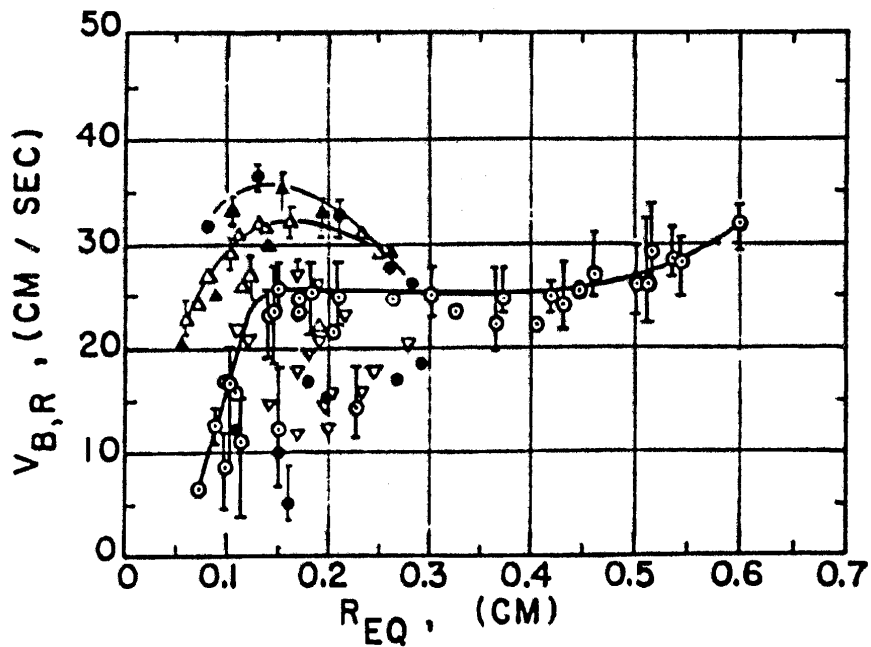


Figure 2.10.a Variation of bubble relative velocity with equivalent radius. [14]

△	D-1	Re _w = 51,500	●	D-4	299,000
⊙	D-2	94,100	▲	D-5	386,000
▽	D-3	131,000			

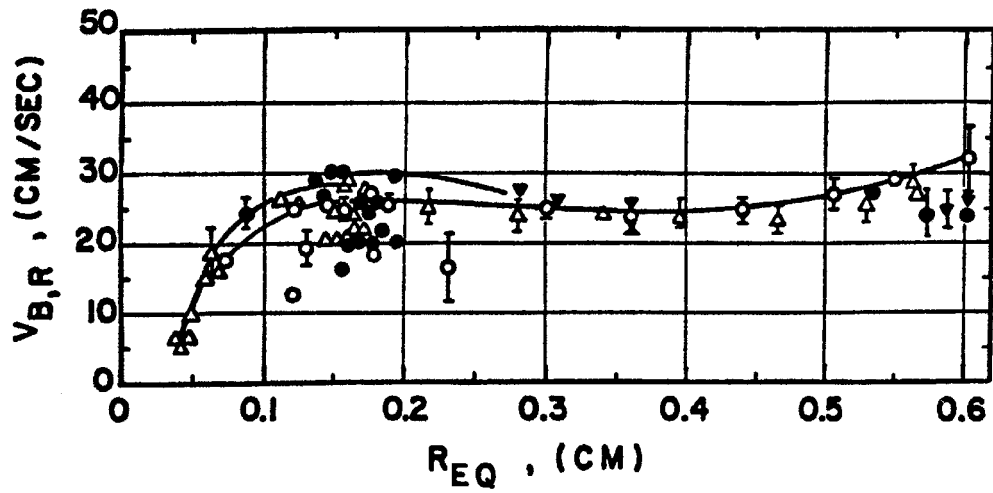


Figure 2.10.b Variation of bubble relative velocity with equivalent radius. [14]

Δ	T-1	$Re_w = 48,600$	∇	T-2*	76,300
\circ	T-2	86,500	\bullet	T-3	124,600

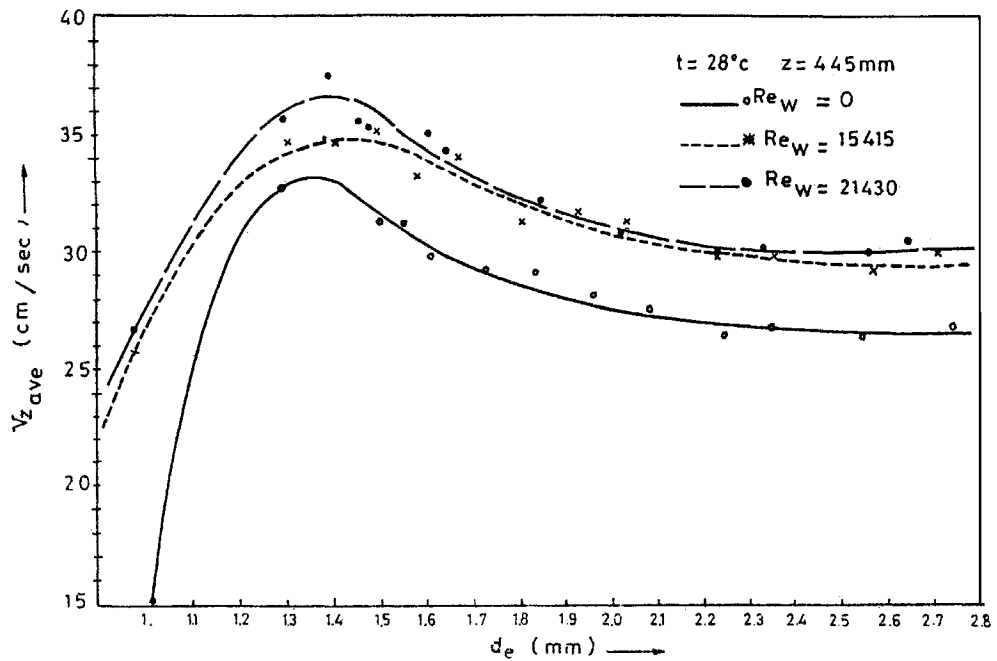


Figure 2.11.a Variation of the average rise velocity with equivalent bubble diameters: for bubbles in co-current water flow. [15]

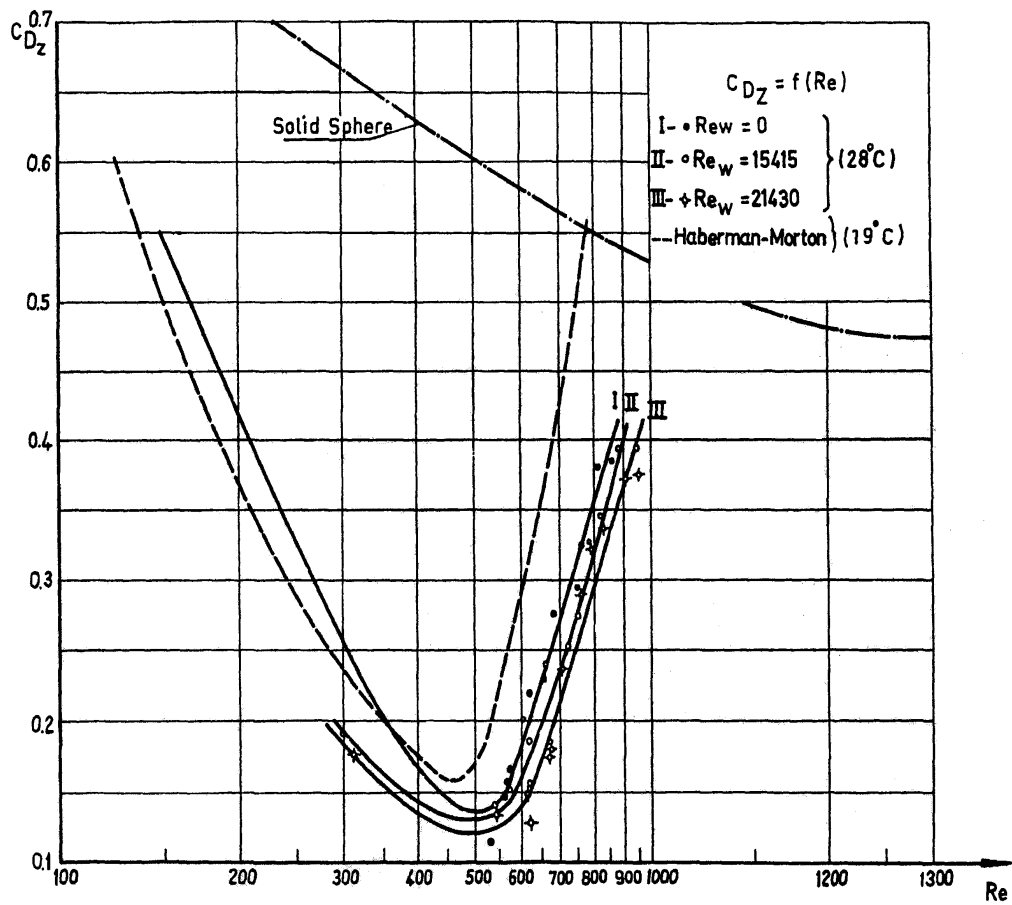


Figure 2.11.b Variation of C_{Dz} with Reynolds number: for bubbles in co-current water flow. [15]

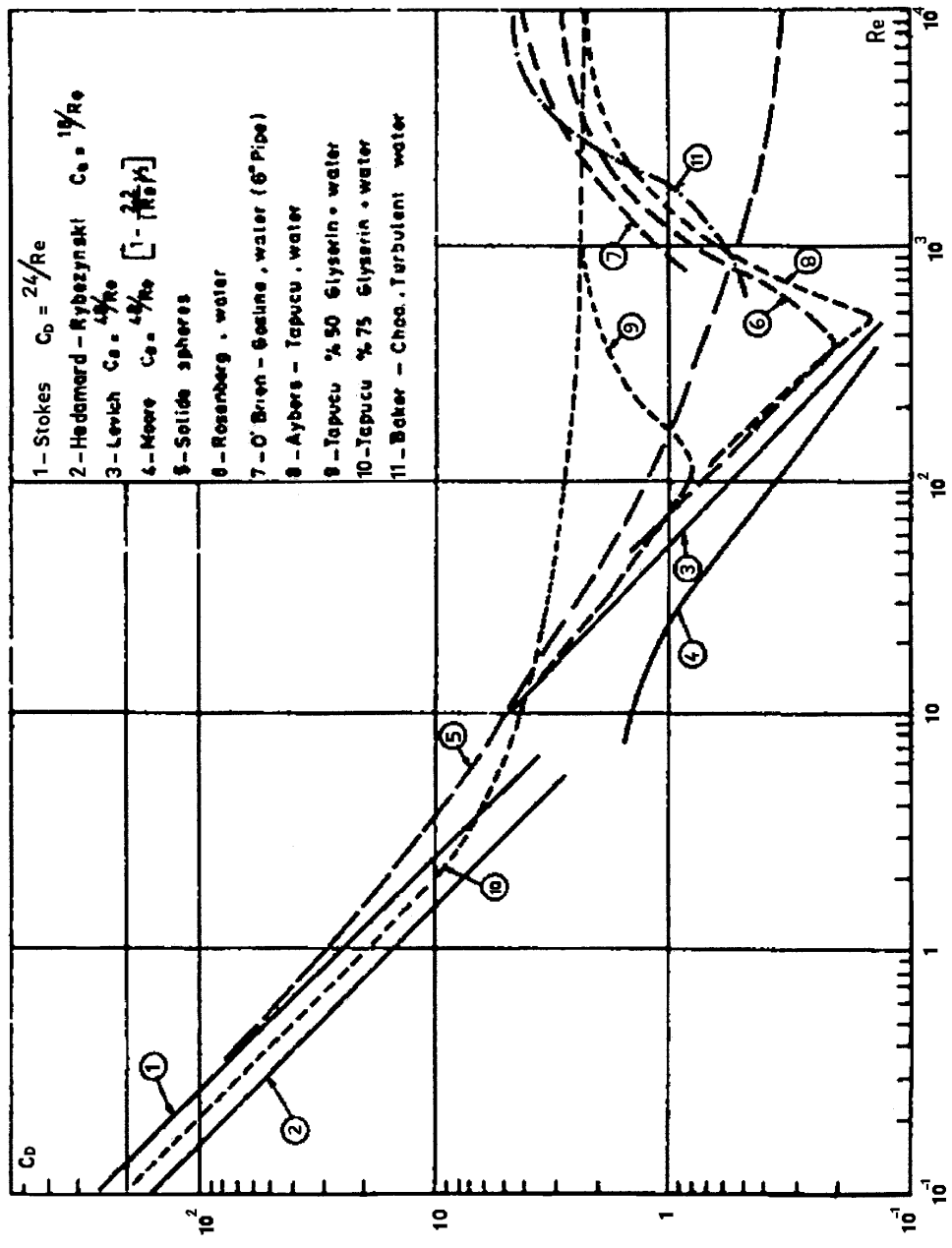


Figure 2.11.c Variation of C_D with Reynolds number. [15]

2.2.6 Simple Analysis of the Motion of an Air Bubble Rising Through Liquid

Consider a spherical air bubble with diameter d_b rising in a linear path through a stagnant liquid from rest. The forces acting on the bubble and governing the motion would be due to drag (F_D) and buoyancy (F_b). Applying the Newton's law, we have

$$\Sigma F = m a = F_b - F_D \quad (2.17)$$

$$F_b = (\rho_l - \rho_b) V_b g \quad (2.18)$$

$$F_D = C_D A \rho_l v^2 / 2 \quad (2.19)$$

$$[\rho_b + (\rho_l/2)] V_b dv/dt = (\rho_l - \rho_b) V_b g - C_D A \rho_l v^2 / 2 \quad (2.20)$$

where V_b is the bubble volume ($\pi d_b^3 / 6$), ρ_b is the bubble density, ρ_l is the liquid density, v is the bubble velocity, g is the gravitational acceleration, C_D is the drag coefficient, and A is the projected area of the bubble ($\pi d_b^2 / 4$).

Equation (2.20) indicates that the bubble, initially at rest, shows an accelerated motion until it reaches a terminal velocity (final velocity), U_T , where the forces acting on the bubble are balanced. When the bubble reaches its terminal velocity, the governing force balance equation (2.20) becomes

$$C_D A \rho_l U_T^2 / 2 = (\rho_l - \rho_b) V_b g \quad (2.21)$$

If the drag coefficient, C_D , is known, the terminal velocity can be calculated from the following equation

$$U_T = [2 (\rho_l - \rho_b) V_b g / C_D A \rho_l]^{1/2} = [4 (\rho_l - \rho_b) d_b g / 3 C_D \rho_l]^{1/2} \quad (2.22)$$

Since $(\rho_l - \rho_b) \approx \rho_l$, Equation (2.22) can be simplified as

$$U_T = \left(\frac{4 g d_b}{3 C_D} \right)^{1/2} \quad (2.23)$$

However, if the terminal velocity of a bubble is known (e.g. measured from an experiment), the drag coefficient can be calculated from the following equation

$$C_D = \frac{4 g d_b}{3 U_T^2} \quad (2.24)$$

For deformed bubbles, it is customary to define an equivalent bubble diameter, d_e , corresponding to the same volume of the observed bubble. Then, Equations (2.20), (2.23) and (2.24) can also be used for any deformed bubble by changing the term d_b with d_e in the equations.

If the surrounding liquid is not stagnant and there is a liquid flow with the known velocity, v_l , Equations (2.20), (2.23) and (2.24) are also valid by changing the velocity terms v and U_T in the equations with v_r and $U_{T,r}$ that are

$$v_r = v_{ob} - v_l \quad \text{and} \quad U_{T,r} = U_{T,ob} - v_l \quad (\text{for co-current liquid flow}) \quad (2.25)$$

$$v_r = v_{ob} + v_l \quad \text{and} \quad U_{T,r} = U_{T,ob} + v_l \quad (\text{for counter-current liquid flow}) \quad (2.26)$$

where v_r and $U_{T,r}$ are bubble relative velocities, v_{ob} and $U_{T,ob}$ are observed or measured bubble velocities.

CHAPTER III

TEST SET-UP AND EXPERIMENT PROCEDURE

3.1 Test Set-up

The design details of the test set-up are shown in Figures 3.1.a and 3.1.b at the end of this chapter.

Distilled water is used in the system and it is stored in a 100 lt. plastic storage tank. There is a supply line at the bottom of this reservoir. It is connected to the pump. The pump is a multistage normal suction, horizontal, high pressure centrifugal pump. The maximum permissible working pressure of the pump is 10 bars and optimum flow rate is 8 m³/h. There is also a by-pass line in order to prevent overpressure of the system. The water flow rate at the test section is adjusted mainly by the exit valve (or outlet valve) for the corresponding water velocities that are 6.5 cm/s, 7.9 cm/s, 10.5 cm/s, 12.9 cm/s, 15.4 cm/s, and 18.2 cm/s ($Re_w = 3477, 4226, 5616, 6900, 8237, \text{ and } 9735$). As it is seen from the Figure 3.1.a, the water pumped through the water supply line enters a buffer tank (see Fig. 3.2) and then it is directed to the transparent test section through a bunch of pipettes assembled in a honeycomb configuration in order to damp down the possible initial flow and pressure disturbances.

The test section gauge pressure is measured by an Omega PX 605-100 GI type pressure transducer from a point 20 cm above the bubble injector location. One of the purposes of the online pressure measurement is to check whether any pressure oscillation exists in the test section. The water flow rate is measured by a turbine flow meter having a five bladed rotor with a permanent magnet integrated into each blade. Both measurements are made online. Output of the flow meter and the pressure transducer are conveyed to a data acquisition system which consists of one multifunctional analog and digital I/O card (PCL-812PG) and two channel

multiplexing daughter boards (PCLD-789D). Each PCLD-789D has 16 differential input channels. Advantech GENIE software is used to read, display and log the measurement data. Advantech GENIE provides an intuitive object oriented graphical use interface that simplifies control strategy and display setups.

Air is supplied to the system from a tank that is connected to an air compressor (see Fig. 3.1.c). There are pressure gages and relief valves at the top of the air tank. The stored air is given to the system with the help of a regulator that adjusts the pressure in the air supply line. Afterwards, air is injected into the test section through the bubble injector after passing through a needle type valve used for the adjustment of the bubble generation frequency. There is a check valve before the needle type valve to prevent water from entering the air supply line.

The main part of the test section is the cylindrical transparent plexiglas pipe enabling the visualization of the bubble motion. Its length, and inner and outer diameters are 170 cm, 4.6 cm and 5 cm, respectively. The distance between the bubble generation point and the exit of the bunch of pipettes is 152 cm. To minimize optical deformations, a plexiglas aquarium (10x10x18 cm) was fixed onto the plexiglas pipe region where the camera shots were taken. It was filled with water.

The design and the manufacturing of the bubble injection section were made to provide proper sealing while enabling to easily change the bubble injector with another one to be able to produce bubbles of different sizes. The detailed design of the bubble injection section is shown in Figure 3.3. Bubble injectors are cylindrical hollow brass pipes of 5.9 mm outer diameter drilled at seven different diameters (1.0-1.8 mm) to generate air bubbles of different sizes. Design details are given in the Figure 3.4.

Other important design parameters of the test set-up are as follows:

- a) The inner diameter of the transparent pipe is 46 mm. To be able satisfy the negligible wall effect conditions ($(d_b / D_h) \leq 0.12$, [2]), the generated bubble diameters should be less than 5.5 mm.

- b) To filter the possible initial flow and pressure disturbances; the water is initially pumped to a cylindrical buffer tank (see Fig. 3.2) and then is directed to the transparent test section through a bunch of pipettes (87 pipettes with 3.6 mm inside diameter and 80 mm length) assembled in a honey comb configuration. Water flow Reynolds numbers in pipettes corresponding to the minimum (6.5 cm/s) and maximum water velocities (18.2 cm/s) in the test section are 512 and 1433, respectively.
- c) The studied range of the water velocities in the test section is 6.5-18.2 cm/s and the corresponding Reynolds numbers for these water velocities is in the range of 3477- 9735. Referring to various fluid mechanics text books for this range of Reynolds numbers and also considering that the water flow exiting from the pipettes to the entrance region of the plexiglas pipe will cause a turbulence at this region due to its behaviour similar to water jets (ratio of the flow areas at the plexiglass pipe section and the pipette section is 1.88), characteristic of the flow is expected to be turbulent.

For turbulent flow conditions, the required length for fully developed flow is:

$$i- L > 0.8 \times D_h \times Re^{1/4} \quad [15]$$

$$L_{max} > 0.8 \times 0.046 \times (9.735)^{1/4} \quad ---- \quad L_{max} > 36.5 \text{ cm} \quad (L/D) = 7.9 ,$$

or

$$ii- L > 1.359 \times D_h \times Re^{1/4} \quad [17]$$

$$L_{max} > 1.359 \times 0.046 \times (9.735)^{1/4} \quad ---- \quad L_{max} > 62 \text{ cm} \quad (L/D) = 13.5$$

Therefore the length of the transparent pipe, 152 cm, is considered as sufficient to satisfy fully developed flow conditions at the observed part of the transparent plexiglas pipe. Therefore, the velocity profile at the core region of the flow is assumed to be flat and value of the water velocity used in the calculation of the bubble relative velocity is assumed to be equal to the value of the average water velocity measured from the calibrated turbine flow meter.

A monochrome camera was used for the visualization of the experiments. Its shutter speed can be adjusted from 1/500 to 1/20000. In practice, it is very difficult to use shutter speeds greater than 1/5000 due to illumination problems.

Camera shots were recorded to computer hard disc by using a capture program and a capture card. For this purpose, a few capture programs were examined, and the software called “Virtual Dub” has given the most satisfactory results. Output of this software is an “avi” file (a kind of video clip). This file is processed by using a photo editor program, called “Adobe Premiere”, to divide them into smaller video clips. Then, desired small clips showing the movement of a single bubble in the range of the camera view area are divided into “tif” type image files (25 frames/sec). By examining those images, the bubble diameter, bubble velocity and characteristics of the bubble motion can be determined.

3.2 Minimization of the Optical Deformations

To be able to minimize the optical deformations, a plexiglas aquarium (10x10x18 cm, see Fig. 3.1.a) was fixed onto the plexiglas pipe region where the camera shots were taken. When a light beam, emitted from a substance inside the cylindrical plexiglas pipe, reaches to an eye which is looking in the direction perpendicular to the surface of the square aquarium, it experiences a linear deviation due to the refraction at the plexiglas pipe wall. The plexiglas pipe, whose inner and outer wall surfaces are parallel, is in the water whose refraction index is very close to the plexiglas material. Linear deviation (δ) of the incoming light beam due refraction at the tube surface is given as [15]

$$\delta = e (1 - (n_1/n_2)) \text{Sin } \theta$$

where

e = plexiglas pipe wall thickness : 2 mm

n_1 = refraction index of the water: 1.33

n_2 = refraction index of the plexiglas pipe: 1.49

θ = angle between the incoming light beam and normal to the plexiglas pipe surface

If it is considered that the camera position corresponds to the mid point of the vertical axis of the aquarium, bubbles are generated at the middle of the plexiglass pipe, the camera is 25 cm far from the plexiglass pipe center and the maximum

bubble diameter is about 4.8 mm, the angle between the incoming light beam and normal to the plexiglas pipe will be 5.98° . Hence, linear deviation of the incoming light beam due refraction at the tube surface will be at the negligible level, 0.022 mm. This corresponds a maximum distortion for the investigated bubble diameter range, $\approx 1\%$. The deviation for 3 mm bubble is 0.0138 mm (0.9%). In conclusion, the system minimizes the optical deformations to a negligible level.

3.3 Experiment Procedure

Experiments were conducted for seven different water flow conditions and for bubbles having diameters in the range of 3.0-4.8 mm which are generated from seven different injectors. Water flow rate was adjusted through an exit valve which is at the end of a plastic pipe connected to the plexiglas pipe (see Fig. 3.1.a). By the adjustments of this exit valve within allowable precision, it was observed that the steady state condition could be maintained only at certain water flow rates which corresponds to 6.5 cm/s, 7.9 cm/s, 10.5 cm/s, 12.9 cm/s, 15.4 cm/s, 18.2 cm/s, 19.3 cm/s and 22.5 cm/s water flow velocities. Corresponding Reynolds numbers for those water flow velocities are 3477, 4226, 5616, 6900, 8237, 9735, 10323, and 12035, respectively. For the flow conditions with the water velocities higher than 18.2 cm/s, it was observed that bubbles began to move in the water flow direction and the bubble generation was out of control. Therefore, the maximum water velocity of 18.2 cm/s was chosen as a limiting condition in all experiment sets.

In order to generate bubbles with various diameters, seven injectors drilled with different diameters were used. In the experiments conducted by using these injectors, bubbles could be generated in diameters approximately between 3 mm and 4.8 mm. The plexiglas pipe has an inner diameter of 4.6 cm and the wall effect is assumed to be negligible for the bubbles with the diameters less than 5.5 mm [2]. As discussed in Chapter II section 2.1, bubbles having diameters less than 4.2 mm keep their spheroid shapes. For greater diameters surface oscillations begin and bubbles get a rather irregular shape for diameters over 4.8 mm. Consequently, it has been decided not to investigate the bubbles having diameters between 4.8 mm and 5.5 mm. Additionally, after analyzing the recorded images, it was seen that

some bubbles having $d_e > 4.5$ mm showed very strong shape oscillations under flowing water conditions and were broken-up into two pieces.

The maximum resolution of the available image capture card is 384x288 pixels. The maximum uncertainty in calculation of the bubble diameter is 1 pixel length that corresponds to ± 0.32 mm. Therefore the maximum error for a bubble with the diameter of 3.0 mm is 11% (see Appendix A). Since a drill with a diameter less than 1 mm was unavailable and the maximum resolution was not good enough for these diameter measurements, bubbles having diameters less than 3 mm were not studied.

Experiments conducted using an injector of a certain size correspond to one experiment set. Briefly, experiments were conducted as follows:

- i. an injector was chosen and mounted in the experimental set-up,
- ii. before operating the pump, the tank water temperature and “ph” were measured,
- iii. the pump was operated while the exit valve was closed and bypass valves were half-open,
- iv. the system was operated for 15 minutes after evacuation of air from the system through the degassing valves (see Fig. 3.2) and the exit valve was opened little bit,
- v. the tank water temperature was re-measured,
- vi. water velocity were adjusted through the exit valve. After ensuring steady state flow conditions by waiting 2-3 minutes, bubbles were tried to be produced with a definite frequency,
- vii. 2-5 video clips with a length of 5-10 seconds were recorded for each flow condition, by using a system consisting of a monochrome camera, a video capture card and “Virtual Dub” software,
- viii. after the recording was accomplished for a certain water flow rate condition, steps “vi-viii” were repeated for the next water flow rate condition. That process continued until all water flow conditions

corresponding to 6.5 cm/s, 7.9 cm/s, 10.5 cm/s, 12.9 cm/s, 15.4 cm/s and 18.2 cm/s water velocities were examined. An experiment set was completed by maintaining stagnant water condition after closing the exit valve and directing the water flow to the water tank through a bypass line, and then by repeating the steps “vi-viii”.

- ix. the temperature of water in the tank was re-measured at the middle and the end of each experiment set.

Based on the information given in previous studies [2,3,13,15], the bubble generation frequency was chosen less than 60 bubbles/min in order to avoid the interference occurring between consecutive bubbles having distances less than a certain value.

There was no problem adjusting the bubble generation frequency during experiments conducted for stagnant water conditions. Also, it was observed that diameters of the bubbles generated from the same injector are almost the same. On the other hand, control of the bubble generation frequency was usually difficult under flowing water conditions. And also, it was observed that bubbles were generated with different diameters from the same injector under the same water flow rate condition due to the external water flow effect.

The flow meter was calibrated before the beginning of each experiment set. For this purpose, 5 samples were taken for each steady state water flow condition. In each sampling, the water discharged through the exit valve was collected into a container for 60 seconds by using a three-way valve and it was weighed. Calibration values were taken as the average of these 5 samplings.

3.4 The Error Arising from Flow-meter Calibration and the Tank Water Temperature Change

Since the valve is opened and closed manually, the plausible maximum timing error may be assumed to be 1 second. The sampling time is 60 sec. Therefore, the plausible maximum error in the water flow rate measurement is $\pm 1.7\%$ ($\pm 1/60$).

In the same sampling group, the maximum difference between the smallest and the biggest value was about 1.5%. Since calibration was made according to average values, the error is expected to be probably less than 1%. The temperature of water inside the tank was measured at the beginning, at the middle and at the end of each experiment set. The temperature rise from the beginning to the end of an experiment is mostly about 3°C. Because the temperature rise of approximately 2°C occurs during the first 10-15 minutes, the system is operated for about 15 minutes before starting each experiment set. In this case, the temperature rise observed between the beginning and the end of an experiment was usually remained under 2°C, generally about 1°C. Because the experiment sets were performed at different times, the measured average water temperatures were different for each experiment set. The average measured water temperatures for the experiment sets were respectively as follows; 25.6°C, 26.3°C, 26.5°C, 26.8°C, 28.2°C, 27.1°C, 27.7°C and 27.0°C. For those 8 experiment sets the average temperature is 26.9°C. So, the physical properties of water such as viscosity and density are taken at 26.9°C. Due to this assumption, the maximum error for the temperature range 25.0-30.0°C is $\pm 0.1\%$. If it is considered that uncertainties arise from the other measurements are $\pm 1\%$ or more (see Appendix A), this error can be assumed as negligible.

The other important point is the effect of water temperature on the bubble velocity. Previous experimental studies [3,5,15] on this subject indicate that 5°C change of water temperature cause about 1 cm/sec change in the velocity of a bubble. When all experiment sets are considered, the maximum tank water temperature difference between its maximum and minimum is 2.6°C. This difference will cause a maximum error of less than 0.5 m/sec ($\approx 2\%$) in the bubble velocity measurements. On the other hand, the common temperature difference of 1.0°C will cause an error of less than 0.2 m/s ($\approx 0.8\%$) in the bubble velocity measurements.

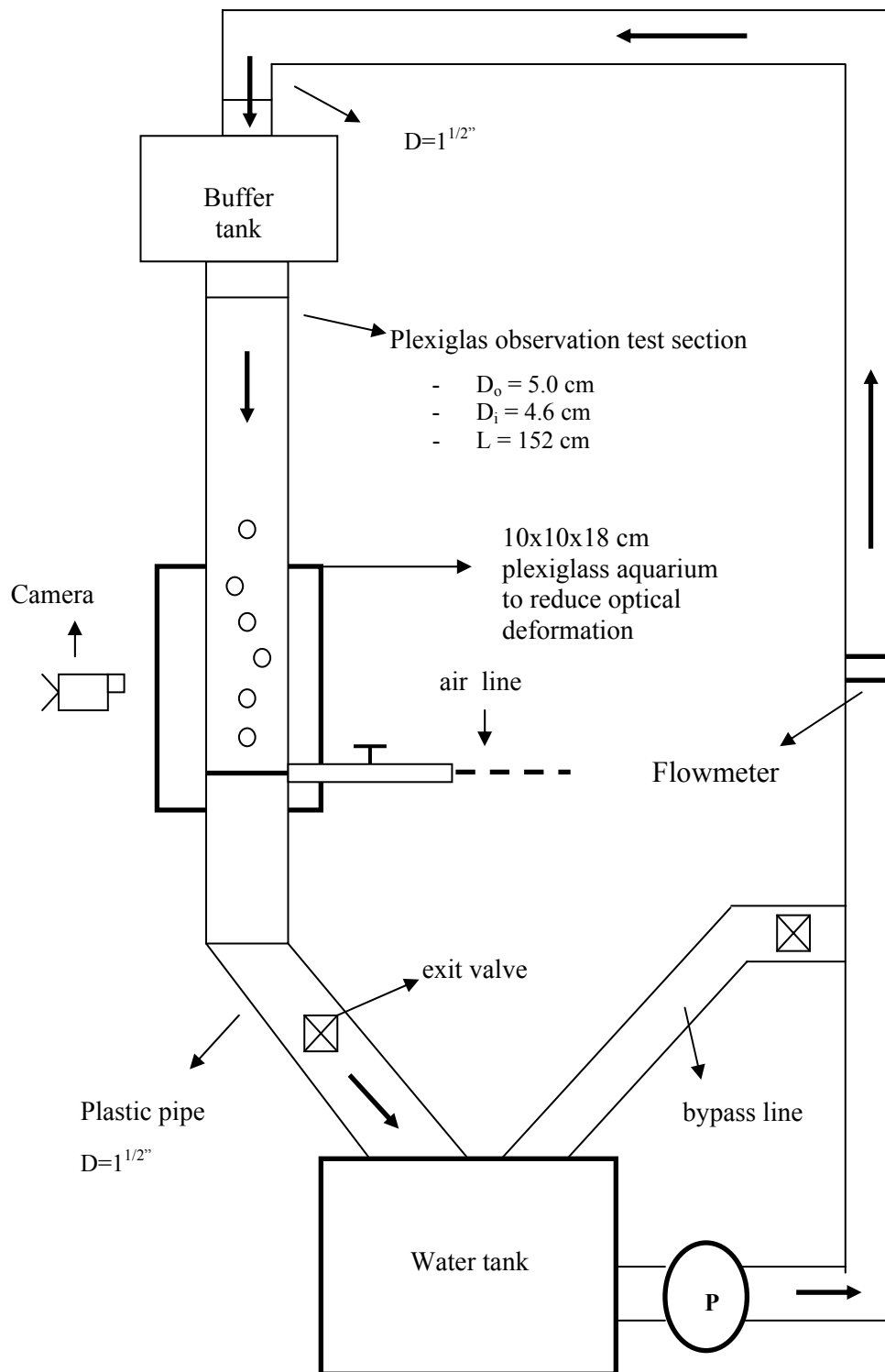


Figure 3.1.a Test Set-up

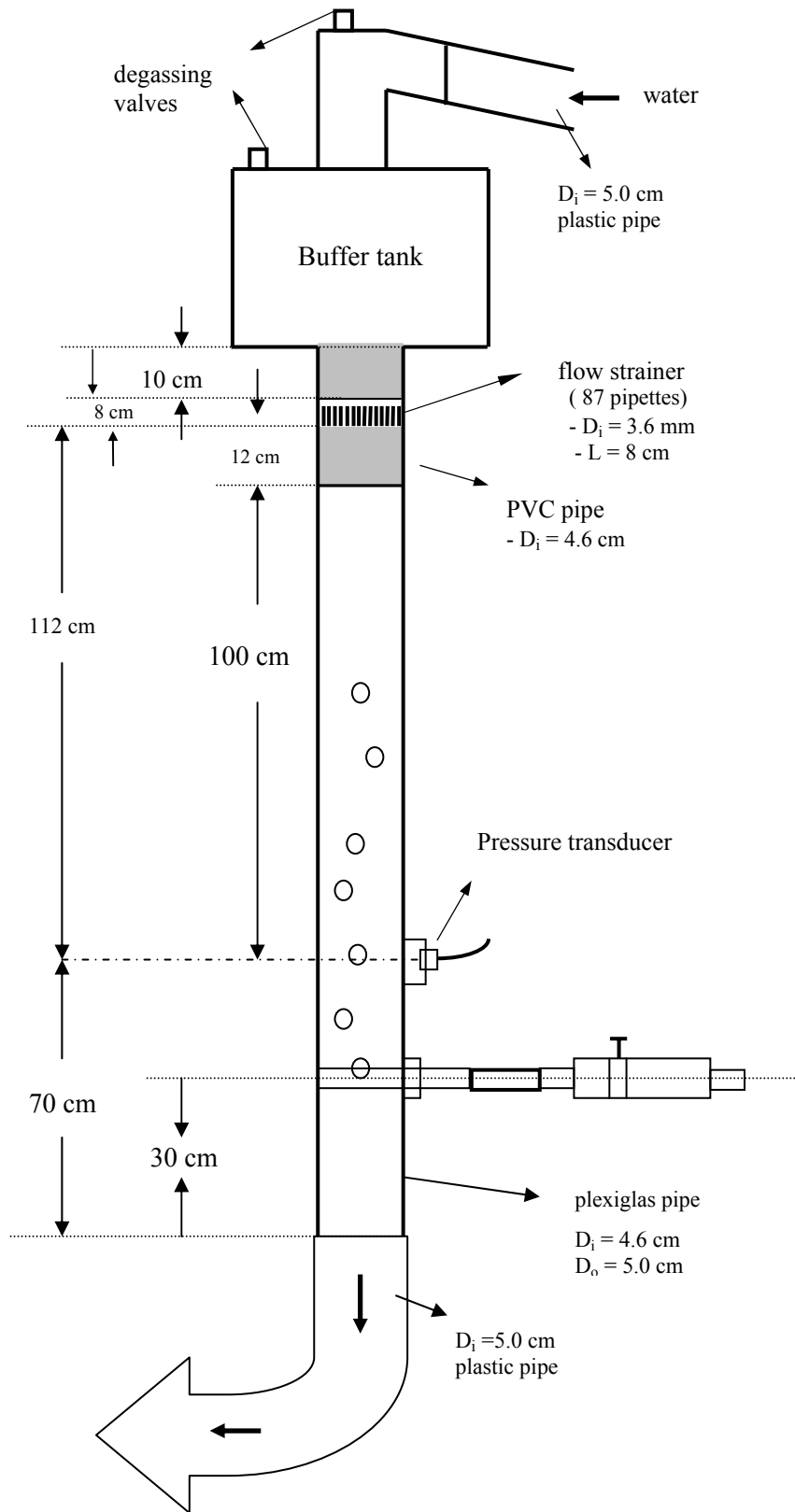


Figure 3.1.b Test Section

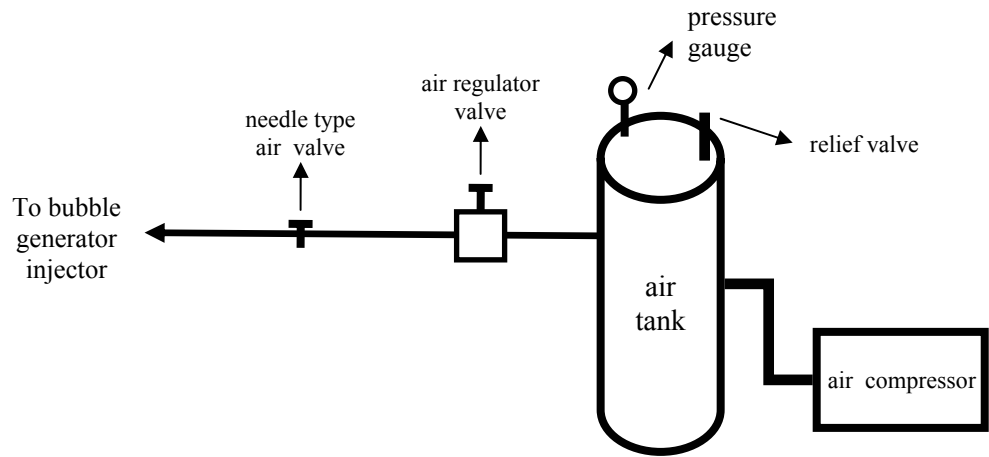


Figure 3.1.c Air line

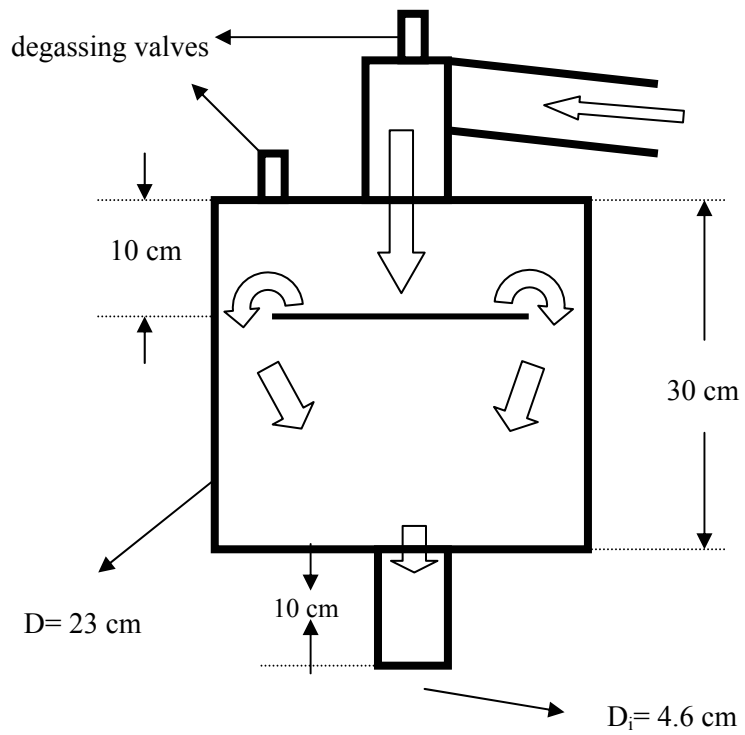


Figure 3.2 Buffer tank

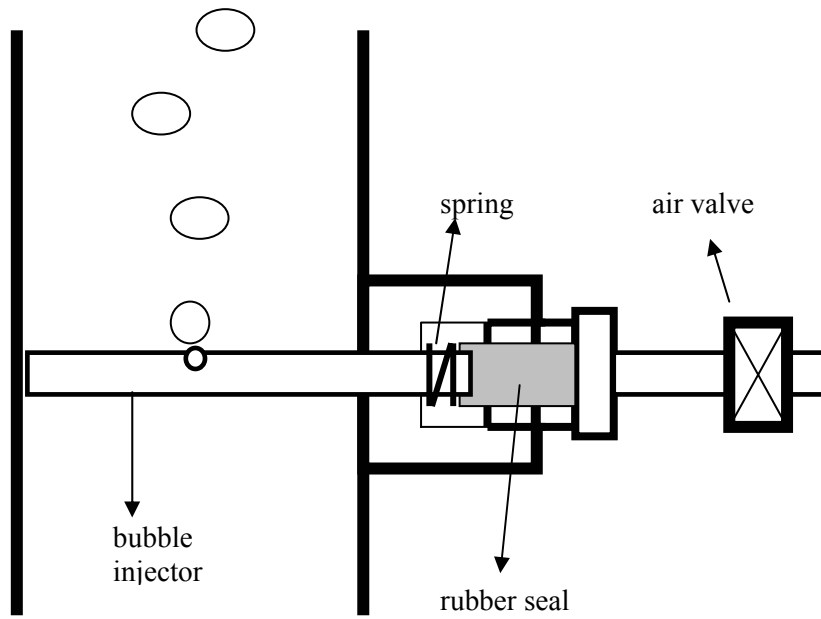


Figure 3.3 The bubble injection section

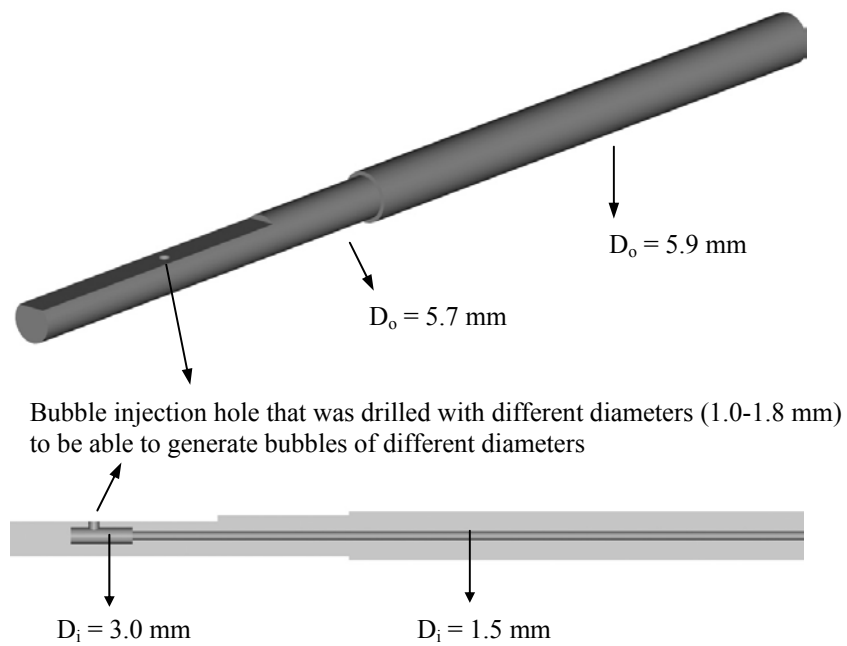


Figure 3.4 Design of the brass bubble injectors

CHAPTER IV

ACQUISITION AND PROCESS OF THE EXPERIMENTAL DATA

The process performed from the acquisition of the raw experimental data to the formation of the final data is as follows:

- Motion of an air bubble is recorded to PC hard disc as an “avi” type video file by using a monochrome camera having 1/5000 shutter speed, a capture card and “Virtual Dub” software. The recording frequency is 25 frames/s and the recording resolution is 384x288 pixels. Those are the maximum limits of the system. Since the velocity of an air bubble is about 25 cm/s, the distortion of the bubble shape image due to shutter speed will be 0.05 mm (see Appendix A). Since this distortion is almost the same for images from which the bubble location is determined, the uncertainty of the bubble travel distance measurement can be disregarded.

Since the bubble velocity attained when the bubble has just detached from the injector surface is less than 2.5 cm/s, the maximum uncertainty in the bubble diameter measurement due to this image distortion is 0.005 mm (see Appendix A), and can be neglected. Therefore, the shutter speed of the camera can be considered as adequate for the purpose of this thesis study.

“Virtual Dub” software has a control mechanism that gives a warning message when recording of a frame is skipped. The time difference between two consecutive recorded images is 1/25 s. This feature is also confirmed by taking a 10 second record of a working chronometer and checking the time difference between two consecutive recorded chronometer images.

- “avi” type video files are divided into “tif” type images that constitute the video file by using “Adobe Premiere” software. The software creates 25 images per 1 second long record.

- Those ".tif" type images, which are showing the motion of a bubble throughout the first 10 cm distance, are grouped under the directory having a label unique to this bubble.

- Images of each group are extensively investigated by using "Paint Shop Pro" software. At first, it is checked whether the group includes an image showing the instant that bubble is mature and just about to detach from the injector surface. Since the bubble is extremely deformed after detaching from the injector surface, an image showing the instant that the bubble is just about to detach from the injector surface is necessary for accurate measurement of bubble diameter. If a group doesn't include this image, it is considered as useless and hence it is discarded from the process. Bubble groups, which include this image, are considered as suitable for the process.

- For a bubble considered as suitable for the process, its diameter is measured in kind of "pixel" from this image. The location of the bubble shown in each image of the group is also determined in kind of "pixel" as it is seen from the Figure 4.1.

In the second step; axial position of this bubble seen from each frame is recorded into a table having the label of the bubble. These are called ".raw data tables".

- A tape meter is attached to the pipe wall as shown in the Figure 4.1 to be able to determine the length of 1 pixel. After the length of 1 pixel (0.32 mm) is determined from the image, the data in the raw data tables are converted in kind of "cm".

- Now, all necessary data can be produced from these new tables which are giving the bubble diameter and bubble locations in kind of "cm". At first, taking into account that the time difference between two consecutive images is 1/25 second, the data tables giving bubble velocity versus bubble location and bubble average relative velocities between the distance 5-10 cm ($V_{av,r} = [(10-5)/\text{travel time}] + V_w$) are produced for each bubble.

- Finally, the drag coefficient, Weber number and Eötvös number are calculated from those tables.

In total, 142 ".avi" type files were recorded. Most of them are showing the motion of more than one bubble. Some are showing the motion of only one bubble. About

8700 images were evaluated. 153 image groups out of 393 were discarded due to the reason that they didn't include an image suitable for accurate measurement of the bubble diameter as noted above. The number of suitable image groups was 240. Therefore, experimental results are based on the data obtained for 240 bubbles.

4.1 Measurement of the Bubble Diameter

As seen from the Figures 4.2, 4.3, 4.4 and 4.5, the shapes of bubbles are almost prolate spheroid ($E \approx 1.18$) when they are mature and about to detach from the bubble injector surface.

For deformed bubbles, it is customary to define an equivalent bubble diameter, d_e , corresponding to the same volume of the observed bubble. Because the recorded images are 2-D, the shapes of the bubbles are seen as ellipsoid. Therefore, the equivalent bubble diameter is calculated from the formula given below

$$d_e = (a \times b)^{1/2} \quad (4-1)$$

where "a" is the length of the major axis of the ellipsoid and "b" is the length of the minor axis of the ellipsoid.

As noted above, the maximum resolution of the available image capture system is 384x288 pixels. The maximum uncertainty in calculation of the bubble diameter is 1 pixel length which corresponds to ± 0.32 mm. Therefore, the maximum uncertainty for a bubble with the diameter of 3.0 mm is 11% and the uncertainty for a bubble with the diameter of 4.8 mm is 7% (see Appendix A).

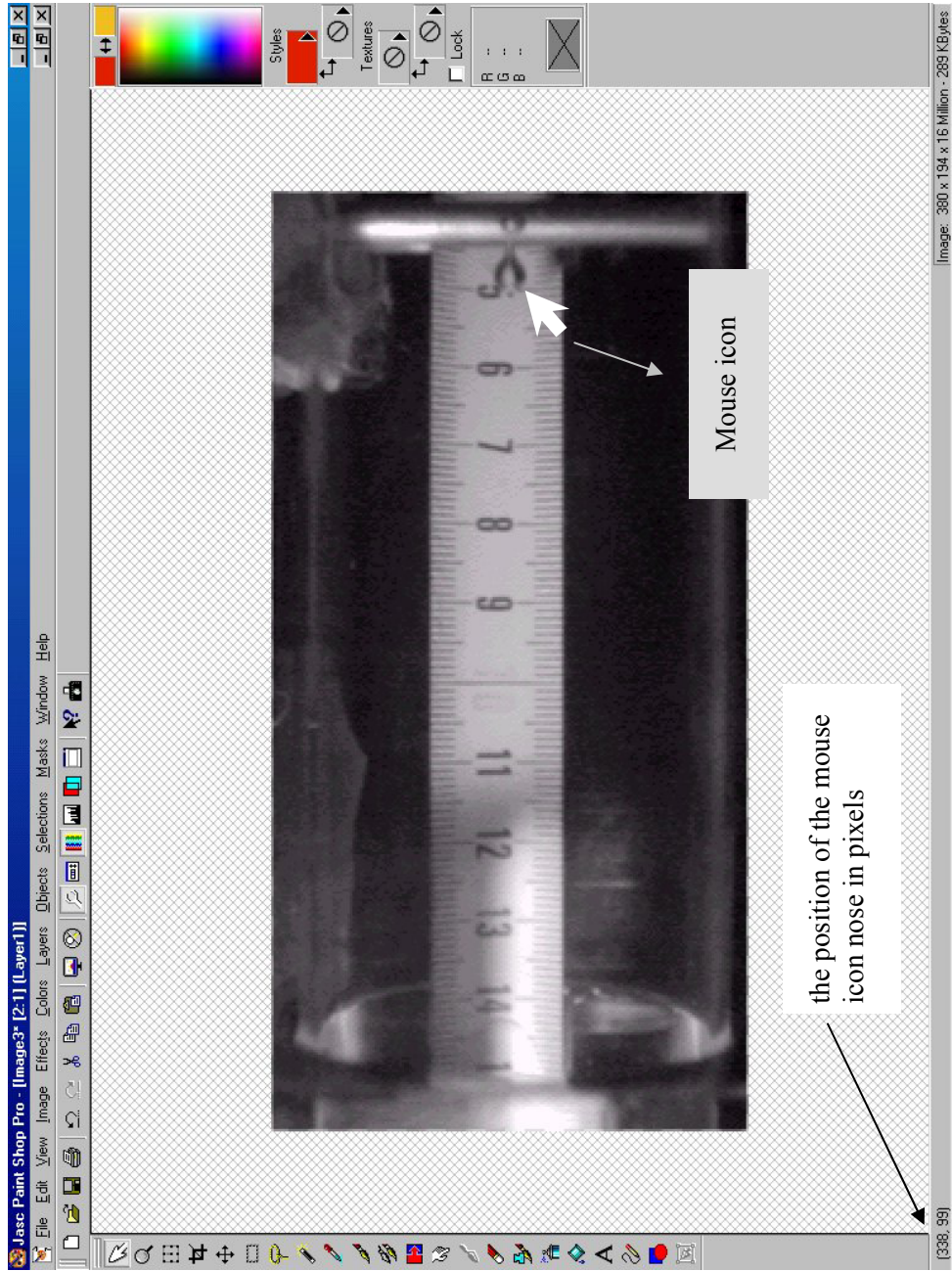


Figure 4.1 Process of the images by using Paint Shop Pro computer program

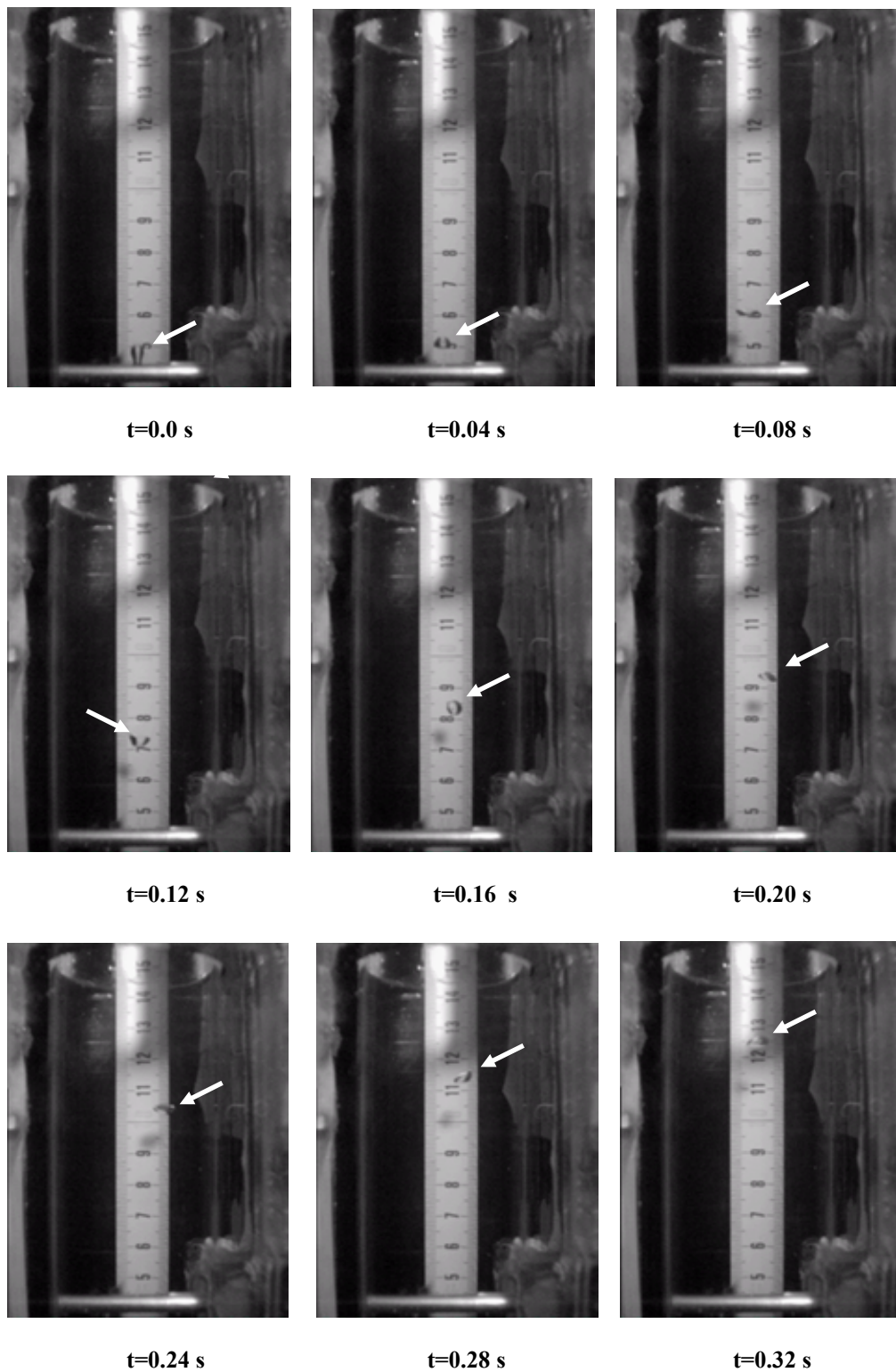


Figure 4.2 Motion of a bubble having 4.60 mm diameter ($V_w = 0.0\text{cm/s}$)

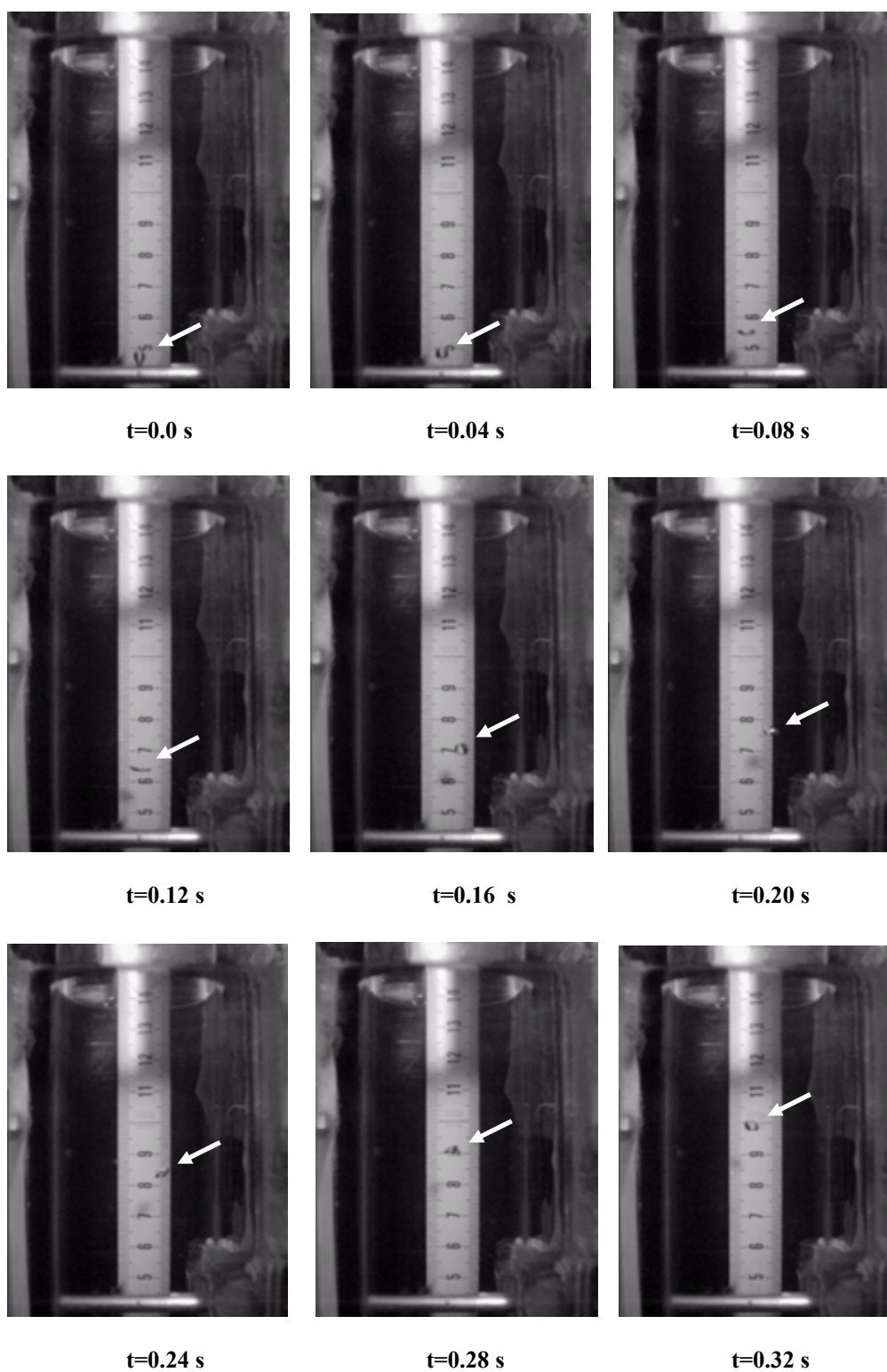


Figure 4.3 Motion of a bubble having 4.30 mm diameter ($V_w = 6.5$ cm/s)

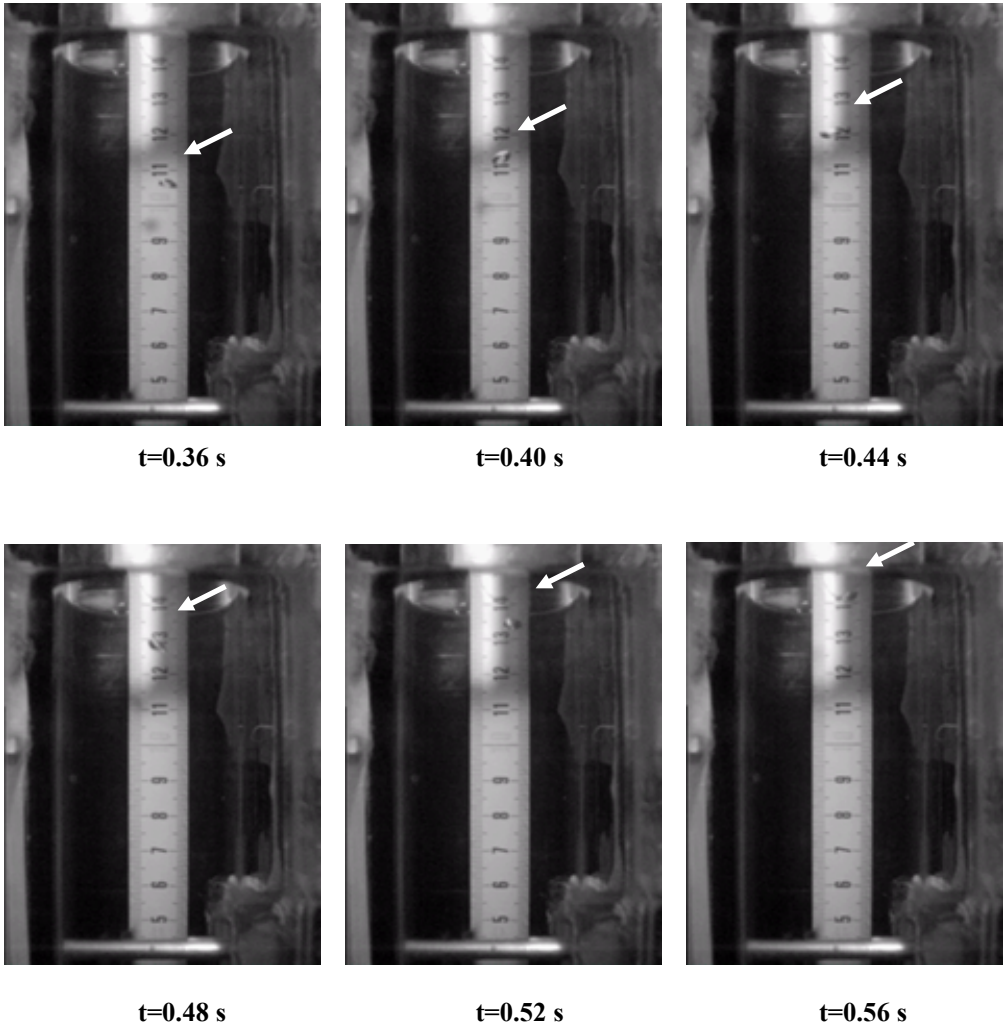


Figure 4.3 (cont.) Motion of a bubble having 4.30 mm diameter ($V_w = 6.5$ cm/s)

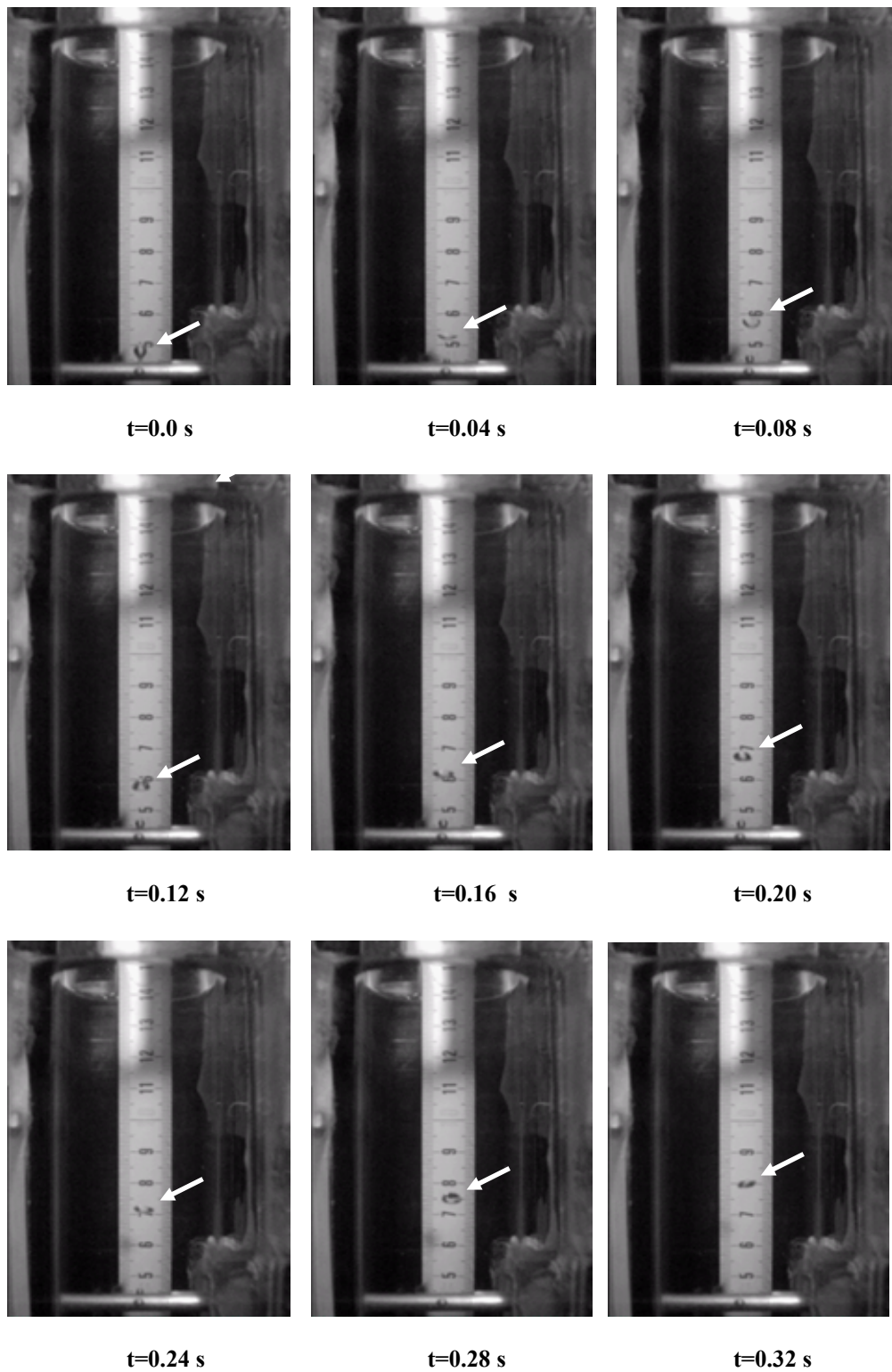


Figure 4.4 Motion of a bubble having 4.53 mm diameter ($V_w = 12.9$ cm/s)

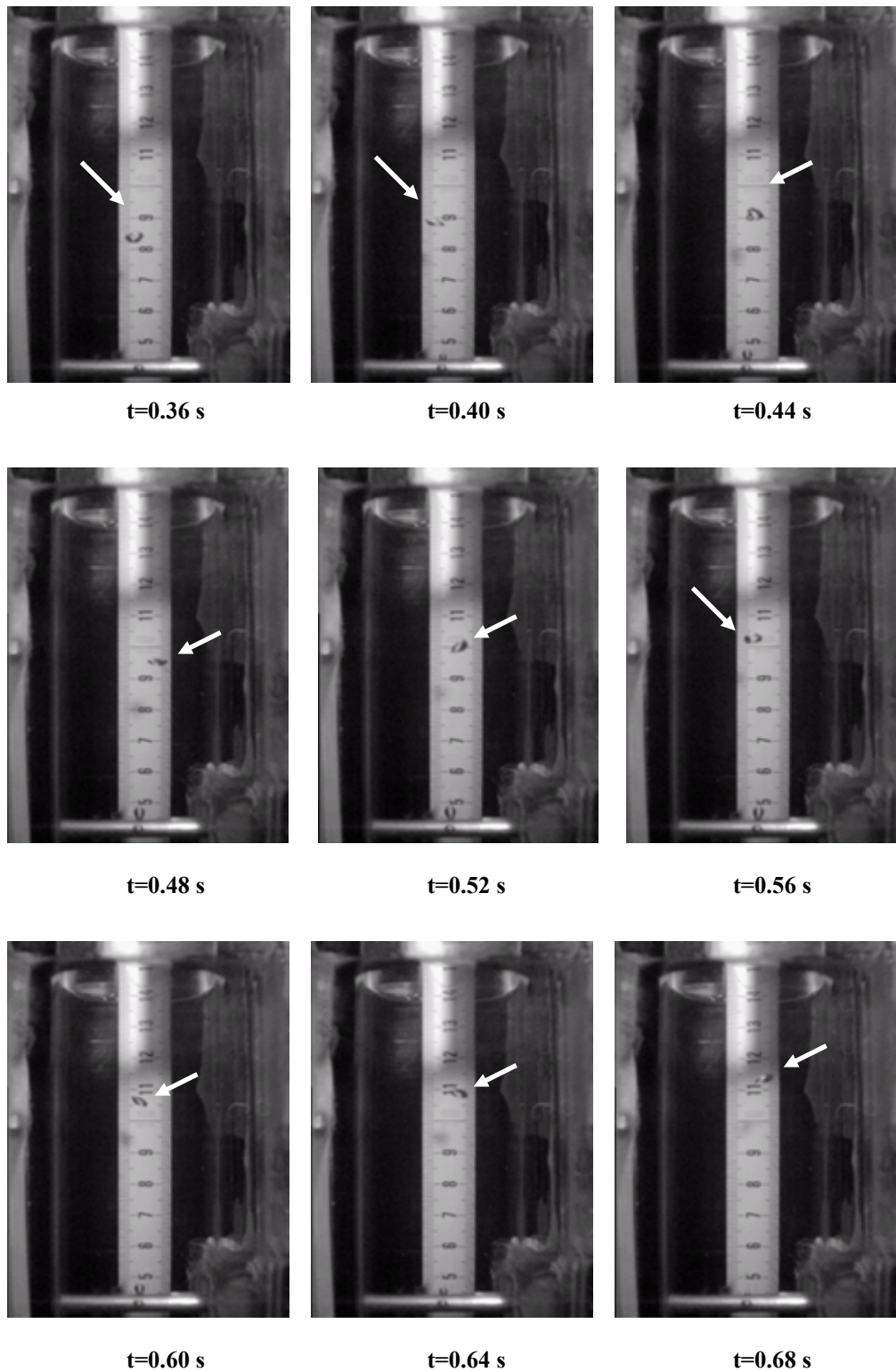


Figure 4.4 (cont.) Motion of a bubble having 4.53 mm diameter ($V_w = 12.9$ cm/s)

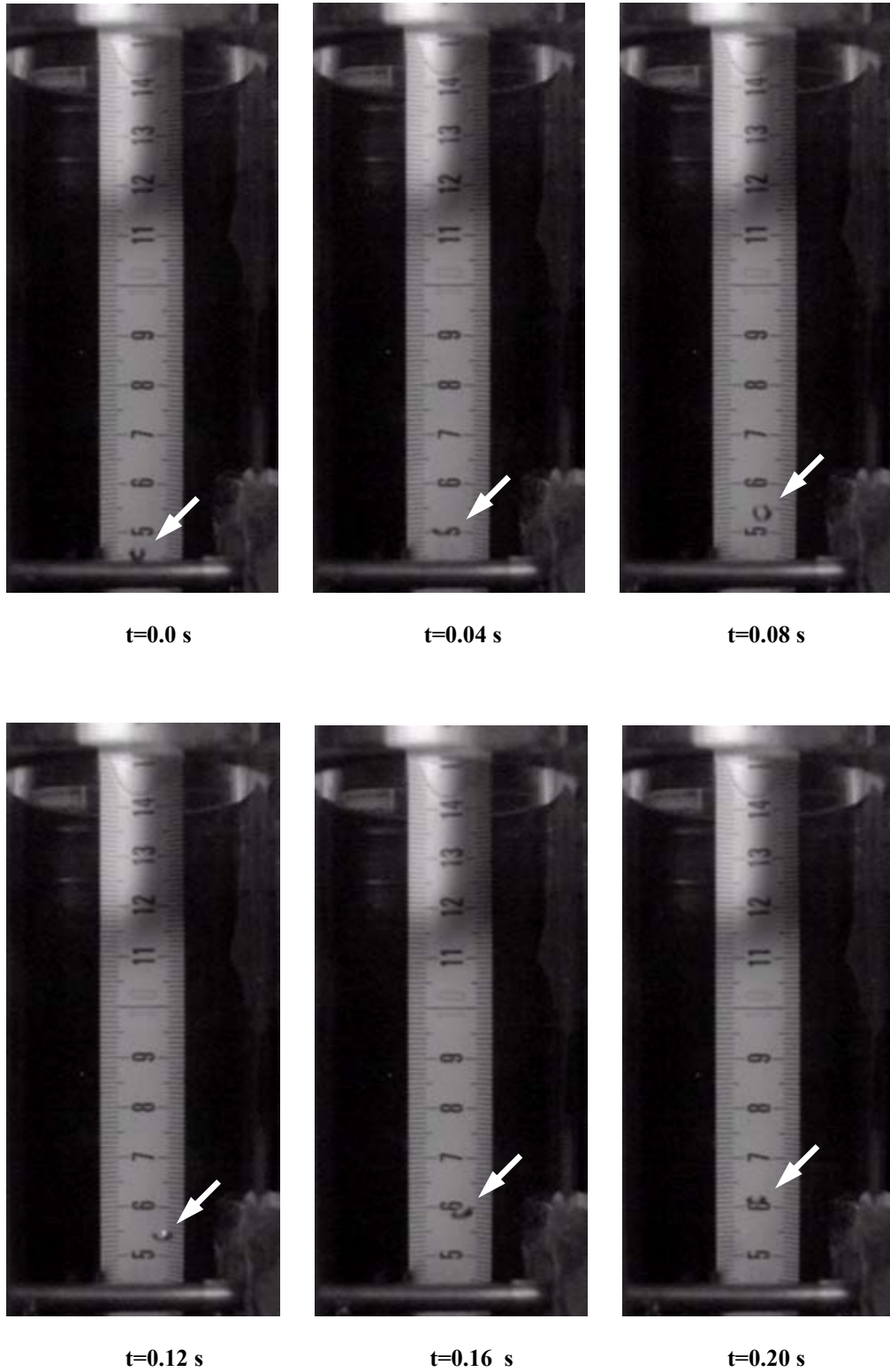
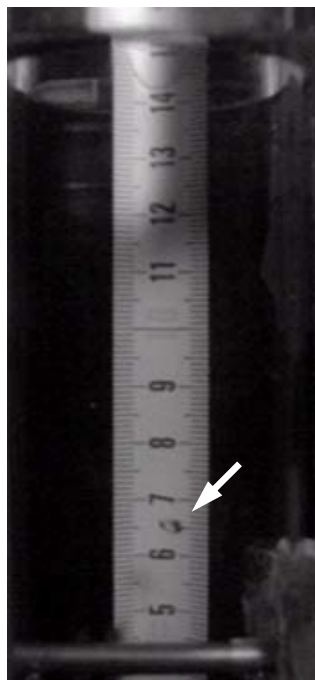
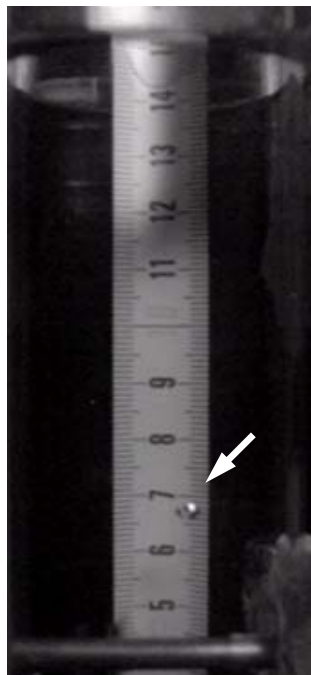


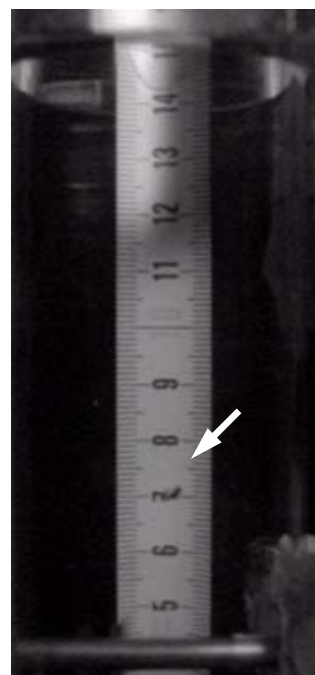
Figure 4.5 Motion of a bubble having 3.28 mm diameter ($V_w = 18.2$ cm/s)



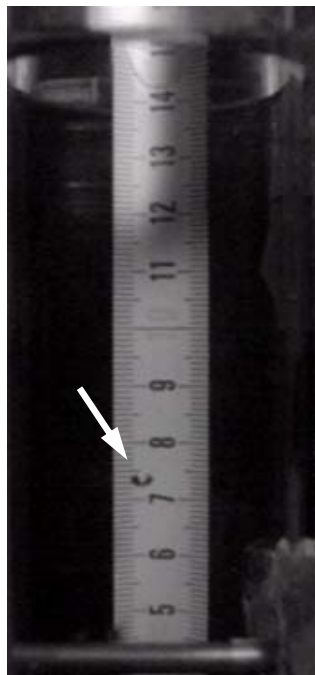
t=0.24 s



t=0.28 s



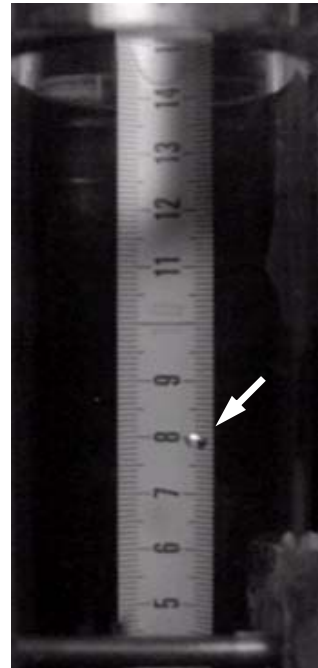
t=0.32 s



t=0.36 s



t=0.40 s



t=0.44 s

Figure 4.5 (cont.) Motion of a bubble having 3.28 mm diameter ($V_w = 18.2$ cm/s)

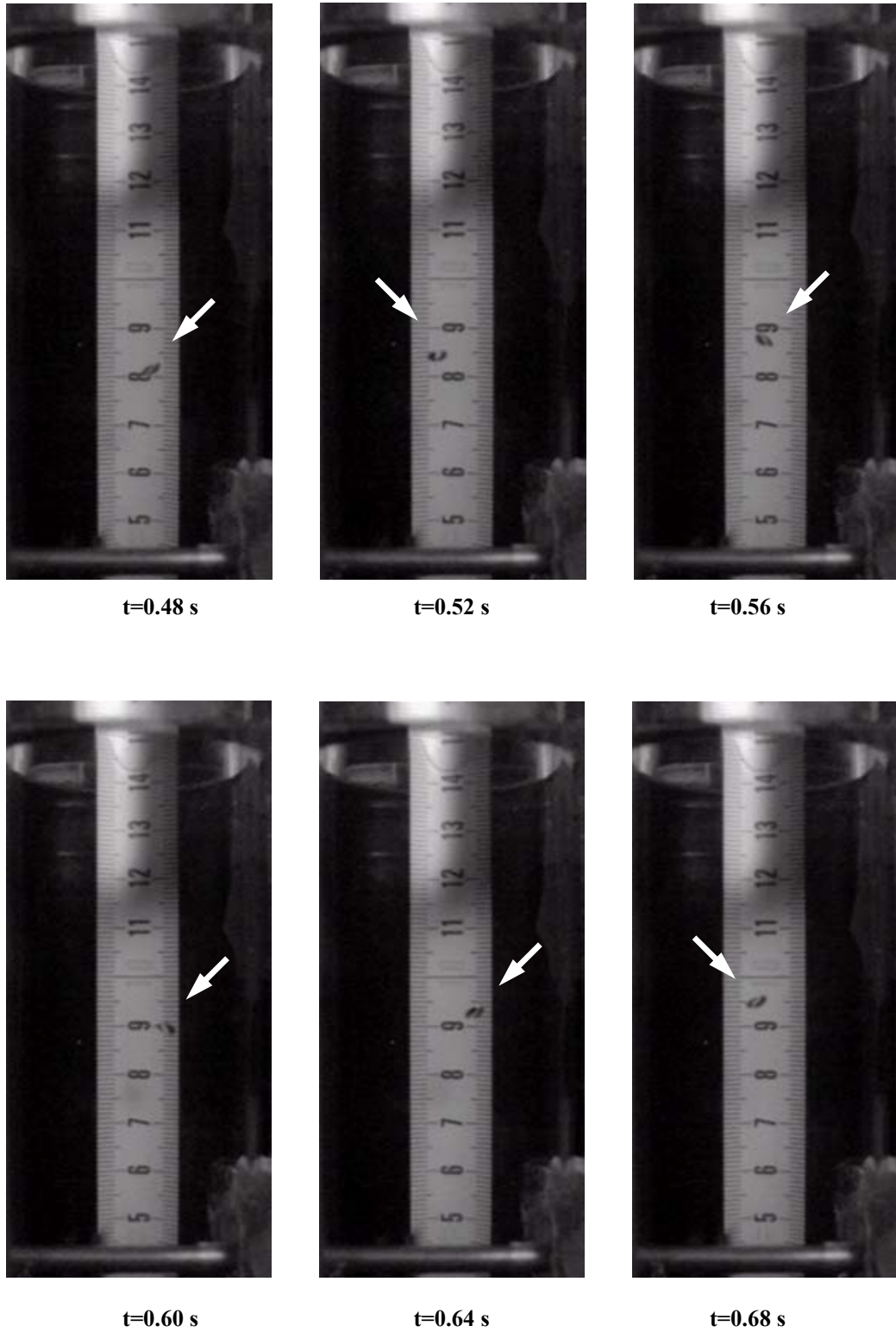
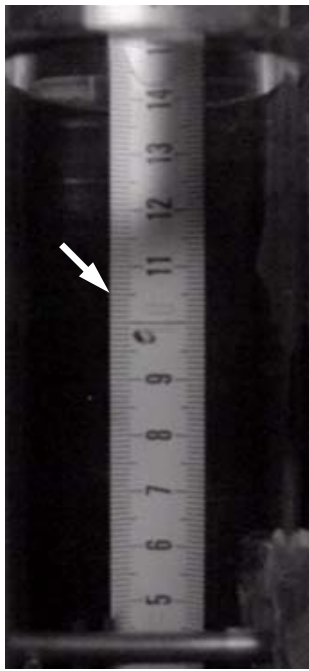
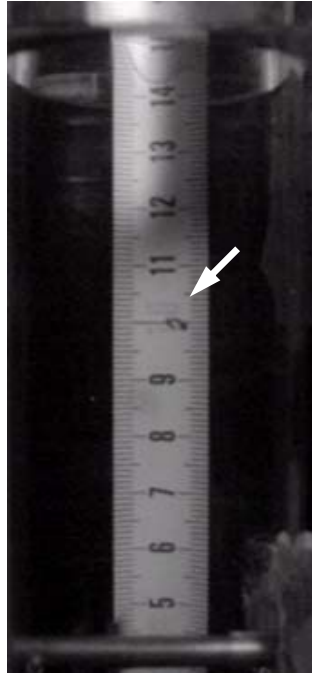


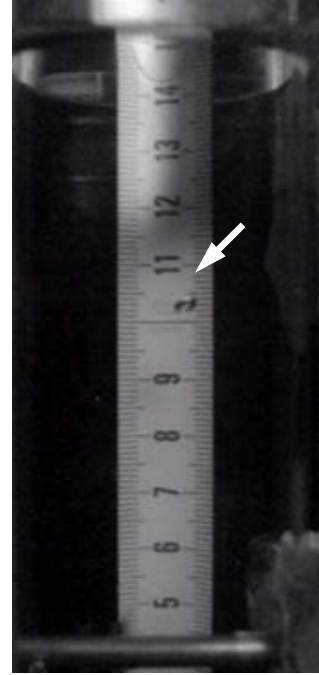
Figure 4.5 (cont.) Motion of a bubble having 3.28 mm diameter ($V_w = 18.2$ cm/s)



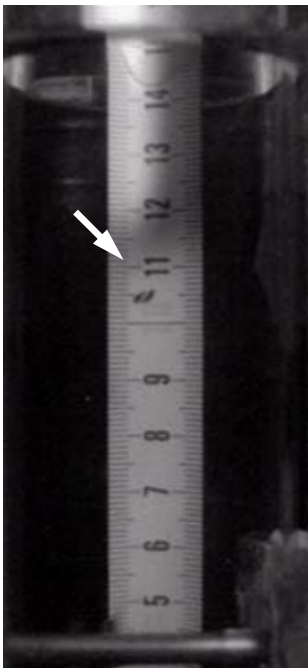
t=0.72 s



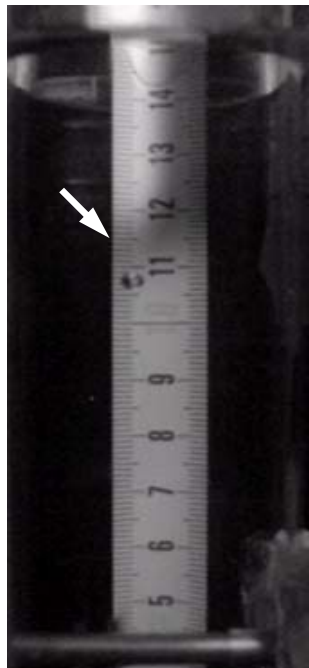
t=0.76 s



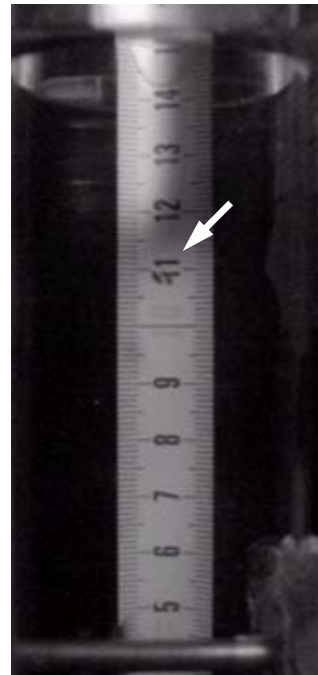
t=0.80 s



t=0.84 s



t=0.88 s



t=0.92 s

Figure 4.5 (cont.) Motion of a bubble having 3.28 mm diameter ($V_w = 18.2$ cm/s)

CHAPTER V

DISCUSSION OF EXPERIMENTAL RESULTS

In this chapter, the experimental results of this thesis study are discussed in detail. In the following sections, results of the study are given in details and compared with the previous experimental results reported in the literature. Also, some observed important phenomena are explained. All figures referred to in this chapter are given at the end of this chapter.

5.1 Bubble Path, Bubble Shape Behavior, Bubble Axial Relative Velocity Change and Effect of the Water Velocity

In the observed bubble diameter range, all bubbles move upward linearly for a few cm after being detached from the bubble injector surface, then show a planer zigzag motion similar to a sinusoidal shape. These observations are in a good consistency with observations given in References 3, 4, 5 and 8 which are investigating the bubble path as a function of air bubble diameter under the stagnant water condition. Figures 4.2, 4.3, 4.4 and 4.5 show the bubble behaviour for some sample bubbles having different diameters and moving under different counter-current water flow conditions ($V_w = 0.0, 6.5, 12.9$ and 18.2 cm/s). As it is seen from these four figures which consist of the images recorded during this thesis study, the shapes of the bubbles are almost prolate spheroid ($E \approx 1.18$) when they are mature and about to detach from the bubble injector surface. Once they detach from the injector surface, the shape begins to be distorted due to the effect of the hydrodynamic pressure force which increases with the increasing bubble velocity. The shape of the bubble becomes like a spherical cap and then oblate spheroid while following a linear path. Then, the bubble follows a zigzag path and begins to change its shape from sphere to disk with irregularly changing orientations or spherical cap. Careful examination

of the recorded images for the stagnant water condition showed that the magnitude of shape oscillations seems to be increasing with the increasing diameter.

Under counter-current water flow conditions, the type of shape oscillations seems to be similar for the entire range of bubble diameters and the bubble shape is wobbling similar to the stagnant water condition. However, during some experiments, some bubbles having $d_e > 4.5$ mm ($E_o \approx 2.7$) showed very strong shape oscillations under counter-current water flow conditions and were broken-up into two pieces.

These observations are generally consistent with References 3, 5 and 8 (see also Fig. 2.1). Since the bubble final average velocities seem to be independent from bubble diameter as shown in Figure 5.1.a, the Weber number, giving the ratio of the hydrodynamic pressure force to the surface tension force, is only a linear function of bubble diameter (see Chapter II section 2.1). On the other hand, the Eötvös number, giving the ratio of the buoyancy force to the surface tension force, is a square function of the bubble diameter. The magnitudes of the forces, which depend on the bubble diameter and act on bubble with a relative velocity of 23 cm/s, are given in Table B.1 and Figure B.1 of Appendix B as an example. Viscous forces are negligible and forces governing the shape are surface tension, buoyancy and hydrodynamic pressure forces (resulting from the drag force). As the bubble diameter increases, the buoyancy and pressure forces, which are trying to distort the shape, increase more rapidly than the surface tension force which is trying to conserve the bubble shape. Because of that reason, shape oscillations increase with the increasing diameter.

Under counter-current water flow conditions, bubble deformation seems to begin in a shorter distance than that for stagnant condition; the higher the water flow rate, the shorter the distance. The hydrodynamic pressure force that the bubble has already been subjected due to water flow while detaching from the injector surface, is probably the cause of this phenomenon.

Figures 5.2, 5.3 and 5.4 show the results of this thesis study and are given for discussion of the bubble relative velocity change in the vertical upward direction and the effect of the water velocity on it. Since the water flow is counter-current,

bubble relative velocity is calculated from the Equation (2.26). These figures give the bubble axial relative velocity as a function of vertical axis position for bubbles having equivalent diameters 3.23 mm, 4.06 mm and 4.63 mm, respectively, which are taken as sample diameters by considering that the investigated bubble diameter range is between 3.0 mm to 4.8 mm. Each data point represents the average of the data obtained from bubbles having the same diameter (see Figs. 5.5, 5.6 and 5.7). The maximum uncertainty due to the limited image resolution for the determination of the vertical position of the bubble is ± 0.032 cm. This uncertainty results in the maximum uncertainty ± 0.8 cm/s for the calculation of the bubble velocity which is an average value between two consecutive frames (see Appendix A).

The phenomena seen from Figures 5.2, 5.3 and 5.4 and their explanation, based on the theoretical information given in the Chapter II section 2.4, are as follows:

(a) Since the buoyancy force is much greater than the drag force [see Eq. (2.20)], the bubble shows an accelerated motion with an increasing bubble velocity during the initial phase of the bubble motion after its detachment from the bubble injector. The increase in the bubble velocity and also the shape deformation cause an increase in the drag force [see Eq. (2.19)], hence the magnitude of the bubble acceleration decreases until it reaches a maximum velocity. The decrease in the slope seen for the initial phase of the bubble motion is the result of this decrease in the acceleration. Thus, the experimental results are in good agreement with the theoretical expectations.

The bubble velocity drops a certain value after passing a maximum velocity value, and then starts to oscillate within a band of 25-30 cm/s for stagnant water flow conditions and of 20-25 cm/s for counter-current water flow conditions. The slope of this band is small and also decreases slightly with the increasing vertical travel distance. Figures 4.2, 4.3, 4.4 and 4.5 show that the bubble initially follows a linear path, then a planer zigzag path. According to References 2 and 8, the cause of this secondary motion mode is wake shedding behind the moving bubble which occurs at Re_b higher than 200.

It is impossible to visualize the wake and its structure behind bubbles by this test set-up. But, the observations from the recorded images have indicated that the

velocity drop coincides with the start of zigzag motion. The bubble velocity oscillation band seems to be proportional to the bubble horizontal displacement width. However, there is no clear indication that horizontal displacement width is dependent on water flow rate. The reason of this bubble velocity drop after passing through a maximum value is the change of bubble path from rectilinear to zigzag. While the bubble velocity vector had one component in the vertical direction during its initial rectilinear motion, with the beginning of the zigzag motion the bubble velocity vector has two components; one in the vertical direction, the other in the horizontal direction. Also, during the zigzag motion, the bubble shows irregular orientations and increased shape oscillations that may contribute to this bubble velocity decrease. The image recording speed is not sufficient to make a detailed analysis of this phenomenon.

On the other hand, observations showed that the length of the linear path seen in the initial phase of the bubble motion decreases with the increasing water flow rate, in other words bubbles reach their maximum velocities in a shorter distance. It can be explained as: when the bubble is detaching from the injector surface under counter-current water flow conditions, the bubble relative velocity is not zero (equals to the water velocity) and hence it has already been subject to a drag force prior to the start of its motion in contrast to the stagnant water condition. Therefore, either the bubble shape deformation or the wake shedding that causes the secondary motion begins in a shorter distance.

There is only one experimental study [3] found in the literature which gives data of bubble velocity change with vertical distance and enables to make a comparison of results of this thesis study for stagnant water condition. Figures 5.8, 5.9 and 5.10 are taken from the study of Tapucu [3]. Tapucu investigated the air bubbles with diameters of 0.83-7.1 mm rising in stagnant water. In this reference study, bubble velocities are measured throughout very small intervals (≈ 5 mm) by using a mobile electronic system. Unfortunately, there is no other such data, showing the bubble velocity behavior as a function of the traveled vertical distance, of previous experimental studies conducted for co-current water flow conditions or stagnant water condition. Bubble velocity behavior in Figures 5.8, 5.9 and 5.10 show

similarity with the results of this thesis study (Figs. 5.2, 5.3, 5.4, 5.5 and 5.7). The difference between bubble velocity values of these two studies is probably due to the effect of surface contaminants (see Figs.2.5 and 2.6 of Chapter II). While distilled water was used in this thesis study, Tapucu conducted his experiments with tap water. Surface contaminants tend to decrease bubble velocities as explained in Chapter II sections 2.2.4 and 2.2.5.

(b) Figures 5.5 and 5.7 give the results of this thesis for repeated experiments of bubbles having diameters 4.0 mm and 4.14 mm and for the stagnant water condition. The bubble velocity drops to a certain value after passing a maximum value, then begin to oscillate within a band of 25-30 cm/s, along the initial vertical distance between 5 cm to 10 cm. The slope of the band is small and decreases slightly with the increasing distance. Figure 5.10 (as well as Figs.5.8 and 5.9) shows that the bubble velocity drops to a certain value after passing a maximum value, then begins to oscillate within a band of 23-26 cm/s along the initial vertical distance between 5 cm to 10 cm. Between the vertical distance 10 cm to 12 cm, the oscillation band narrows to the value of 0.3 cm/s (24.5 cm/s-24.2 cm/s) with a slightly decreasing slope. After the distance of 12 cm, the bubble velocity remains almost constant at the value of 24.3 cm/s. Figure 5.10 (as well as Figs. 5.8 and 5.9) shows that the bubble velocity behavior is similar to that seen in Figures 5.5 and 5.7.

There are two important points that can be concluded from the experimental results of Reference 3, given in Figures 5.8, 5.9, 5.10 and Figure 2.8.b:

- i. the bubble terminal velocity values are approximately equal to the average value of the velocities measured between the initial travel distance 5 cm to 10 cm,
- ii. the distance in which the bubble terminal velocity is reached decreases with the increasing bubble diameter.

The bubble velocity measurements in this reference study [3] were conducted with a mobile electronic system that enables measurements throughout a long distance. But the measurement technique used in this thesis study is based on images

recorded by a camera. The recordings were taken for the first 10 cm distance. The recordable bubble vertical travel length can only be increased by increasing the camera's field of view. It can be attained by increasing the distance between the camera and the test section. Unfortunately, further increase in distance between the camera and the test section causes poor quality in the recorded image which leads to higher uncertainties for the bubble diameter measurements. The accuracies of the bubble velocity and bubble diameter measurements are both of the same importance. With the available recording equipment, when the accuracy of the measurement for one of them is increased, the accuracy of the measurement for the other is considerably decreased. So, an optimization is necessary. Therefore, the camera position was adjusted in order to take the shots of the first 10 cm bubble travel distance considering the information concluded from Reference 3 (the conclusions i and ii stated above) that the bubble terminal velocity values are approximately equal to the average values of the bubble velocities measured between the initial vertical distance 5 cm and 10 cm. In the light of Reference 3 (see Fig. 2.8.b), it is expected that the bubble average velocity measured between the vertical distance 5 cm to 10 cm is about 0.5-1.5 cm/s higher than the bubble terminal velocity that is attained beyond 10 cm distance and this difference decreases with the increasing bubble diameter.

In this thesis study, observations beyond 10 cm travel distance showed that bubbles continue to move in a zigzag path, having a narrower width, with similar shape oscillations and irregular rotations (or orientations) throughout the 1.5 m long pipe.

Figures showing the maximum velocities as a function of the bubble diameter are not given, because the 25 frames/s recording speed of the capture card is not adequate to catch the exact maximum velocity value and the point where it is attained. If it is considered that the maximum bubble velocities are about 35 cm/s for the stagnant water condition, it means bubbles move approximately 1.4 cm between two consecutive images (frames). Also, bubble velocity values are average values calculated from two consecutive images rather than being instantaneous velocity values. The smaller the time interval between two consecutive images, the more accurate the calculated bubble maximum velocity value and bubble position

where the bubble maximum velocity is attained. The bubble maximum velocities are given in Tables C.1-14.

Because the observed (not relative) bubble maximum velocities are lower (10 – 20 cm/s) than values for the stagnant water condition, the bubble maximum velocity data obtained from the recorded images for counter-current water flow conditions are closer to the actual values.

Tables C.8-14 (as well as Figs. 5.2, 5.3 and 5.4) indicate that the bubble maximum velocity for a certain bubble diameter is higher in the stagnant water condition than that in the counter-current water flow conditions.

5.2 Bubble Average Relative Velocity and Effect of the Water Velocity

Figure 5.1.a, which is obtained from this thesis experiments, gives bubble average relative velocity as a function of bubble diameter for various water velocities. As explained in Chapter IV, bubble velocity is the average relative value calculated from the raw data corresponding to the bubble travel distance between 5 cm to 10 cm.

5.2.1 Stagnant Water Condition

When Figure 5.1.a is examined for the stagnant water condition, it is seen that the velocity decreases from the value, 30 cm/s, to the value, 27 cm/s, between the bubble diameter range 3 mm to 4.2 mm and then this decrease becomes very slight for the rest of the bubble diameter range. According to References 2, 3 and 8, and Figure 2.3 of Chapter II, the rate of the bubble shape change (characterized by E) is decreasing with the increasing bubble diameter. Figure 2.3 shows that (for air bubble, $\kappa=0.02$) the aspect ratio, E , decreases more rapidly for smaller diameters. Therefore, while the buoyancy force, having positive contribution to the bubble velocity, is increasing with the bubble diameter in the range of 3 mm to 4.2 mm, the drag force (causing a pressure force on the bubble) is also increasing more rapidly due to relatively rapid bubble deformation. As the rate of deformation decreases for $d_c > 4.2$ mm, the rate of drag force increase versus the rate of buoyancy force increase is almost balanced.

This velocity behavior observed in this thesis experiments shows a good consistency with the data found in References 2, 3, 5, 6, 8, 13 and 16. Figures 2.5, 2.7.a and 2.8.b are sampled from those references and give the experimental results for the stagnant water condition. For a certain bubble diameter, the bubble average relative velocity values of this thesis study is 1.5-3 cm/s higher than the ones seen in these figures. There are two reasons of that:

- (i) Figures 2.5, 2.7.a and 2.8.b give the bubble terminal velocities, but Figure 5.1.a gives the bubble average velocities that are calculated for the initial distance between 5 cm to 10 cm. Therefore, Figure 5.1.a data are giving 0.5-1.5 cm/s higher values than the actual bubble terminal velocity values that could have been observed if the recorded portion of the observation section had been long enough.
- (ii) It is known that the pure water results give a few cm/s higher velocity values (see Fig. 2.5). Figure 2.8.b shows the results for tap water that is probably contaminated with surfactants, and the error in velocity measurements of Reference 3 is about $\pm 3\%$ ($\approx \pm 1$ cm/s).

Therefore, it can be concluded that the results of this thesis study for stagnant water condition are consistent with relevant theoretical and reliable experimental data found in the literature. Figure 5.1.b gives a comparison of the results of this thesis study with the results of two reliable experimental studies [3, 15].

There are sometimes considerable differences between the experimental data found in the literature as shown in Figure 2.9. It gives the results of three different experimental studies conducted for stagnant water condition. As it is seen, the difference between the velocity values for a certain bubble diameter is about 40%. One of the reasons is different contamination level of the water used in experiments. The other one is the usage of different bubble velocity measurement techniques or instruments having different uncertainties.

In this thesis study, it is seen that although the bubble motion behavior is similar for bubbles having the same diameter, it is not exactly replicated, in other words, it is not exactly the same. Because of that reason, it was tried to take suitable

recordings as much as possible for bubbles having almost the same diameter despite the following practical difficulties.

- i) Before performing the time consuming manual image processing explained in Chapter III, it is not possible to know the diameter of the bubble whose motion was recorded.
- ii) Bubbles generated from the same bubble injector under the same water flow conditions may not have the same diameter, especially under counter-current water flow conditions due to the external flow field effect.
- iii) Although many recordings were obtained for bubbles probably having the same diameter, they may not make any contribution to the test data produced for this diameter. Because the moment that the bubble is about to depart from the injector surface, and when bubble diameter can be measured more reliably, was not captured.

There are at least 3-4 samples obtained from suitable recordings for each bubble diameter referred in figures and tables. The number of samples is 7 for some bubble diameters. All of the data are given in Tables C.8-14 (see Appendix C) give the average values obtained from Tables C.1-7. The maximum deviations of samples from the averaged values are mostly ± 0.7 cm/s, and rarely greater than ± 1 cm/s.

The results found in the literature are generally based on 2-3 samples for a specific bubble diameter if the measurement techniques are not based on automated process or direct bubble velocity measuring systems.

5.2.2 Counter-Current Water Flow Conditions

The phenomenon that the initial decrease in the average velocity with the increasing bubble diameter is not seen for counter-current water flow conditions in the results of this thesis study (Fig.5.1.a). For a certain bubble diameter, the surface tension and buoyancy force values are the same as for the stagnant water condition and not affected by external water flow. On the other hand, the drag force, which is

governing the bubble motion, may be affected by external flow water by means of the following mechanisms;

- (i) bubble shape might be affected by the external water flow field, which may change the pressure distribution at the frontal side of the bubble, and
- (ii) wake size and wake structure behind the bubble might be affected by the external flow field.

The rapid bubble deformation phase probably occurs at smaller bubble diameters than it does under stagnant water condition due to the external flow effect explained in (i). Therefore, the drag force increase due to bubble deformation is in the moderate region and the drag force increase has been already in balance with the buoyancy force increase.

Another possibility is that the drag force increase due to wake structure change is in a way that it is in balance with the buoyancy force increase. Both mechanisms may also be effective at the same time and in different or same intensities. However, it is not possible to investigate and to clarify this issue with the available instrumentation. Also, there is not any experimental study conducted for counter-current water flow conditions reported in the literature, enabling to make any comparison or to get information in order to make a certain conclusion.

The most important outcome of this thesis study is that the bubble average relative velocity for a certain bubble diameter is less under counter-current flow conditions than that under stagnant water condition (see Fig.5.1.a). For the range of the investigated bubble diameter and water flow rates, the difference in velocity values from the stagnant case is about 4-5 cm/s. Figures 5.11 and 5.12 show the drag coefficient change as a function of Eötvös number and Weber number, respectively. These two dimensionless numbers are used for analysis of the bubble shape as explained in Chapter II section 2.1. These figures show that for the same Eötvös number and Weber number, drag coefficient values for counter-current water flow conditions are higher than those for the stagnant water condition. For the same Eötvös number and Weber number, the effect of external flow on the

bubble shape is probably limited and not sufficient to increase the drag coefficient values to these values seen in the figures. Therefore, the main reason of the drag increase seen for counter-current water flow conditions is probably the wake size or the wake structure change due to counter-current external flow in a way that the drag force increases. Unfortunately, there is not any study available in the literature to confirm or deny this argument and to give another plausible explanation.

Although it is not evident enough, the velocity of a bubble for a certain diameter seems to be slightly decreasing with the increasing water flow rate.

The uncertainty in the bubble velocity measurement is dependent on the recorded image resolution. The maximum uncertainty value for the determination of the travel distance is ± 1 pixel. Because the bubble velocities are averaged on 5 cm long distance, the maximum uncertainty is $\pm 0.65\%$ for the bubble average velocities (see Appendix A). It is negligibly small. On the other hand, the deviation from the averaged values is mostly ± 0.7 cm/s, rarely greater than ± 1 cm/s (see Tables C.1-14) for the repeated samples of the same diameter.

Figures 2.10 and 2.11 show data for co-current water flow conditions [14,15]. They indicate that external water flow has an effect on the bubble terminal velocities: the bubble velocity for a certain bubble diameter is higher under co-current flow conditions than that under stagnant water condition. On the other hand, as explained above, the results of this thesis study show that the situation is opposite for the counter-current flow conditions. The bubble velocity for a certain bubble diameter is lower under counter-current flow conditions than that under stagnant water condition. Figure 5.1.b gives a comparison of the results of this thesis study with the results of References 3 and 15.

According to the Figure 2.11.a which was taken from the studies of Yavuz [15], the difference between the bubble velocity values for co-current and stagnant water condition is about 3 cm/s and slightly increases with the increasing water flow rate. Yavuz investigated the air bubbles with diameters of 1.0-2.7 mm rising in the stagnant and two different co-current water conditions ($Re_w=154445$ and 21430). The maximum deviation from the averaged values for the repeated samples is about ± 2.5 cm/s in Reference 15.

Figures 2.10.a and 2.10.b, which were taken from the studies of Baker and Chao [14], show a similar trend. Baker and Chao investigated the air bubbles with diameters of 0.38-7.0 mm rising in the stagnant and nine different co-current water conditions. The data of Reference 14 have an uncertainty of about ± 5 cm/s.

Explanations given in both references for this velocity difference are based on the assumption that wake size and structure behind the bubble are affected by the external water flow. Nevertheless, they have not confirmed their explanations by any experimental study visualizing the wake behind the bubble.

5.3 Drag Coefficient

Figure 5.13.a shows the drag coefficient data of this thesis study as a function of bubble diameter and water flow rate. As it is seen from the figure, $C_{D,av}$ increases with the increasing diameter. It is a consequence of bubble deformation which also increases with the diameter. Change of Eötvös number and Weber number with bubble diameter are also given in Figures 5.14 and 5.15. Increase of Eötvös number and Weber number with the increasing bubble diameter also indicates the bubble deformation. $C_{D,av}$ values are higher for counter-current water flow conditions than those for the stagnant water condition. The explanation has already been given in the previous section.

Although it is not evident enough, $C_{D,av}$ values for a certain bubble diameter seem to be slightly increasing with the increasing water flow rate.

Similar $C_{D,av}$ behavior is seen in Figures 5.16.a and 5.16.b which show the change of $C_{D,av}$ as a function of the bubble Reynolds number. Since the bubble Reynolds number gives the ratio of the pressure forces to viscous forces, as it is explained in the Chapter II section 2.1, it is clear that viscous effects are negligible for this range of bubble diameter and hence the main contribution to drag force comes from the pressure drag (form drag) component. Because of that reason, the level of the bubble deformation is important for the drag force. If it is considered that the bubble velocities are approximately constant for the investigated range of bubble diameter (Fig. 5.1.a) and the bubble Reynolds number formula, $Re_b = \rho_l U d_b / \mu_l$, it can be assumed that Re_b is only dependent on the bubble diameter and is a linear

function of the bubble diameter as seen from the given formula above. Therefore, $C_{D,av}$ behavior is very similar to the one seen in Figure 5.13.a. It can be concluded that factors explained for Figure 5.13.a are also governing the behavior seen in Figure 5.16.b in the same manner.

Figure 2.11.b shows the results of the studies of Yavuz [15], which was performed for the co-current water flow conditions. The drag coefficient increases exponentially with the increasing Re_b . The similar trend has been seen in this thesis study (see Figs. 5.16.a and b). Another important point seen in Figure 2.11.b is that for a certain Re_b , the drag coefficient values under co-current water flow conditions are lower than those under stagnant water condition and the difference increase with the increasing water flow rate. On the other hand, the results of this thesis study show that the situation is opposite for the counter-current water flow conditions. Contrary to the co-current water flow conditions, the drag coefficient values of a certain Re_b are higher under counter-current flow conditions than those under stagnant water condition. Figures 5.13.b, 5.16.c and 5.16.d show the comparison of the data of this thesis study with the results of References of 3 and 15. The explanation of this phenomenon is the same with that is given under section 5.2.2 (i) and (ii).

5.4 Conclusion and Recommendations for Future Studies

This is the first study investigating the air bubble motion under counter-current water flow conditions where the bubble motion is in the upward direction while the water flow is downward. For the investigated bubble diameter range, the results for stagnant water condition are in good agreement with theoretical expectations and reliable experimental data available in the literature.

The most important outcome of this thesis study is that the bubble average relative velocity for a certain bubble diameter is less under counter-current flow conditions than that under stagnant water condition and the drag coefficient value for a certain bubble diameter is higher under counter-current flow conditions than that under stagnant water condition.

In comparison with the results of experimental studies reported in the literature which were performed for the co-current water flow conditions, the results of this thesis study show that the bubble velocity of a certain bubble diameter is lower under counter-current flow conditions than that under stagnant water condition contrary to the co-current water flow conditions.

Considering the importance of the subject of this thesis study for its application in many heat generation systems as explained in the Chapter I, a contribution has been made in this study area and a gap in the literature for air bubbles having diameters 3.0-4.8 mm moving under counter-current water flow conditions has been filled.

With a convenient test set-up, this study might be performed for smaller and larger bubble diameter range. Also, it might be useful to use a high-speed high-resolution digital camera to investigate the bubble axial and vertical velocity change more precisely.

Another future study subject might be the mapping of the bubble aspect ratio, E , and bubble orientation change by using software enabling automatic digital image processing with a high-speed high-resolution digital camera.

The most important future study subject might be the visualization of the wake structure behind the air bubble having a certain diameter for the stagnant, co-current and counter-current water flow conditions to better understand the reason of the bubble velocity differences among those cases.

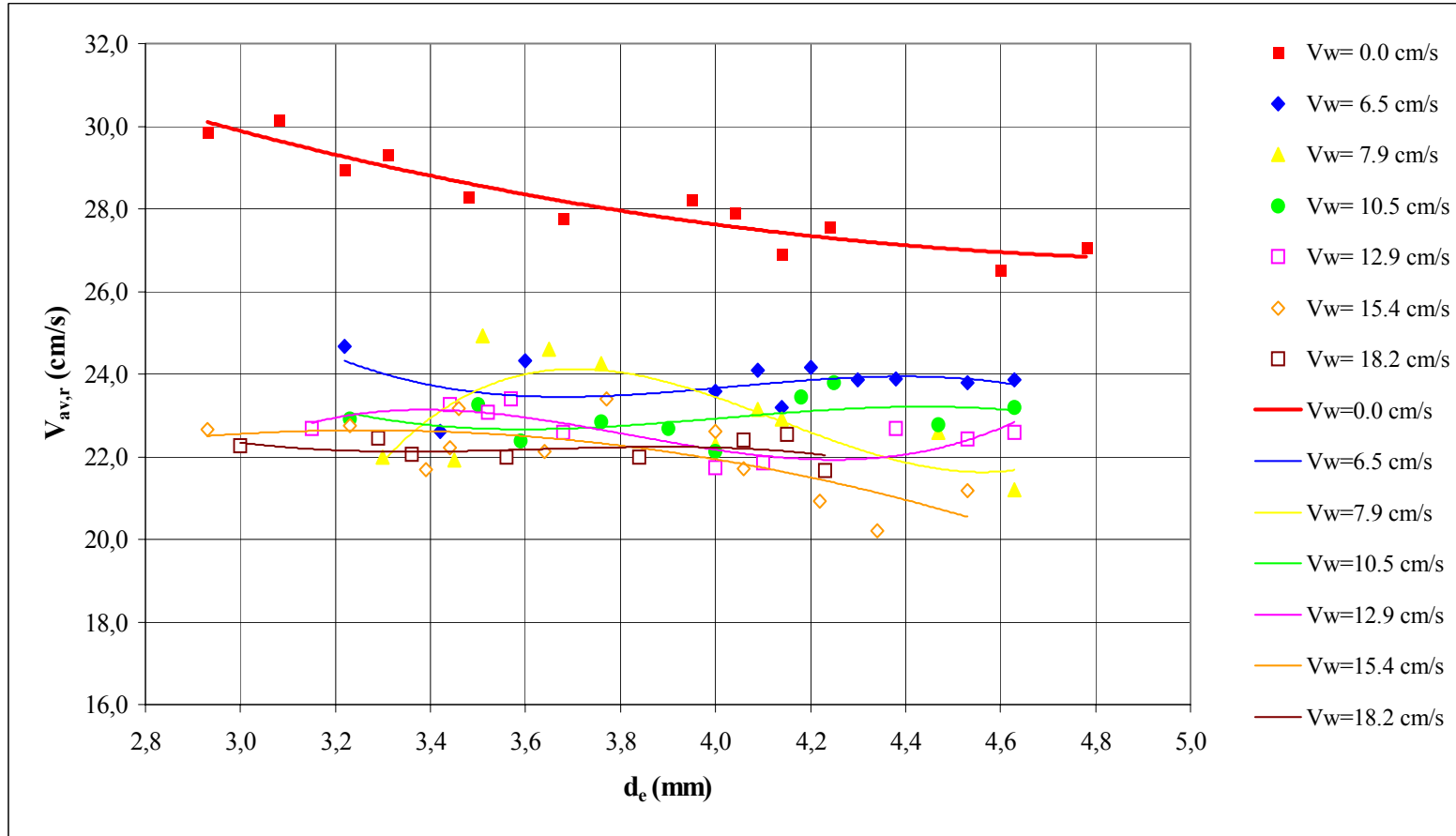


Figure 5.1.a The bubble average relative velocity change as a function of the equivalent bubble diameter and water velocity

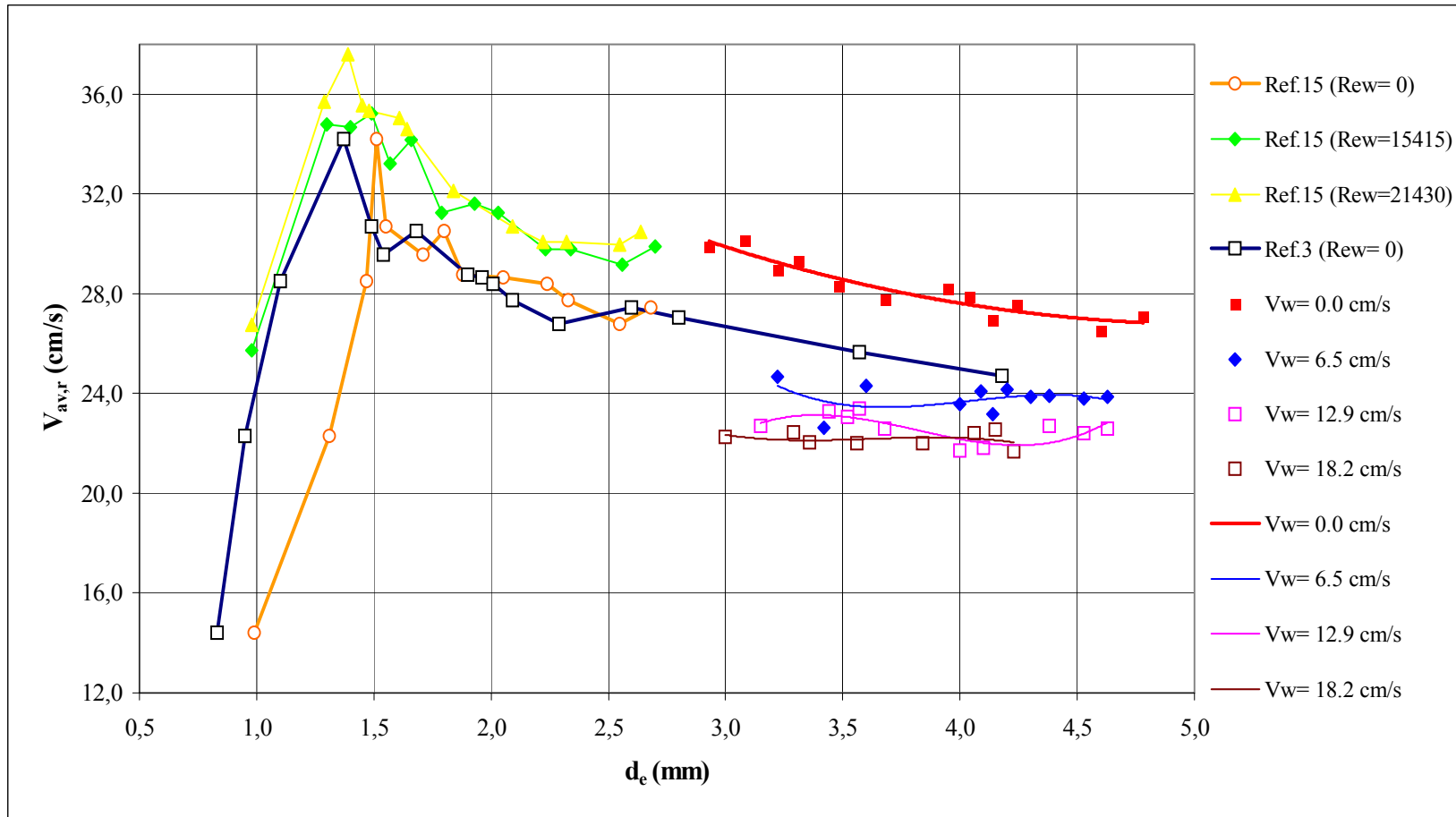


Figure 5.1.b The bubble average relative velocity change as a function of d_e (comparison with the results of Ref.3 and Ref.15) (Ref.3 : stagnant water condition , Ref.15 : stagnant water and co-current water flow conditions)

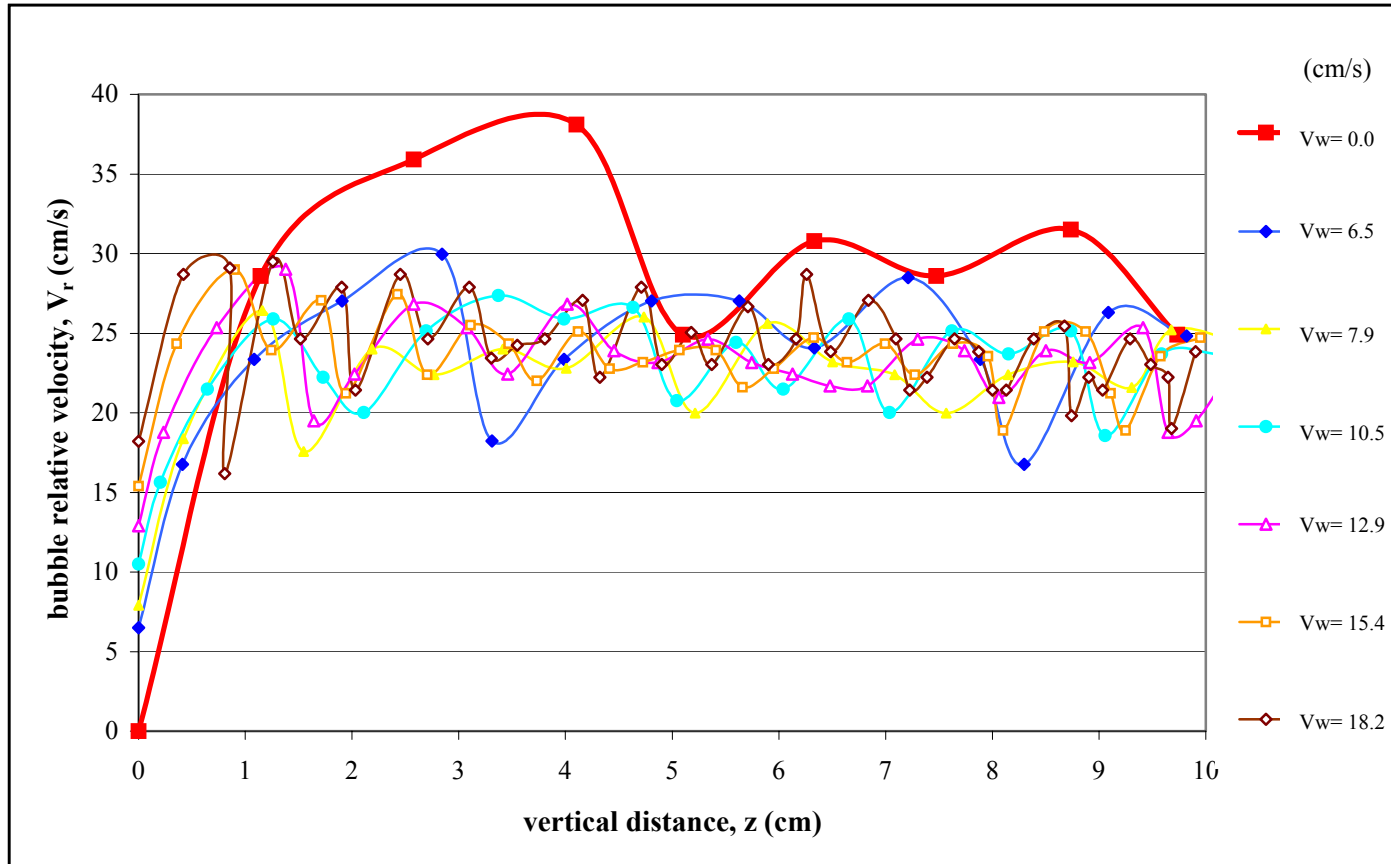


Figure 5.2 The bubble relative velocity change with the vertical distance ($d_c = 3.23$ mm)

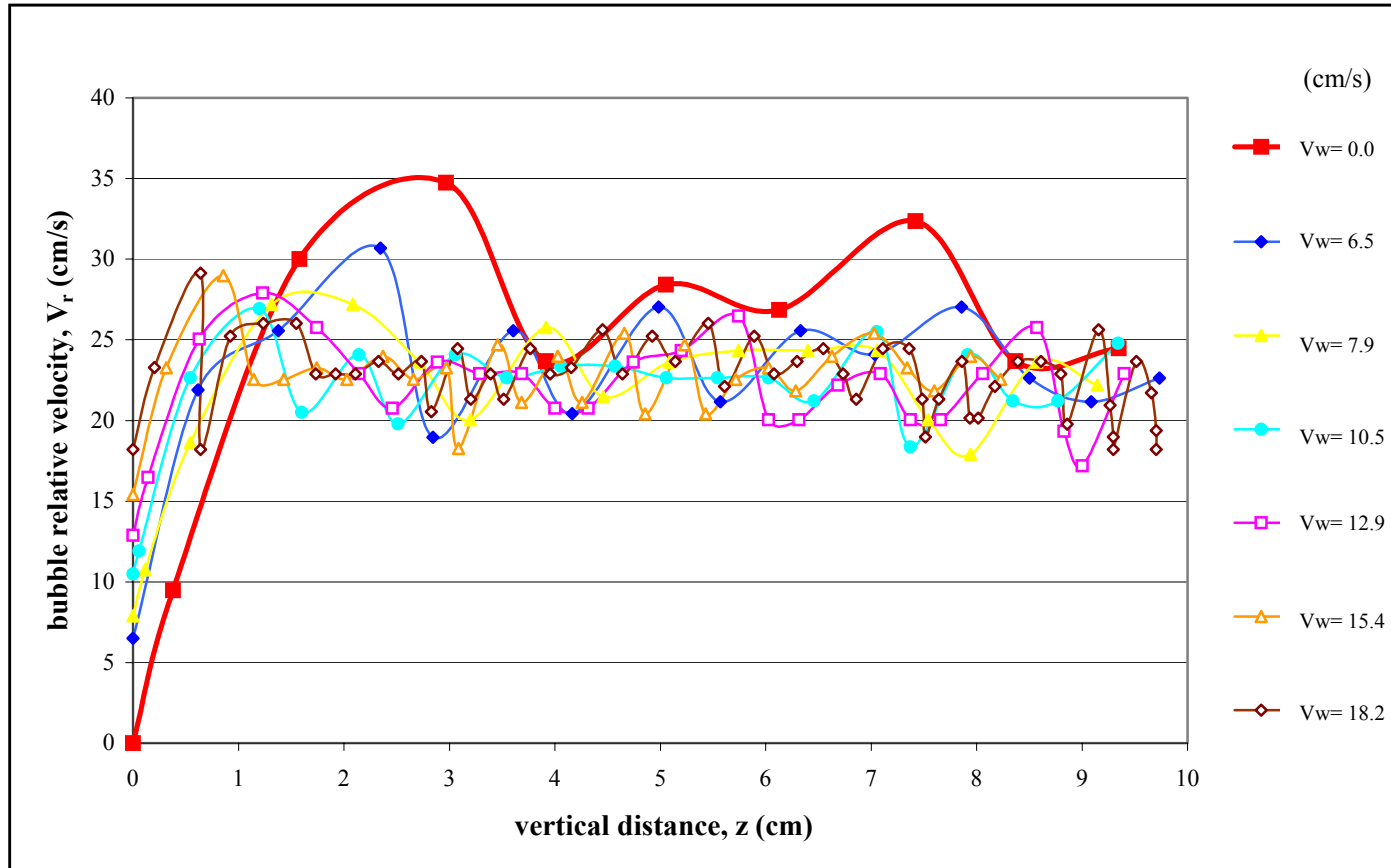


Figure 5.3 The bubble relative velocity change with the vertical distance ($d_c = 4.06$ mm)

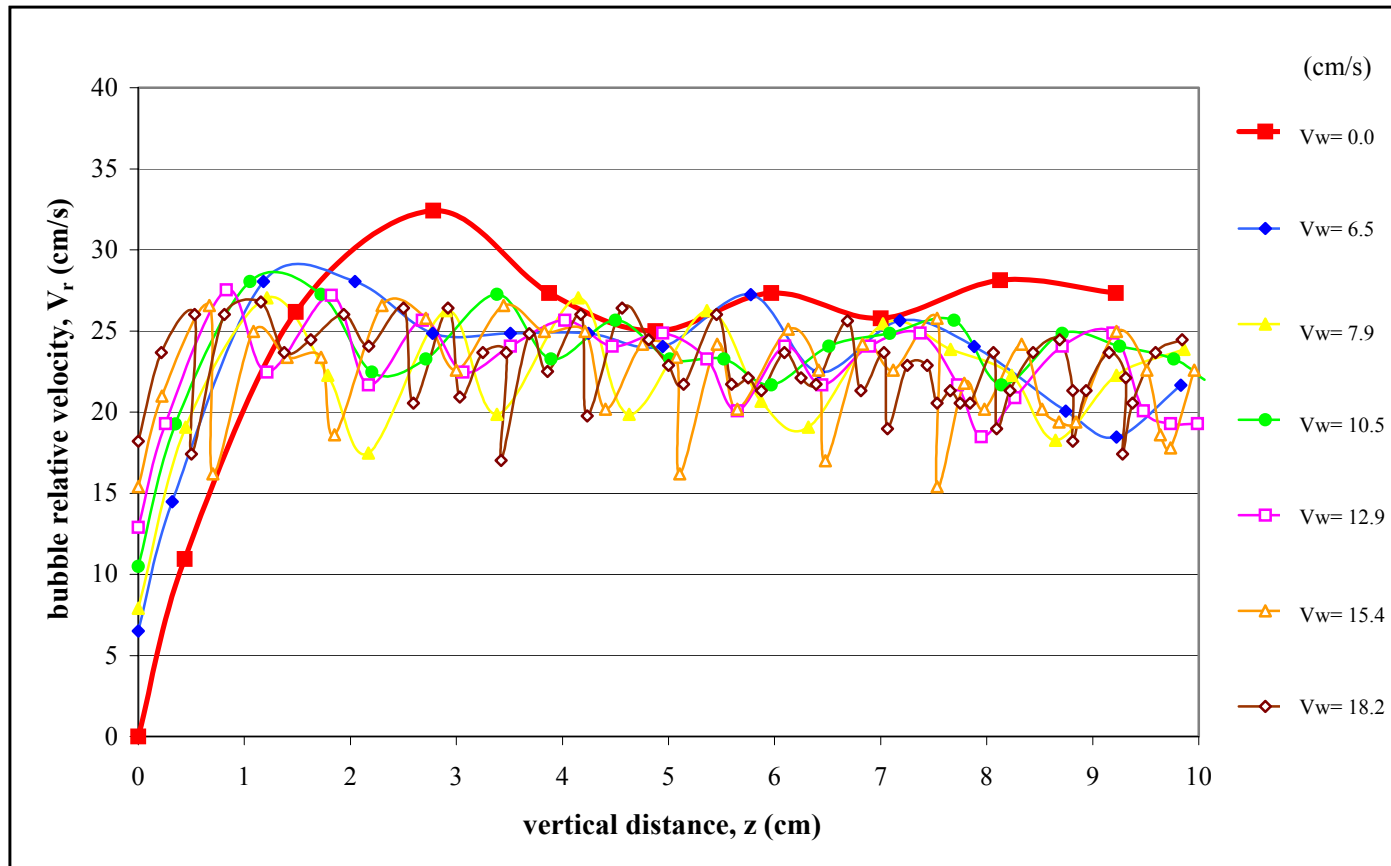


Figure 5.4 The bubble relative velocity change with the vertical distance ($d_c = 4.63$ mm)

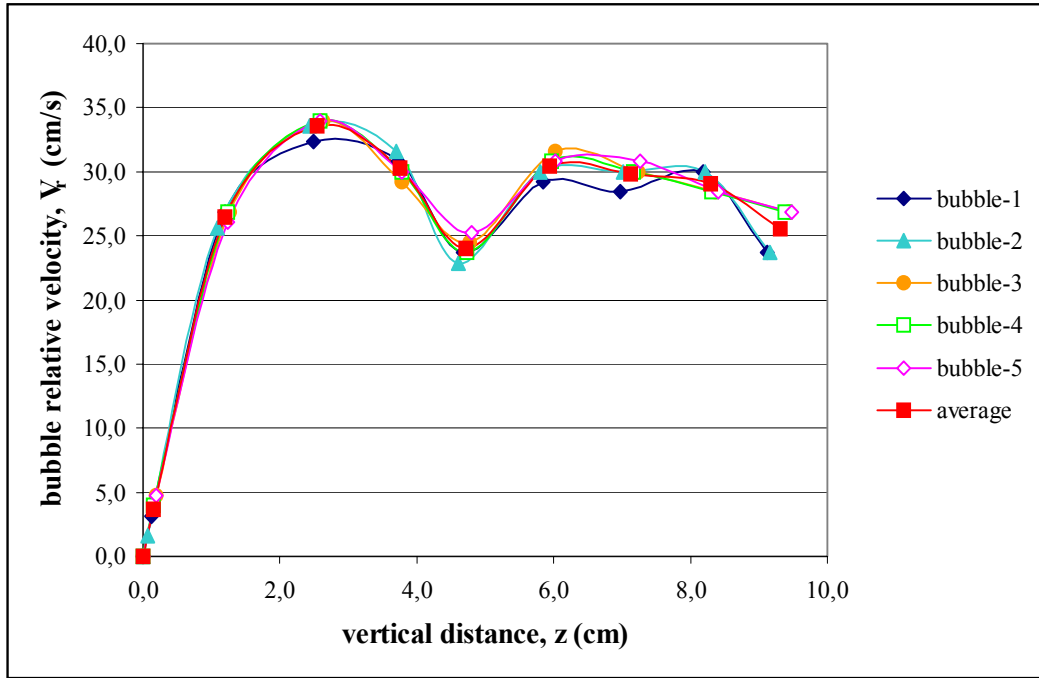


Figure 5.5 Change of the bubble relative velocity with the vertical distance ($d_e=4.0$ mm, $V_w=0$ cm/s)

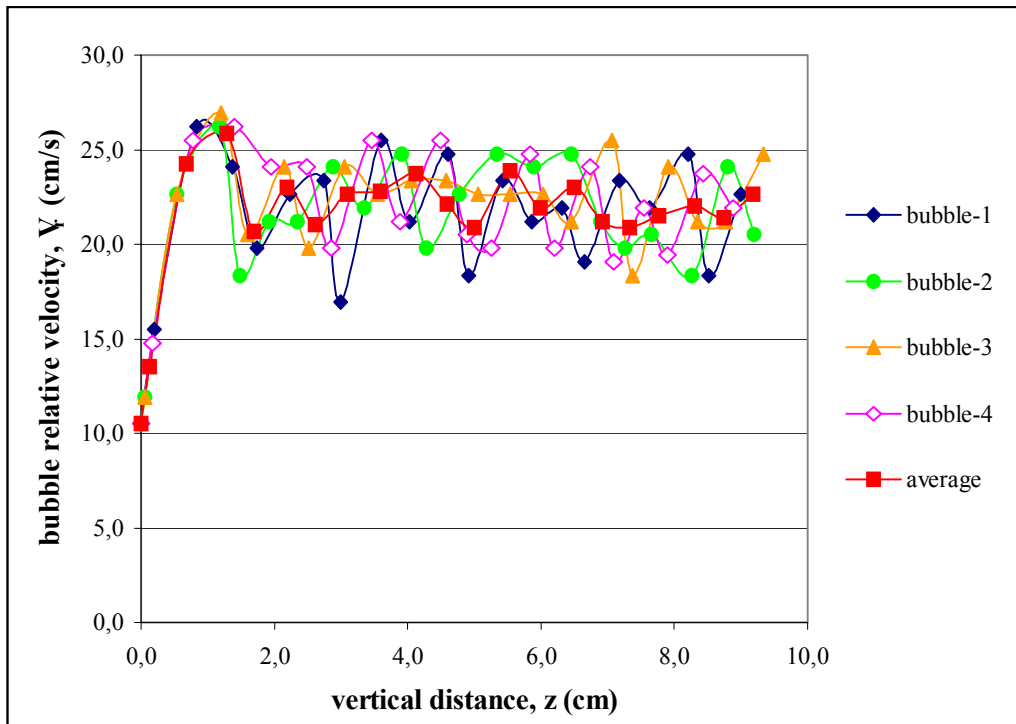


Figure 5.6 Change of the bubble relative velocity with the vertical distance ($d_e=4.0$ mm, $V_w=10.5$ cm/s)

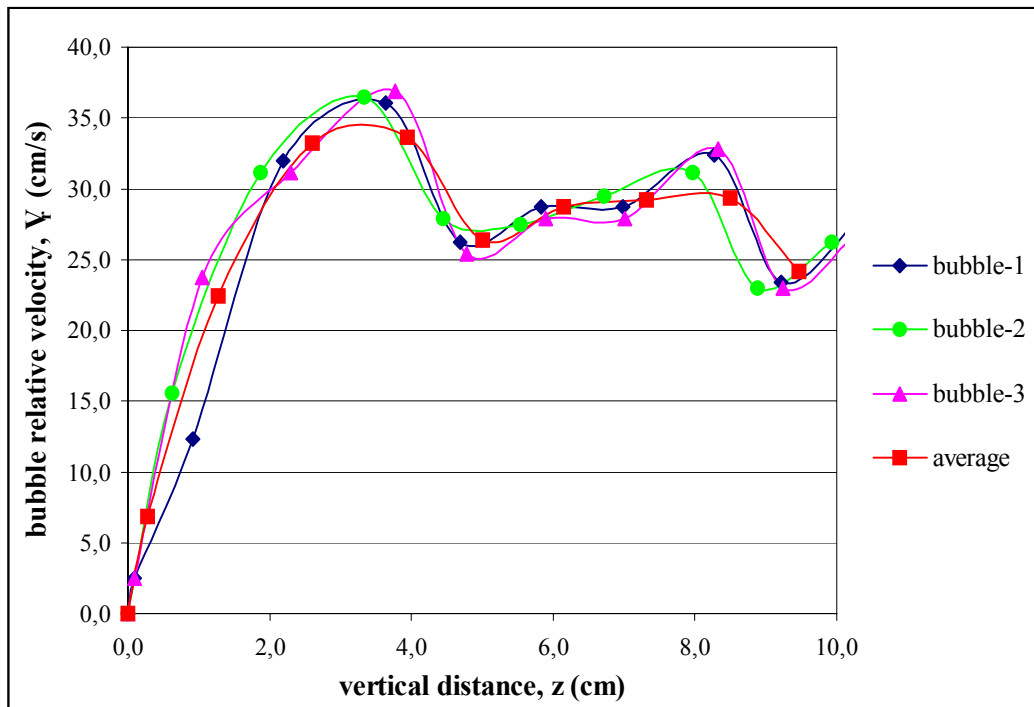


Figure 5.7 Change of the bubble relative velocity with the vertical distance
 ($d_e=4.14$ mm, $V_w=0$ cm/s)

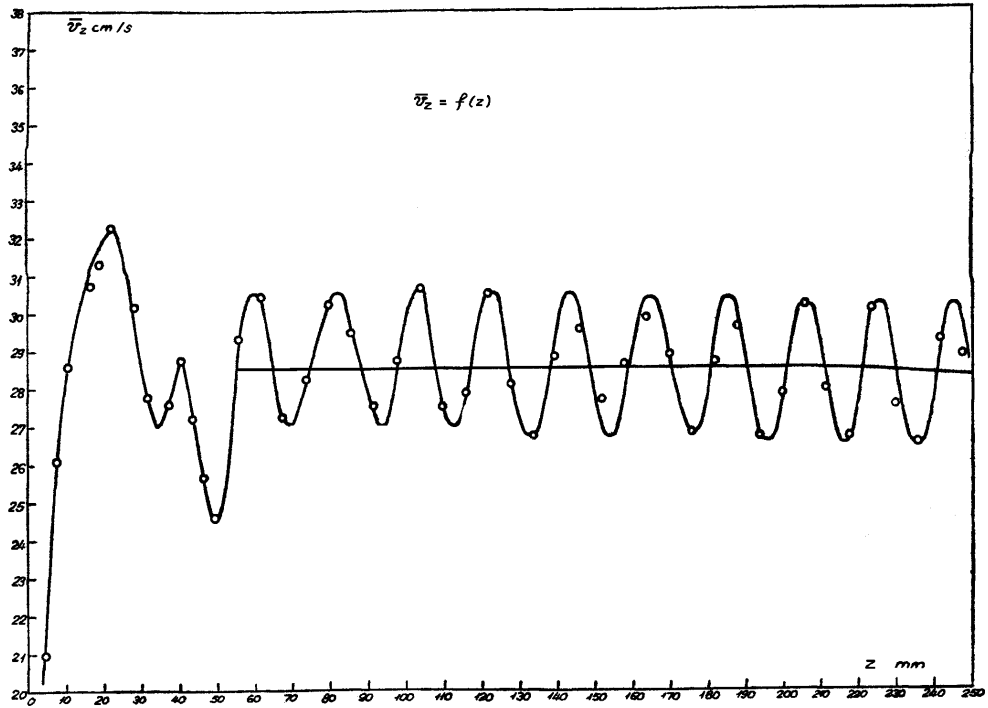


Figure 5.8.a The bubble relative vertical velocity change with the vertical distance (de=2.8 mm) [3]

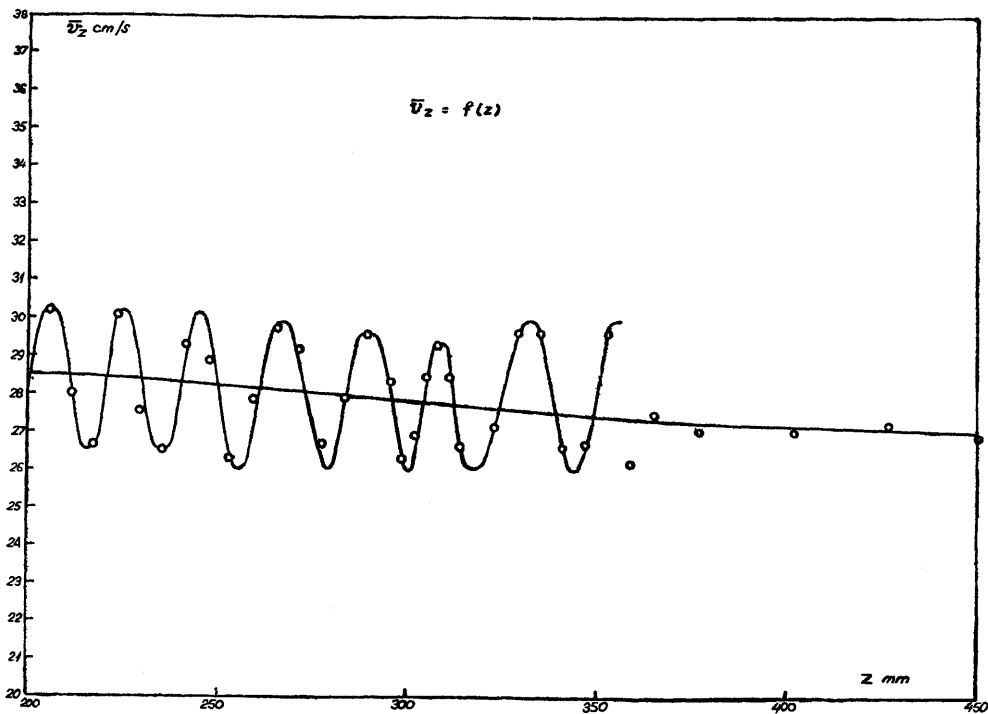


Figure 5.8.b The bubble relative vertical velocity change with the vertical distance (de=2.8 mm) [3]

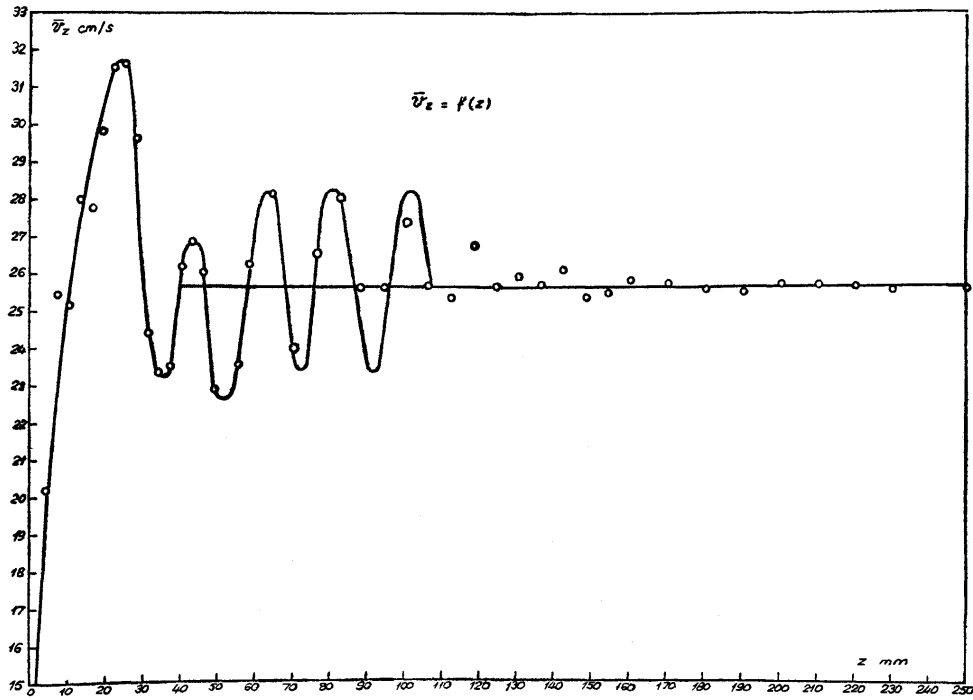


Figure 5.9.a The bubble relative vertical velocity change with the vertical distance ($d_e=3.57$ mm) [3]

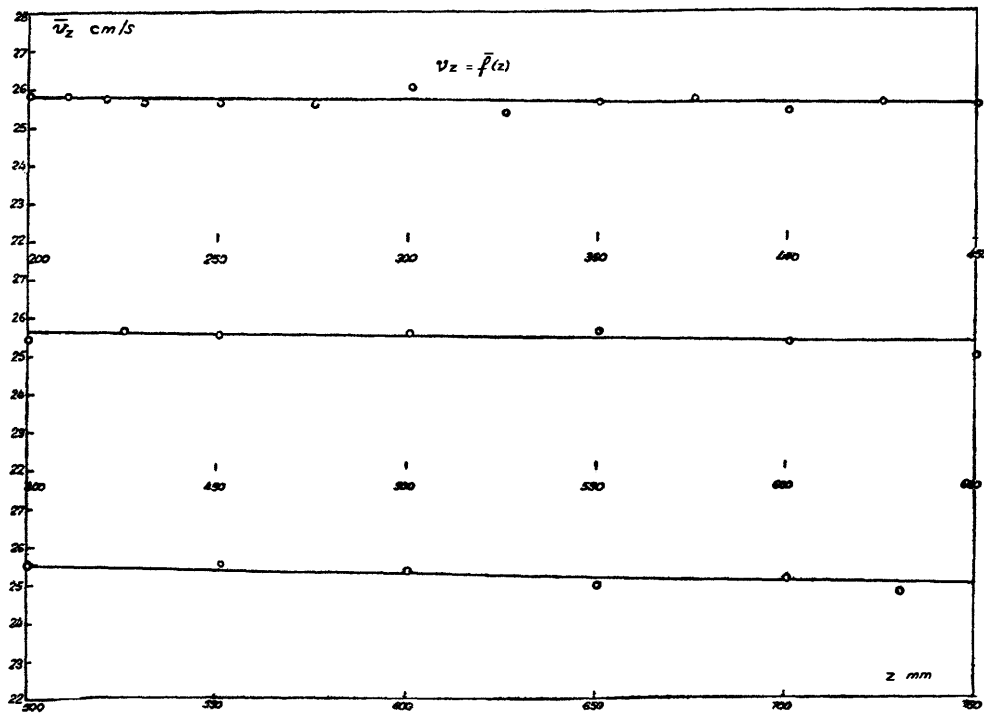


Figure 5.9.b The bubble relative vertical velocity change with the vertical distance ($d_e=3.57$ mm) [3]

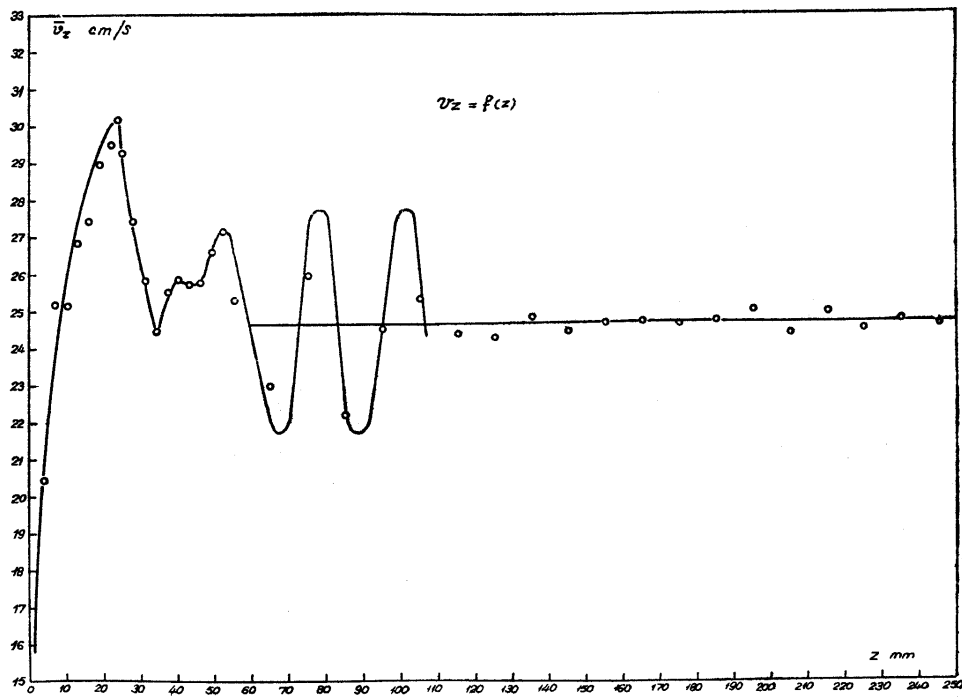


Figure 5.10.a The bubble relative vertical velocity change with the vertical distance (de=4.18 mm) [3]

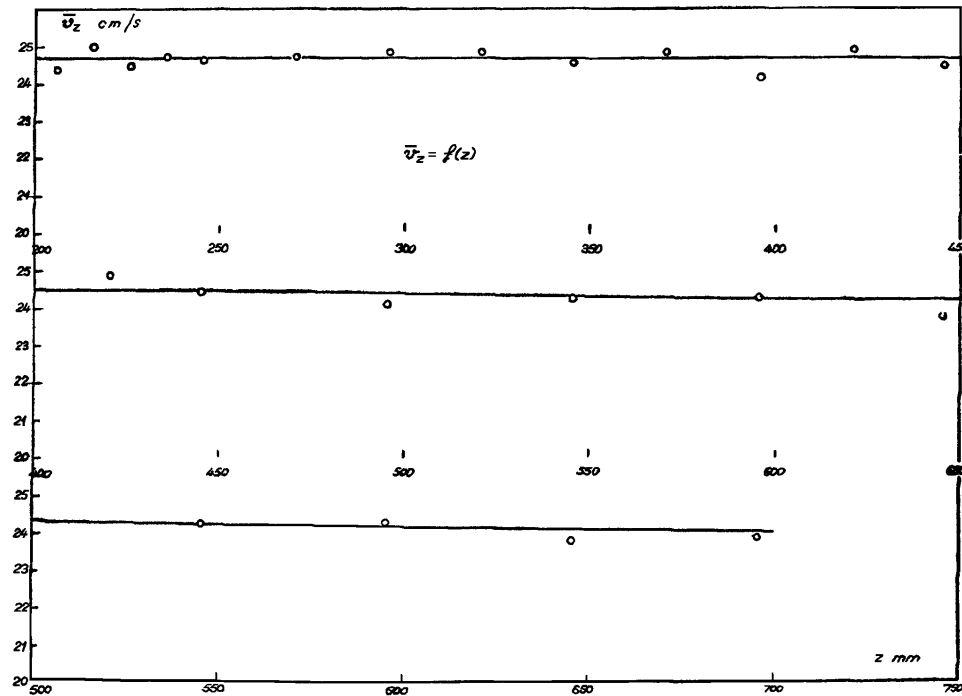


Figure 5.10.b The bubble relative vertical velocity change with the vertical distance (de=4.18 mm) [3]

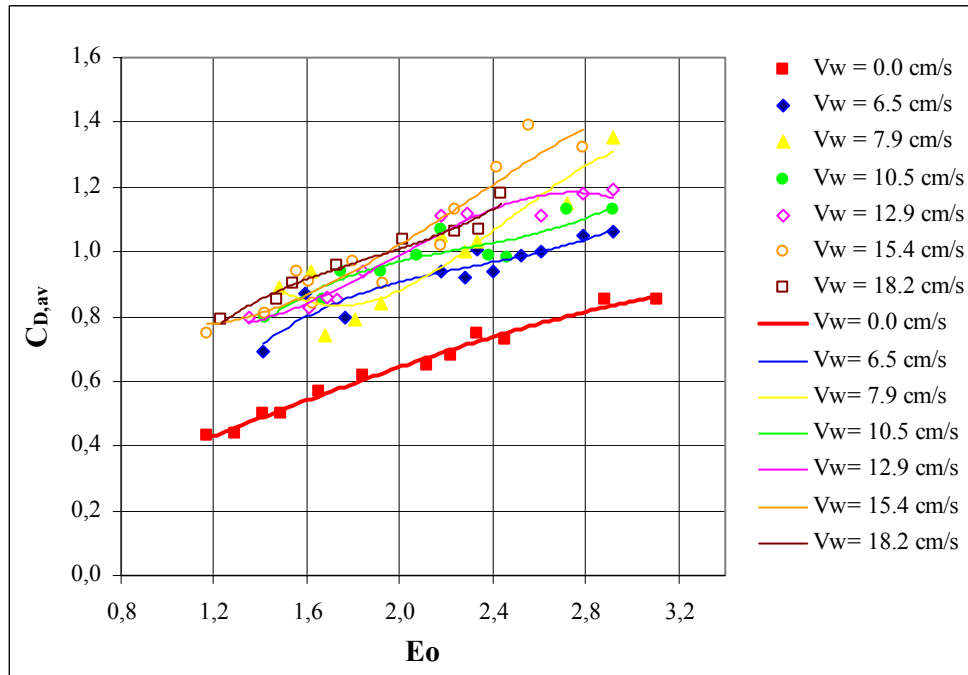


Figure 5.11 Drag coefficient change as a function of Eötvös number

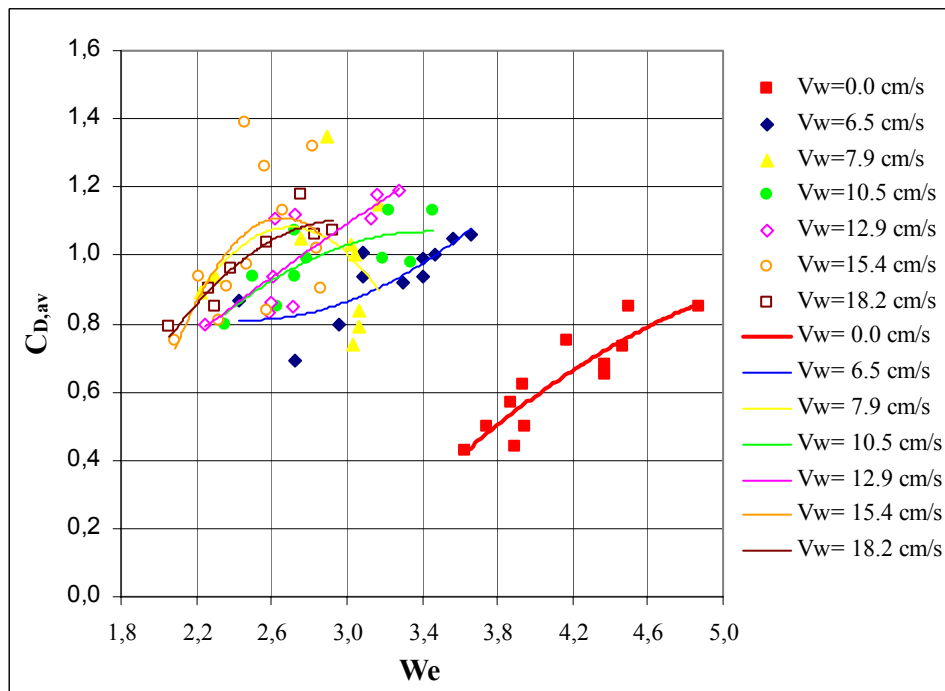


Figure 5.12 Drag coefficient change as a function of Weber number

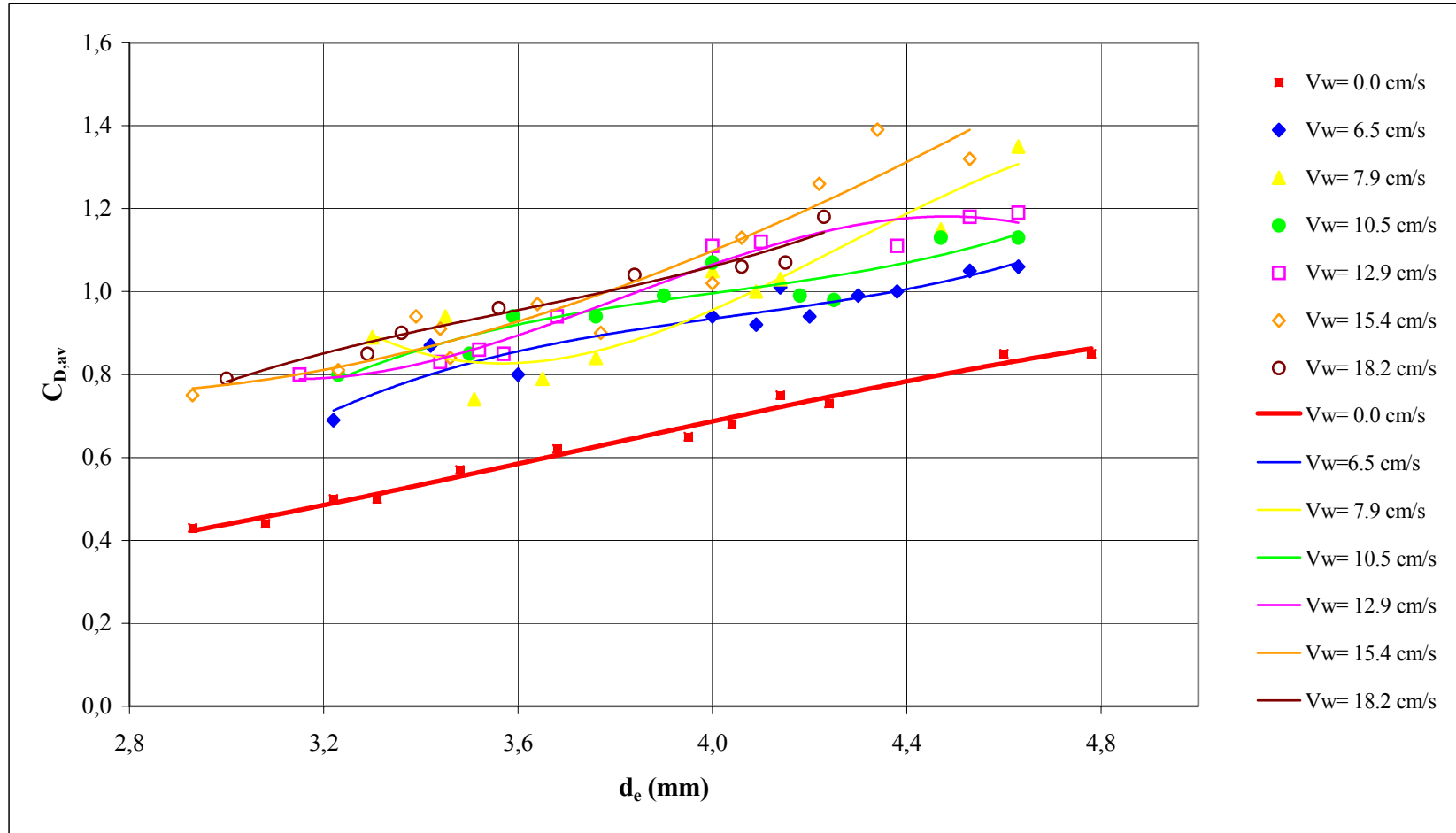
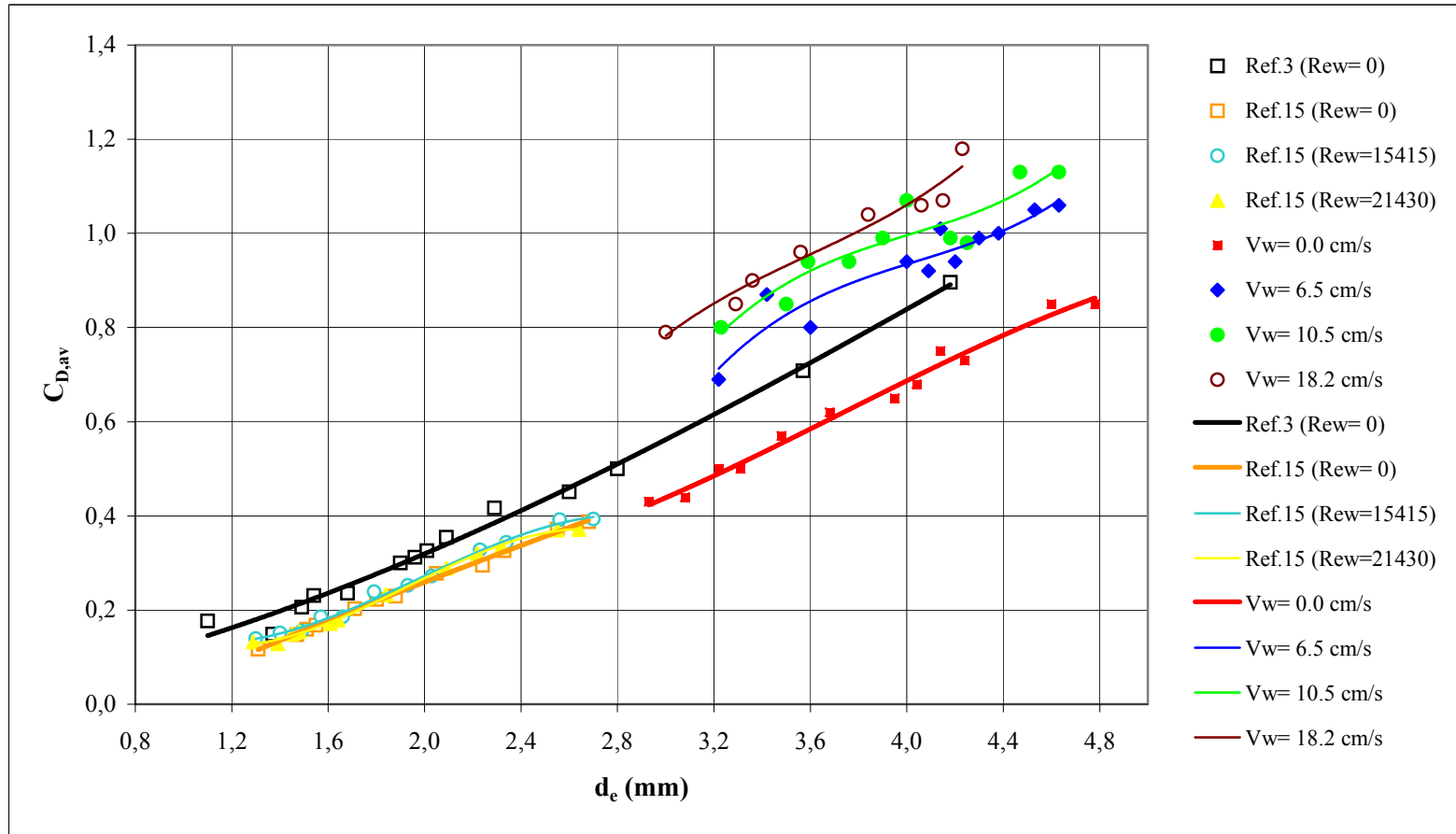


Figure 5.13.a Drag coefficient change as a function of the equivalent bubble diameter and the water velocity



**Figure 5.13.b Drag coefficient change as a function of d_c (comparison with the results of Ref.3 and Ref.15)
(Ref.3 : stagnant water condition , Ref.15 : co-current water flow conditions)**

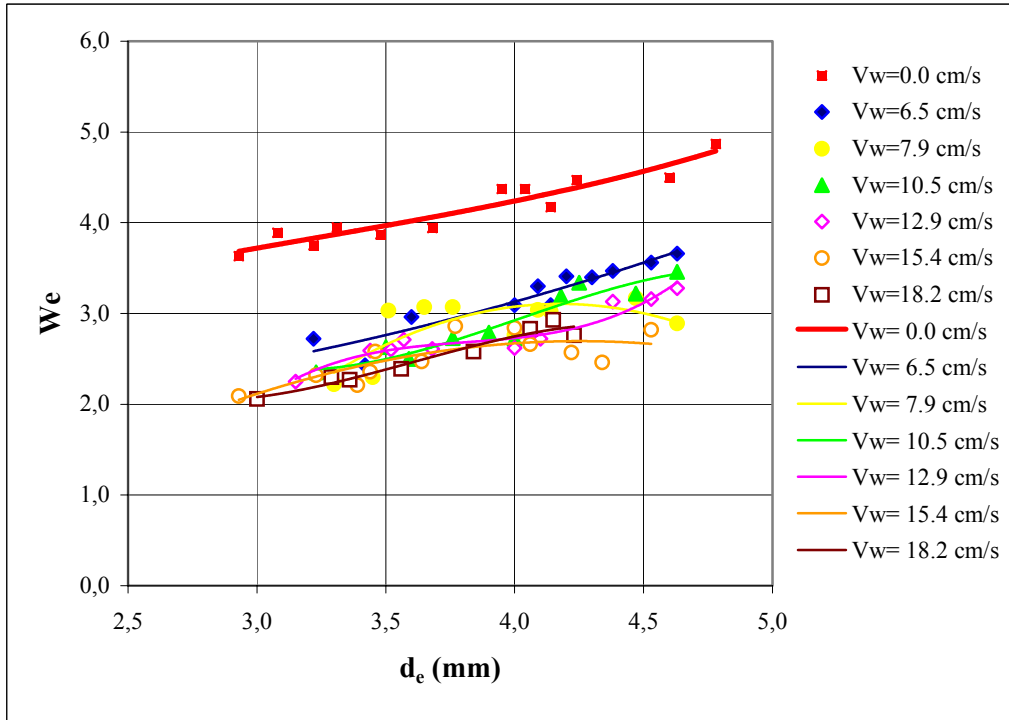


Figure 5.14 Change of Weber number as a function of the bubble diameter

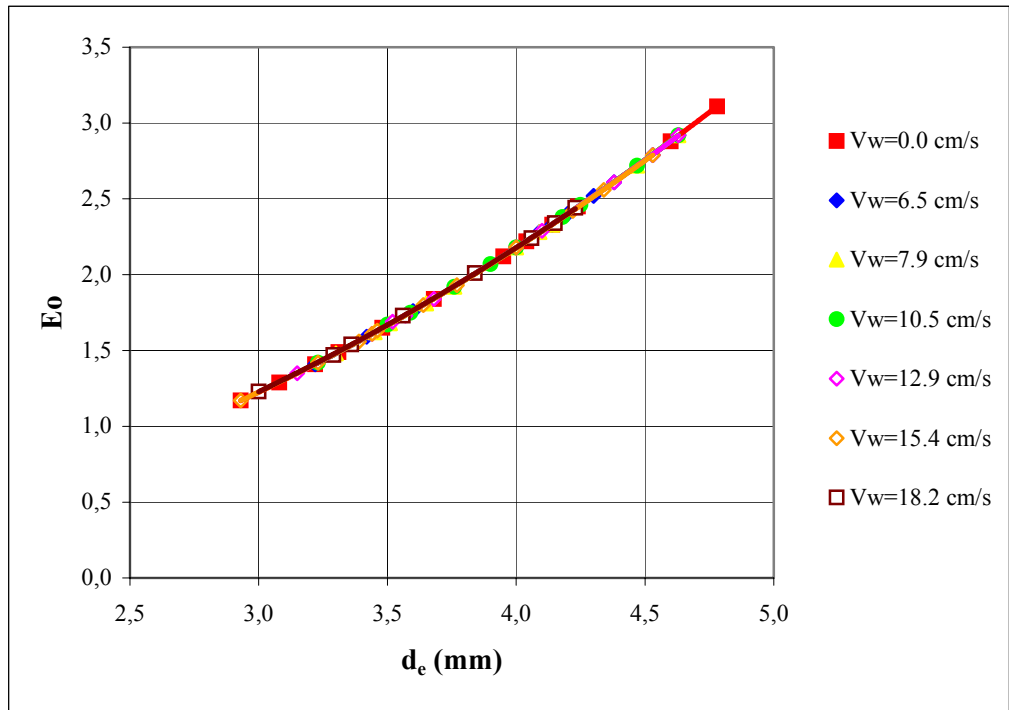


Figure 5.15 Change of Eötvös number as a function of the bubble diameter

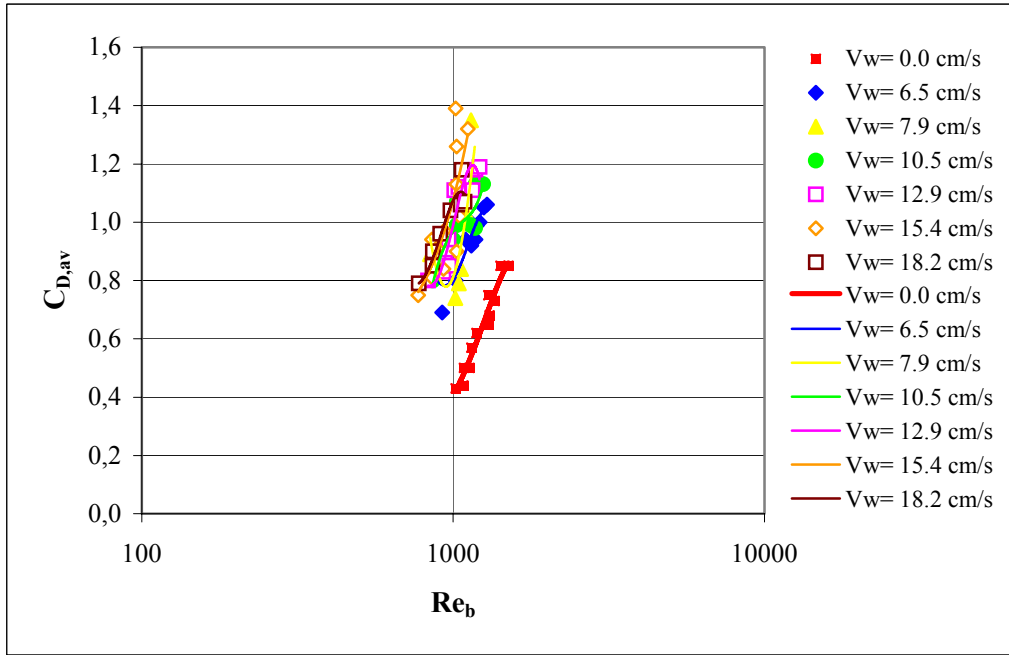


Figure 5.16.a Drag coefficient change as a function of the bubble Reynolds number and water velocity

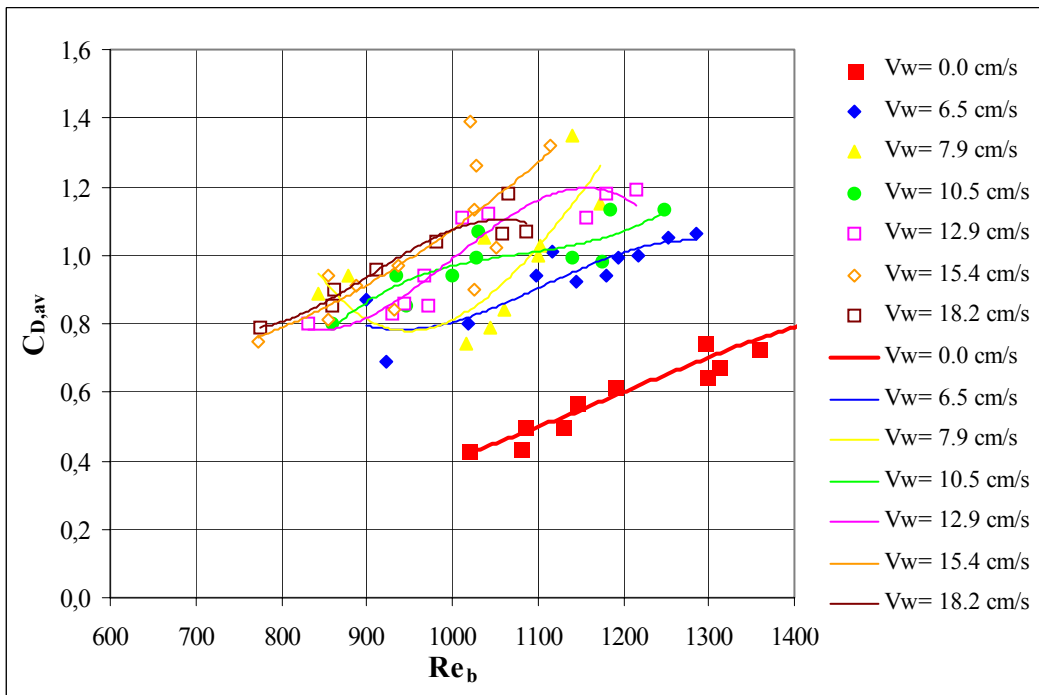
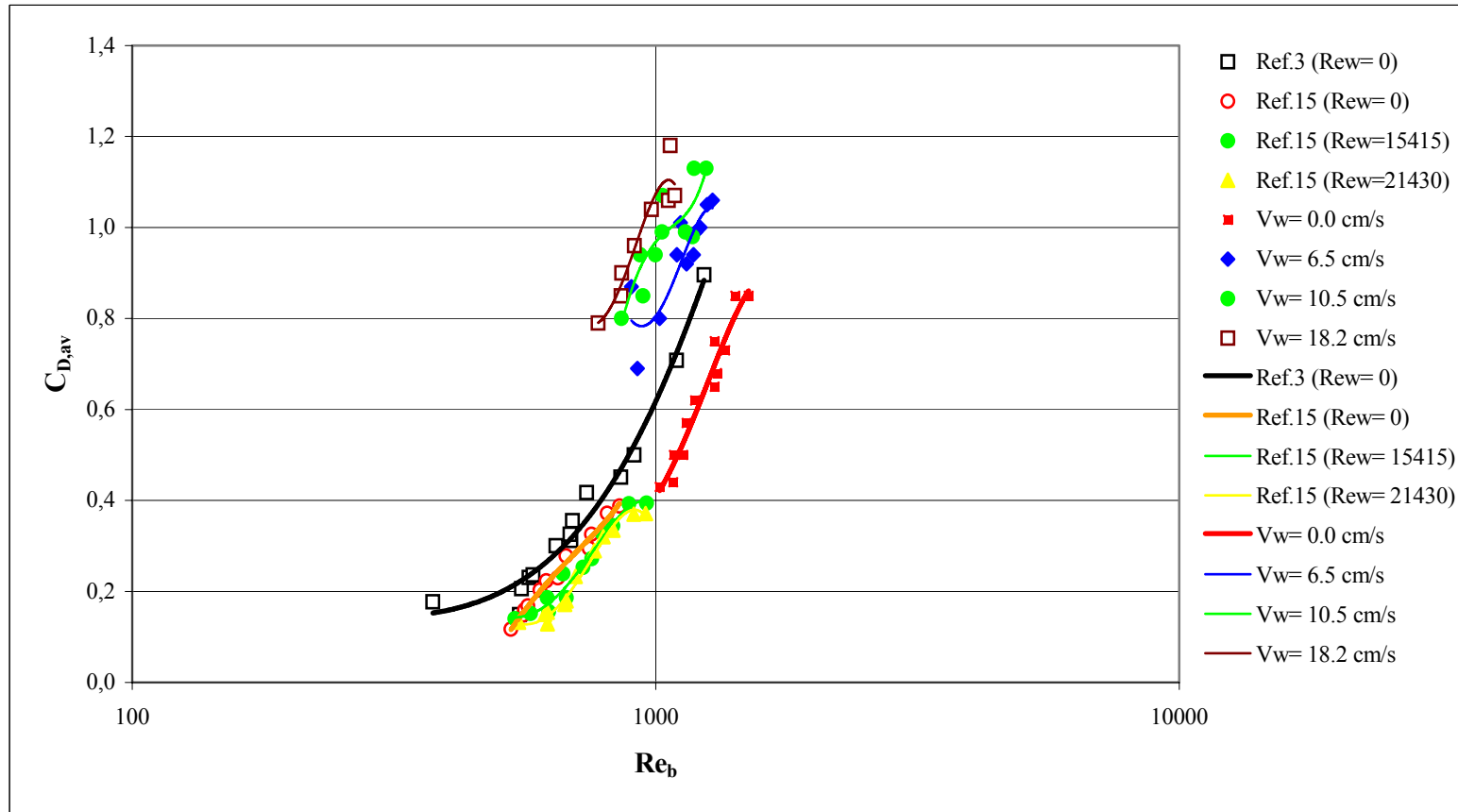


Figure 5.16.b Drag coefficient change as a function of the bubble Reynolds number and water velocity



**Figure 5.16.c Drag coefficient change as a function of Re_b and water velocity (comparison with the results of Ref.3 and Ref.15)
(Ref.3 : stagnant water condition , Ref.15 : stagnant water and co-current water flow conditions)**

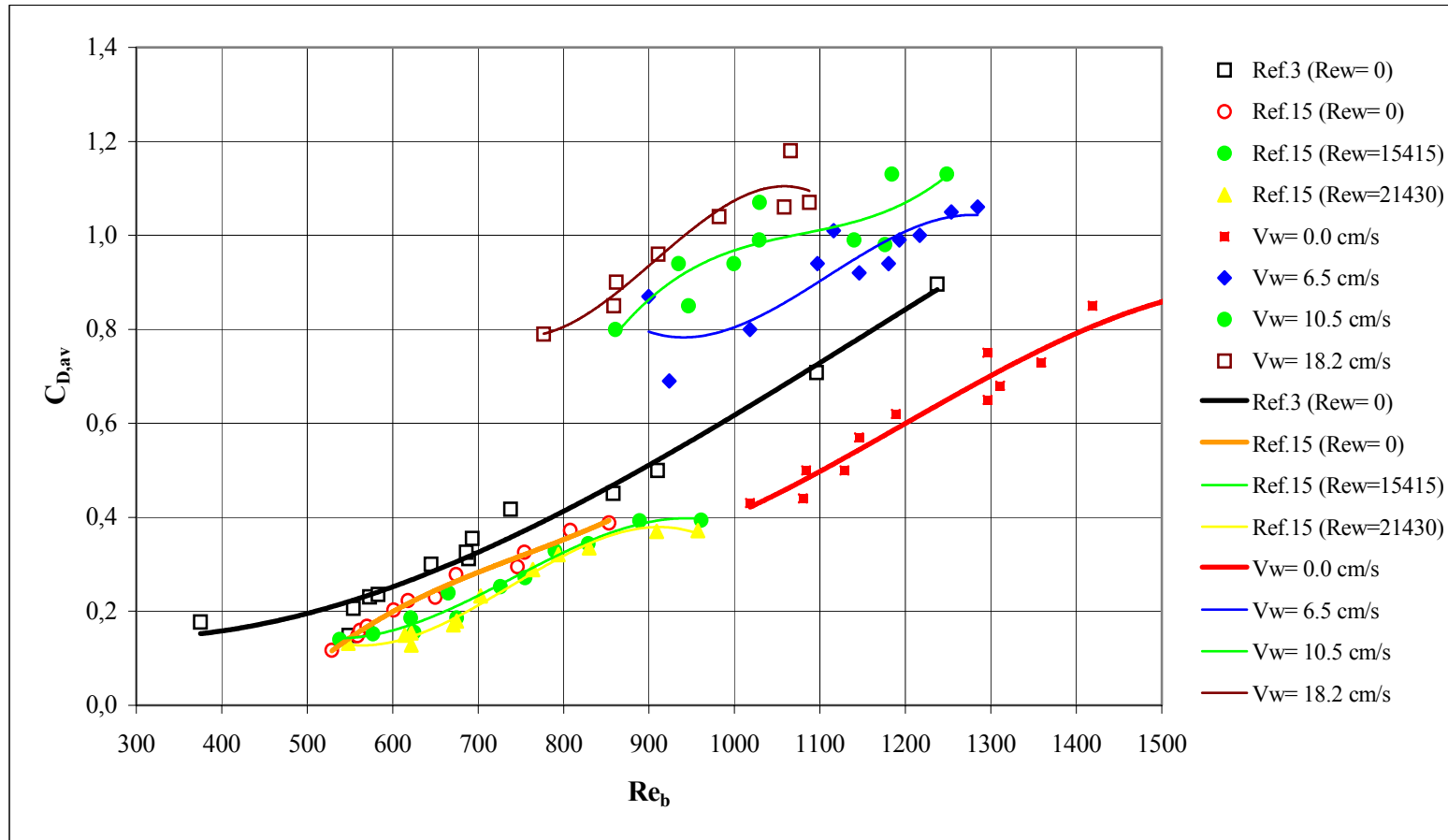


Figure 5.16.d Drag coefficient change as a function of Re_b and water velocity (comparison with the results of Ref.3 and Ref.15)
 (Ref.3 : stagnant water condition , Ref.15 : stagnant water and co-current water flow conditions)

REFERENCES

- 1- S.S. Sadhal, P.S. Ayyaswamy, and J.N. Chung, "Transport Phenomena with Drops and Bubbles", Mechanical Engineering Series, Springer, 1997
- 2- R. Clift, J.R. Grace and M.E. Weber, "Bubbles, Drops and Particles", Academic Press, New York, 1978
- 3- Altan Tapucu, "Durgun Sıvılar İçinde Yükselen Gaz Habbelerinin Hareketlerinin Etüdü", Ph.D. Thesis, İTÜ- Faculty of Machine, 1968
- 4- N.M. Aybers and A. Tapucu, İTÜ INER Bulletin, No.18, 1969
- 5- N.M. Aybers, Two Phase Flows and Heat Transfer, Vol. I, Hemisphere, Washington, DC, 357-380, 1977
- 6- N.M. Aybers and A. Tapucu, İTÜ INER Bulletin, No.17, 1969
- 7- N.M. Aybers and H. Yavuz, İTÜ INER Bulletin, No.23, 1976
- 8- A.W.G. de Vries, "Path and Wake of a Rising Bubble", Ph.D. Thesis, Twente University, The Netherlands, 2001
- 9- P.G. Saffman, J. Fluid Mech., 1, 249-275, 1956
- 10- D.W. Moore, J. Fluid Mech., 23, 749-766, 1965
- 11- J.F. Harper, Adv. Appl. Mech., 12, 59-129, 1972
- 12- P.C. Duineveld, J. Fluid Mech., 292, 325-336, 1995
- 13- I. Zun and J. Groselj, Nuc. Eng. and Design, 163, 99-115, 1996
- 14- James L.L. Baker and Bei T. Chao, AIChE Journal, 268-273, 1965
- 15- H. Yavuz, "Tabii Sirkulasyonlu Kaynar Sulu Reaktörlerde Buhar Habbelerinin Aşağı Sürüklenmesinin Etüdü, Ph.D. Thesis, İTÜ- Faculty of Machine, 1970

- 16- S.S. Sami, Nuclear Technology, 60, 124-136, 1983
- 17- W.S. Janna, "Introduction to Fluid Mechanics", 3. Edition, PWS-KENT, Boston, 1993
- 18- J.F. Douglas, J.M. Gasiorek, J.A. Swaffield, "Fluid Mechanics", 3. Edition, Longman Scientific and Technical, Essex, 1985
- 19- F.M. White, "Fluid Mechanics" 4. Edition, Mc Graw-Hill, Boston, 1999
- 20- R.W. Fox, A.T. McDonald, "Introduction to Fluid Mechanics", SI Version, 4. Edition, Wiley, NewYork, 1994
- 21- S.F. Hoerner, "Fluid-Dynamic Drag", 1958, 2. Edition, Midland park, N.J., 1958
- 22- T.E. Faber, "Fluid Dynamics for Physicists", Cambridge University Press, Cambridge, 1995
- 23- M.J. Miksis and J. Vanden-Broeck, J. Fluid Mech., 23, 31-41, 1982
- 24- G. Ryskin and L.G. Leal, J. Fluid Mech., 148, 19-35, 1984
- 25- G.F. Andrews, R. Fike and S. Wong, Chemical Engineering Science, 43, No.7, 1467-1477, 1988
- 26- K. Tsuchiya and L.S. Fan, Chemical Engineering Science, 43, No.5, 1167-1181, 1988
- 27- P.C. Duineveld, J. Fluid Mech., 292, 325-332, 1995
- 28- D.S. Dandy and L.G. Leal, J. Fluid Mech., 208, 161-192, 1989
- 29- C. Pozrikidis, J. Fluid Mech., 210, 1-21, 1990
- 30- T.S. Lundgren and N.N. Mansour, J. Fluid Mech., 224, 177-196, 1991
- 31- T.B. Benjamin, J. Fluid Mech., 181, 349-379, 1987
- 32- D. Bhaga and M.E. Weber, J. Fluid Mech., 105, 61-85, 1981
- 33- T. Maxworthy, C. Gnann, M. Kürten, and F. Durst, J. Fluid Mech., 321, 421-441, 1996

- 34- L.E. Seeley, R.L. Hummel, and J.W. Smith, *J. Fluid Mech.*, 68, 591-608, 1975
- 35- M.S.L. Higgins, B.R. Kerman, and K. Lunde, *J. Fluid Mech.*, 230, 365-390, 1991
- 36- M. Lance and J. Bataille, *J. Fluid Mech.*, 222, 95-118, 1991
- 37- R. Natarajan and A. Acrivos, *J. Fluid Mech.*, 254, 323-344, 1993
- 38- P.D.M. Spelt and A. Biesheuvel, *J. Fluid Mech.*, 336, 221-244, 1997
- 39- L.V. Wijngaarden, *J. Fluid Mech.*, 77, part 1, 27-44, 1976
- 40- W. Matthes, W. Riebold, and E. De Cooman, *The Review of Scientific Instruments*, 41, No.6, 843-845, 1970
- 41- D.C. Brabston and H.B. Keller, *J. Fluid Mech.*, 69, part 1, 179-189, 1975
- 42- G.B. Wallis, *Int. J. Multiphase Flow*, Vol.1, 491-511, 1974
- 43- T. Okawa, Y. Suzuki, I. Kataoka, M. Aritomi, and M. Mori, *Journal of Nuclear Science and Technology*, Vol.37, No.4, 387-396, 2000
- 44- A. Tomiyama, I. Zun, A. Sou and T. Sakaguchi, *Nuclear Engineering and Design*, 141, 69-82, 1993
- 45- G.P. Celata, M. Cumo, F. D'Annibale, and A. Tomiyama, *Experimental Heat Transfer, Fluid Mechanics, and Thermodynamics*, 1319-1328, 2001
- 46- A. Tomiyama, Y. Nakahara, and G. Morita, 4th Int. Conference on Multiphase Flow, ICMF'01, New Orleans, U.S.A., May 27 – June 1, 2001
- 47- C.E. Brennen, "Cavitation and Bubble Dynamics", Oxford University Press, 1995
- 48- F. Takemura, S. Takagi, J. Magnaudet, and Y. Matsumoto, *J. Fluid Mechanics*, 461, 277-300, 2002
- 49- S. Takagi, *Proceedings of ASME-FEDSM01*, New Orleans, 2001
- 50- S. Takagi and Y. Matsumoto, Y., *Proceedings of ASME-FEDSM00*, Boston, 2000

- 51- S. Takagi, A. Yamamoto, and Y. Matsumoto, Proceeding of FEDSM-99, 3rd ASME/JSME Joint Conf., San Francisco, 1999
- 52- S. Takagi and Y. Matsumoto, 3rd International Conference on Multiphase Flows, Lyon, 1998

APPENDIX A

UNCERTAINTIES

Important parameters used for the calculation of uncertainties:

- frame rate = 1/ 25 ; time difference between two consecutive frames= 0,04 sec
- one pixel length = 0.32 mm
- shutter speed = 1/5000 s
- the recording frequency = 25 frames/s
- bubble terminal velocities \approx 250 mm/s
- bubble velocities when the bubble has already detached from the injector surface \approx 25 mm/s

Uncertainties in the experimental data are calculated as follows:

1- Error due to optical deformation is negligible.

2- Maximum error in water properties due to water temperature difference is ± 0.1 % and hence, it is negligible.

3- Maximum uncertainty in bubble diameter due to image recording resolution;

$$E_{de} = \pm 1 \text{ pixel length} = \pm 0.32 \text{ mm} \quad E_{de} = \pm ((de \pm 0.32\text{mm}) / de) \%$$

4- The distortion on the bubble shape image due to shutter speed when the bubble is moving with its terminal speed

$$250/5000 = 0.05 \text{ mm} \quad (\text{hence, it is } \underline{\text{negligible}})$$

5- The maximum distortion on the bubble shape image due to shutter speed when the bubble has already detached from the injector surface

$$25/5000 = 0.005 \text{ mm} \quad (\text{hence, it is } \underline{\text{negligible}})$$

6- Maximum uncertainty in the distance traveled by the bubble between two consecutive frames, due to image recording resolution;

$$E_z = \pm 1 \text{ pixel length} = \pm 0.32 \text{ mm}$$

7- Maximum error might occur in local velocity (V_r) calculations due to the uncertainty in the distance traveled by the bubble between two consecutive frames;

$$E_{V_r} = E_z / 0.04 \text{ sec} = \pm 0.8 \text{ cm/sec}$$

8- Maximum error might occur in the bubble average velocity ($V_{av,r}$ between the first 5-10 cm distance) calculations due to uncertainty in the distance traveled by the bubble between the first and the last frames;

$$E_{V_{av,r}} = E_z / (5.0 / (V_{av,r} - V_w)) = \pm 0.0064 (V_{av,r} - V_w) \text{ cm/sec}$$

$$E_{V_{av,r}} = \pm 0.0064 (V_{av,r} - V_w) / V_{av,r} = \pm (0.0064 (1 - V_w / V_{av,r})) \%$$

Max $E_{V_{av,r}} = \pm 0.16 \text{ cm/sec}$, Max $E_{V_{av,r}} = \pm 0.64 \%$ (for stagnant water condition)

Max $E_{V_{av,r}} = \pm 0.12 \text{ cm/sec}$ (for $V_w=6.5 \text{ cm/s}$), (hence, it is negligible)

Max $E_{V_{av,r}} = \pm 0.044 \text{ cm/sec}$ (for $V_w=18.2 \text{ cm/s}$), (hence, it is negligible)

9- Maximum error might occur in bubble drag coefficient calculations due to uncertainties in the related parameters;

$$C_D = 4 g d_e / 3 V_{av,r}^2$$

Because the maximum error might occur in average velocity is negligible, the error comes from the uncertainty in bubble diameter measurement.

$$E_{C_D} = E_d = \pm ((d_e \pm 0.32\text{mm}) / d_e) \%$$

$$E_{C_D} = \pm 10.7 \% \text{ for } (d_e=3.0 \text{ mm}), \quad E_{C_D} = \pm 6.7 \% \text{ for } (d_e=4.8 \text{ mm})$$

10- Maximum error might occur in bubble Reynolds number calculations due to uncertainties in the related parameters;

$$Re = d_e V_{av,r} / \nu$$

Because the maximum error might occur in average velocity and water kinematic viscosity is negligible, the error comes from the uncertainty in bubble diameter.

$$E_{Re} = E_d = \pm ((d_e \pm 0.32\text{mm}) / d_e) \%$$

$$E_{Re} = \pm 10.7 \% \text{ for } (d_e=3.0 \text{ mm}), \quad E_{Re} = \pm 6.7 \% \text{ for } (d_e=4.8 \text{ mm})$$

11- Maximum error might occur in bubble Eo number calculations due to uncertainties in the related parameters;

$$E_o = \rho_l g d_e^2 / \sigma$$

Because the maximum error in determination of water properties is negligible, the error comes from the uncertainty in bubble diameter measurement.

$$E_{E_o} = E_d^2 = \pm ((d_e \pm 0.32\text{mm}) / d_e)^2 \%$$

$$E_{E_o} = + 22.5 \%, \quad - 20.2\% \text{ for } (d_e=3.0 \text{ mm}),$$

$$E_{E_o} = + 13.8 \%, \quad - 12.9 \% \text{ for } (d_e=4.8 \text{ mm})$$

12- Maximum error might occur in bubble We number calculations due to uncertainties in the related parameters;

Because the maximum error in determination of water and air properties is negligible, the error comes from the uncertainty in bubble diameter measurement.

$$We = V_{av,r}^2 d_e \Delta\rho / \sigma$$

$$E_{We} = E_d = \pm ((d_e \pm 0.32\text{mm}) / d_e) \%$$

$$E_{We} = \pm 10.7 \% \text{ for } (d_e=3.0 \text{ mm}), \quad E_{E_o} = \pm 6.7 \% \text{ for } (d_e=4.8 \text{ mm})$$

APPENDIX B

FORCES AFFECTING SHAPE OF AN AIR BUBBLE RISING IN WATER

As it is discussed in Chapter II section 2.1 in details, an air bubble adopts a shape where surface tension force, hydrostatic forces and hydrodynamic forces are in balance at every point of the bubble surface. Nevertheless, when the shape of the bubble is deformed significantly, theoretical approaches have limited success to predict the exact bubble shape due to the complexity of the phenomenon. Therefore, analyses mostly rely on the relevant dimensionless numbers and benefit from the relevant experimental data. Besides that, for analysis or interpretation of the observed bubble shape and motion of a bubble under consideration, it may also be helpful to know the magnitude of each force that governs the bubble shape.

The dynamic force due to internal gas motion is usually negligible [2]. Important forces governing the shape and changing with bubble diameter are the surface tension, buoyancy, viscous, and hydrodynamic pressure forces. The viscous, buoyancy and hydrodynamic pressure forces are trying to distort the shape, while the surface tension force is trying to conserve the bubble shape. For a gas bubble moving with a relative terminal velocity, v_r , in a linear path, the hydrodynamic force results from the drag force. If the system pressure and temperature are constant or their variations are negligible, the magnitudes of those forces can be calculated from the following equations:

$$\text{Surface tension force:} \quad F_{st} = \pi d_b \sigma \quad (\text{B.1})$$

$$\text{Viscous force:} \quad F_{vis} = \mu_l \pi d_b v_r \quad (\text{B.2})$$

$$\text{Buoyancy force:} \quad F_{buo} = g \rho_l \pi d_b^3 / 24 \quad (\text{B.3})$$

$$\text{Drag force:} \quad F_D = C_D \rho_l \pi d_b^2 v_r^2 / 8 \quad (\text{B.4})$$

where d_b is air bubble diameter, ρ_l is liquid density, g is gravitational acceleration, μ_l is liquid viscosity and σ is air-liquid surface tension.

Effect of the viscous force can be disregarded when Re_b is greater than 1. It may necessary to remind that for the theoretical calculation of the exact shape of the bubble, exact distribution of those forces on the bubble surface should be known.

B.1. Calculations for Example Cases

For analysis and interpretation of the observed shape and motion of bubbles investigated by this thesis study, magnitudes of some important forces that govern the bubble shape were calculated from the Equations (B.1) to (B.4) with the following assumptions:

- Analyzed bubble equivalent diameter range is 2.9-4.7 mm,
- Bubbles having diameters in this range are moving with the same relative axial velocity, $v_r = 23$ cm/s, (see Fig.5.1)
- C_D is a linear function of d_b and increasing with the diameter increase and given by the following correlation obtained from Figure 5.13.a:

$$C_D = 0.278 (d_b - 2.9) + 0.8$$

- $\sigma \approx 7.2 \times 10^{-2}$ (N/m, at 25°C); $\mu_l \approx 8.9 \times 10^{-4}$ (Ns/m², at 25°C); and
 $\rho_l \approx 997$ (kg/m³, at 25°C)

The calculated results are given in Table B.1 and their graphical representation is shown in Figure B.1.

Table B.1 Forces affecting on bubble shape (mili Newton)

Diameter (mm)	F_{vis} (mili N)	F_{buo} (mili N)	F_{st} (mili N)	F_D (mili N)	We	Eo	Re
2,90	0,019	0,03	0,66	0,136	2,09	1,127	746
3,10	0,020	0,038	0,71	0,171	2,24	1,29	798
3,30	0,021	0,045	0,76	0,209	2,38	1,46	849
3,50	0,023	0,055	0,80	0,241	2,53	1,64	901
3,70	0,024	0,065	0,85	0,286	2,67	1,83	952
3,90	0,025	0,075	0,89	0,334	2,82	2,04	1004
4,10	0,026	0,088	0,94	0,396	2,96	2,25	1055
4,30	0,028	0,103	0,99	0,451	3,11	2,48	1107
4,50	0,029	0,118	1,03	0,521	3,25	2,71	1158
4,70	0,030	0,133	1,08	0,597	3,39	2,96	1210

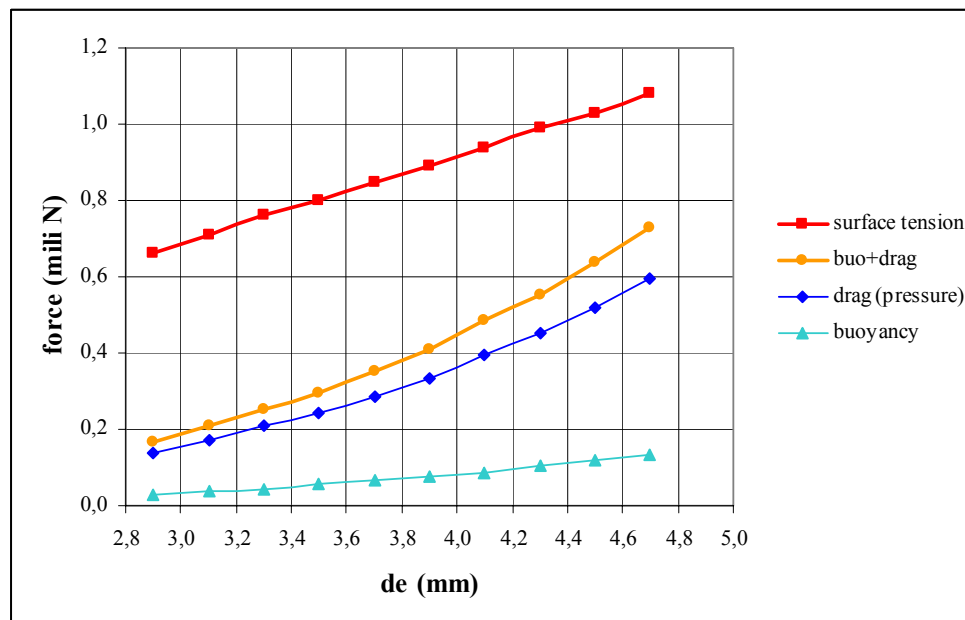


Figure B.1 Magnitudes of some important forces affecting the bubble shape

APPENDIX C
EXPERIMENTAL RESULTS

Table C.1 Data for $V_w = 0.0$ cm/s

d_e (mm)	$V_{max,r}$ (cm/s)	$V_{av,r}$ (cm/s)
2,93	39,06	30,28
2,93	38,62	29,48
3,08	39,28	30,69
3,08	36,94	29,61
3,22	39,41	29,15
3,22	38,27	28,75
3,31	38,11	28,96
3,31	38,11	29,69
3,48	34,02	28,53
3,48	34,02	28,09
3,68	32,47	27,30
3,68	34,00	26,07
3,68	31,57	27,01
3,68	34,00	26,24
3,68	35,62	27,22
3,95	33,95	28,62
3,95	33,55	27,82
4,04	34,74	26,65
4,04	33,95	28,64
4,04	33,95	28,41
4,14	32,37	27,33

Table C.1 (cont.) Data for $V_w = 0.0$ cm/s

d_e (mm)	$V_{max,r}$ (cm/s)	$V_{av,r}$ (cm/s)
4,14	30,71	26,05
4,14	29,29	24,79
4,14	30,71	25,63
4,14	30,71	24,64
4,24	36,48	27,41
4,24	34,02	27,70
4,60	32,81	25,59
4,60	32,03	25,83
4,60	33,20	25,29
4,60	30,47	27,83
4,60	32,42	26,84
4,60	32,81	27,28
4,60	32,81	27,05
4,78	32,71	27,44
4,78	34,31	26,10
4,78	31,91	26,33
4,78	33,51	27,39
4,78	31,91	27,06
4,78	35,11	28,01
4,78	33,51	27,12

Table C.2 Data for $V_w = 6.5$ cm/s

d_e (mm)	$V_{max,r}$ (cm/s)	$V_{av,r}$ (cm/s)
3,22	29,95	24,41
3,22	29,95	24,51
3,22	28,64	23,17
3,22	28,61	26,30
3,42	25,02	22,00
3,42	26,22	20,50
3,42	29,78	25,35
3,42	25,02	22,00
3,42	26,22	20,50
3,42	29,78	25,35
4,00	28,64	22,85
4,00	30,69	23,46
4,00	30,69	23,15
4,00	29,45	24,88
4,09	28,63	23,83
4,09	29,04	24,77
4,09	29,45	23,68
4,14	34,36	22,65
4,14	27,93	23,98
4,14	28,64	22,91
4,20	30,27	23,68
4,20	29,04	24,65
4,30	28,53	24,16
4,30	28,23	23,56
4,38	27,98	23,26
4,38	29,94	23,92
4,38	29,94	24,50
4,53	28,38	23,54
4,53	29,16	24,06
4,63	28,04	23,69
4,63	28,04	23,93
4,63	28,84	23,46
4,63	29,16	24,40

Table C.3 Data for $V_w = 7.9$ cm/s

d_e (mm)	$V_{max,r}$ (cm/s)	$V_{av,r}$ (cm/s)
3,30	26,42	22,13
3,30	28,03	21,83
3,45	27,69	22,55
3,45	28,42	22,19
3,45	25,61	21,04
3,51	30,83	25,10
3,51	28,11	24,80
3,51	30,40	24,86
3,65	29,27	23,92
3,65	31,67	27,50
3,65	29,52	24,11
3,65	28,64	22,85
3,76	26,96	22,23
3,76	30,88	26,28
4,00	27,19	22,35
4,00	27,19	22,22
4,09	29,62	25,07
4,09	26,65	22,74
4,09	29,78	22,84
4,09	29,78	23,54
4,09	28,99	23,00
4,09	28,99	23,07
4,09	28,21	22,64
4,09	26,96	22,29
4,14	29,21	24,30
4,14	27,43	22,84
4,14	26,47	22,35
4,14	27,19	22,21
4,47	27,05	23,12
4,47	26,25	22,45
4,47	27,05	22,18
4,63	26,25	20,37
4,63	27,85	22,03

Table C.4 Data for $V_w = 10.5$ cm/s

d_e (mm)	$V_{max,r}$ (cm/s)	$V_{av,r}$ (cm/s)
3,23	27,36	23,17
3,23	28,24	22,67
3,23	26,63	22,89
3,50	29,54	23,77
3,50	28,38	22,80
3,50	27,60	23,20
3,59	31,10	23,76
3,59	25,89	21,82
3,59	27,36	21,57
3,76	28,12	23,05
3,76	28,53	22,65
3,90	25,16	21,13
3,90	28,53	23,49
3,90	30,17	23,42
4,00	26,21	21,83
4,00	26,21	22,66
4,00	26,93	22,37
4,00	26,21	21,66
4,18	27,69	23,95
4,18	28,47	22,62
4,18	28,47	23,77
4,25	30,03	24,12
4,25	30,03	24,73
4,25	27,69	23,15
4,25	28,47	23,17
4,47	28,05	23,31
4,47	27,26	22,82
4,47	28,05	22,23
4,63	27,26	24,27
4,63	28,85	24,29
4,63	28,05	23,59
4,63	28,05	23,04
4,63	28,05	21,89
4,63	27,86	22,10
4,63	28,05	23,11

Table C.5 Data for $V_w = 12.9$ cm/s

d_e (mm)	$V_{max,r}$ (cm/s)	$V_{av,r}$ (cm/s)
3,15	29,76	23,23
3,15	27,56	22,14
3,15	29,02	22,54
3,15	27,82	22,86
3,44	30,00	23,46
3,44	27,42	23,00
3,44	29,22	23,64
3,44	28,06	24,00
3,44	29,54	23,14
3,44	26,61	22,38
3,52	28,63	23,15
3,52	27,56	23,00
3,57	30,33	23,24
3,57	26,89	23,00
3,57	27,67	23,92
3,68	24,63	21,76
3,68	28,47	23,41
4,00	26,47	21,64
4,00	27,90	21,70
4,00	27,90	22,19
4,00	28,61	21,38
4,10	28,47	22,47
4,10	26,09	21,24
4,38	29,31	23,71
4,38	27,74	22,14
4,38	26,18	22,58
4,38	27,74	22,34
4,53	26,96	21,85
4,53	27,26	21,65
4,53	28,06	23,27
4,53	27,26	23,33
4,53	28,53	21,98
4,63	26,46	22,40
4,63	28,06	23,73
4,63	28,06	21,64

Table C.6 Data for $V_w = 15.4$ cm/s

d_e (mm)	$V_{max,r}$ (cm/s)	$V_{av,r}$ (cm/s)
2,93	31,13	23,62
2,93	30,42	21,18
2,93	29,26	23,18
3,23	28,59	20,98
3,23	28,59	24,38
3,23	29,00	22,93
3,39	27,13	20,67
3,39	26,29	20,65
3,39	28,59	23,72
3,44	28,22	21,26
3,44	26,67	21,80
3,44	28,51	23,58
3,46	27,84	22,43
3,46	30,06	25,36
3,46	26,39	21,96
3,46	29,39	22,86
3,64	27,70	23,59
3,64	24,93	20,66
3,77	31,79	23,15
3,77	27,70	23,44
3,77	28,51	23,59
4,00	27,54	22,15
4,00	28,97	23,05
4,06	28,17	21,94
4,06	25,37	21,46
4,22	27,37	21,06
4,22	27,12	20,64
4,22	27,90	21,52
4,22	27,12	20,53
4,34	26,34	20,53
4,34	24,78	19,82
4,34	26,57	20,37
4,34	25,56	19,69
4,34	24,78	20,61
4,53	26,57	20,93
4,53	25,77	21,41

Table C.7 Data for $V_w = 18.2$ cm/s

d_e (mm)	$V_{max,r}$ (cm/s)	$V_{av,r}$ (cm/s)
3,00	30,66	22,12
3,00	29,93	23,00
3,00	28,69	21,65
3,29	29,49	22,77
3,29	27,73	22,13
3,36	31,91	22,11
3,36	27,73	22,00
3,56	28,30	21,64
3,56	30,08	22,36
3,84	30,34	21,85
3,84	28,91	21,78
3,84	30,34	21,83
3,84	26,77	22,50
4,06	29,92	20,73
4,06	28,36	21,47
4,06	28,36	21,44
4,06	29,14	22,01
4,15	28,36	22,16
4,15	29,40	22,44
4,15	30,20	23,26
4,15	27,80	21,75
4,15	28,57	23,05
4,23	26,79	21,71
4,23	28,36	21,20
4,23	28,36	20,87
4,23	26,79	22,58
4,23	29,37	21,94

Table C.8 Data for $V_w = 0.0$ cm/s

d_e (mm)	$V_{max,r}$ (cm/s)	$V_{av,r}$ (cm/s)
2,93	38,84	29,88
3,08	38,11	30,15
3,22	38,84	28,95
3,31	38,11	29,32
3,48	34,02	28,31
3,68	33,53	26,77
3,95	33,75	28,22
4,04	34,21	27,90
4,14	30,76	25,69
4,24	35,25	27,56
4,60	32,36	26,53
4,78	33,28	27,07

Table C.9 Data for $V_w = 6.5$ cm/s

d_e (mm)	$V_{max,r}$ (cm/s)	$V_{av,r}$ (cm/s)
3,22	29,07	24,67
3,42	27,00	22,62
3,60	31,42	24,32
4,00	29,87	23,59
4,09	29,04	24,09
4,14	30,31	23,18
4,20	29,65	24,17
4,30	28,38	23,86
4,38	29,29	23,89
4,53	28,77	23,80
4,63	28,52	23,86

Table C.10 Data for $V_w = 7.9$ cm/s

d_e (mm)	$V_{max,r}$ (cm/s)	$V_{av,r}$ (cm/s)
3,30	27,23	21,99
3,45	27,24	21,92
3,51	29,78	24,92
3,65	29,77	24,60
3,76	28,92	24,25
4,00	27,19	22,29
4,09	28,62	23,15
4,14	27,58	22,92
4,47	26,78	22,58
4,63	27,05	21,20

Table C.11 Data for $V_w = 10.5$ cm/s

d_e (mm)	$V_{max,r}$ (cm/s)	$V_{av,r}$ (cm/s)
3,23	27,41	22,91
3,50	28,51	23,25
3,59	28,11	22,39
3,76	28,32	22,85
3,90	27,95	22,69
4,00	26,39	22,13
4,18	28,21	23,45
4,25	29,06	23,80
4,47	27,79	22,78
4,63	28,02	23,19

Table C.12 Data for $V_w = 12.9$ cm/s

d_e (mm)	$V_{max,r}$ (cm/s)	$V_{av,r}$ (cm/s)
3,15	28,54	22,69
3,44	28,48	23,27
3,52	28,63	23,07
3,57	28,30	23,39
3,68	26,55	22,59
4,00	27,72	21,73
4,10	27,28	21,84
4,38	27,74	22,69
4,53	27,61	22,42
4,63	27,53	22,58

Table C.13 Data for $V_w = 15.4$ cm/s

d_e (mm)	$V_{max,r}$ (cm/s)	$V_{av,r}$ (cm/s)
2,93	30,27	22,66
3,23	28,73	22,76
3,39	27,34	21,68
3,44	27,80	22,21
3,46	28,42	23,16
3,64	26,32	22,12
3,77	29,33	23,39
4,00	28,25	22,61
4,06	26,77	21,71
4,22	27,38	20,93
4,34	25,61	20,21
4,53	26,17	21,17

Table C.14 Data for $V_w = 18.2$ cm/s

d_e (mm)	$V_{max,r}$ (cm/s)	$V_{av,r}$ (cm/s)
3,00	29,76	22,26
3,29	28,61	22,45
3,36	29,82	22,05
3,56	29,19	22,00
3,84	29,09	21,99
4,06	28,95	22,41
4,15	28,87	22,54
4,23	27,94	21,66

VITA

Uğur Bezdegümeli was born in Tire-İzmir on July 22, 1968. He received his B.S. degree on Nuclear Engineering from the Hacettepe University (HU) in June 1990 and his M.S. degree on Nuclear Engineering from the Hacettepe University in January 1994. He worked at the Department of Nuclear Engineering (HU) as a graduate assistant from 1990 to 1992. Since then he has been working at the Nuclear Safety Department of Turkish Atomic Energy Authority as a safety analyst. His main areas of interest is nuclear safety, thermal-hydraulic analysis and related international regulations.